1043

Some fundamental and practical aspects of CHEMFETs

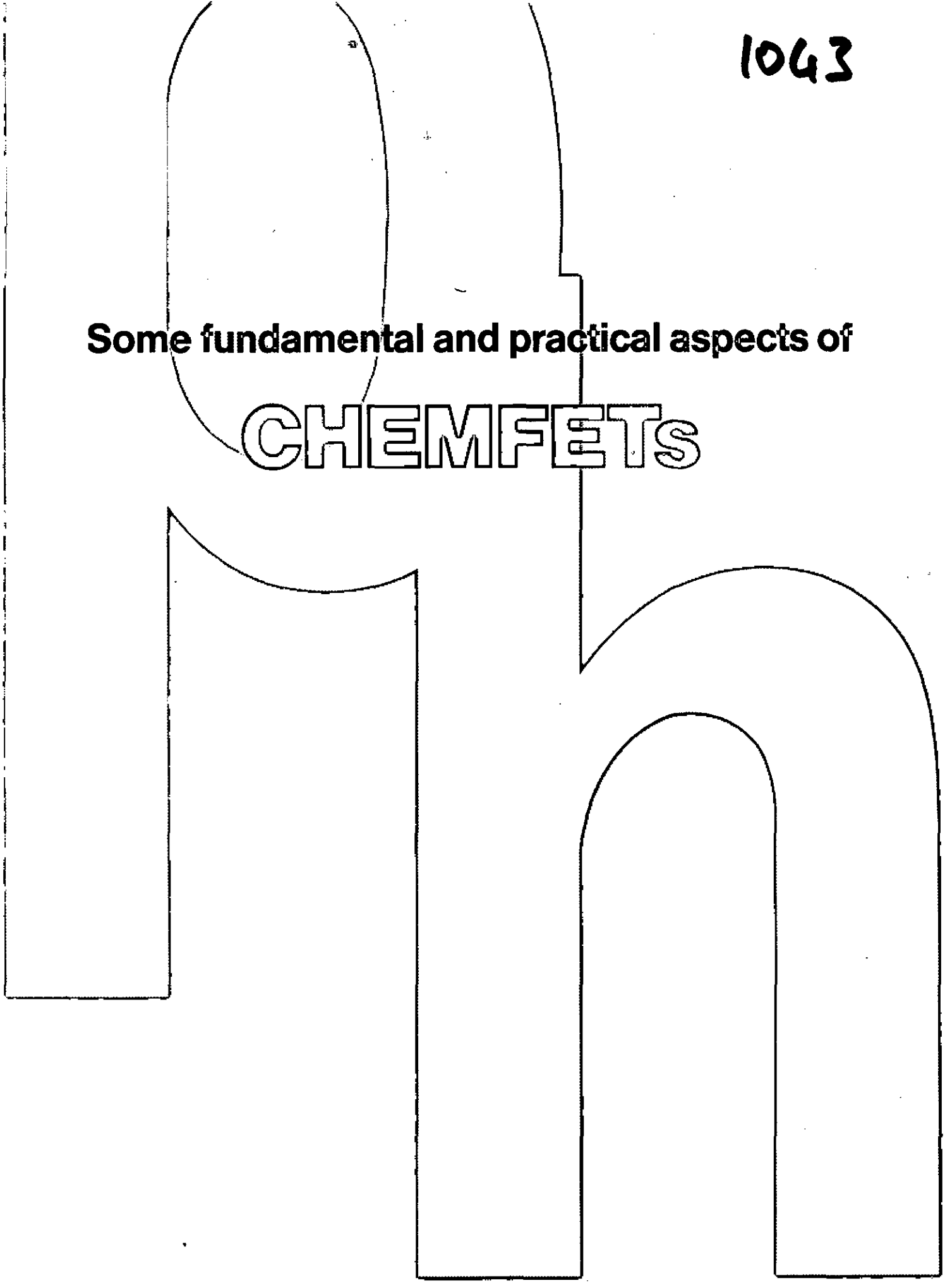

H. H. van den Vlekkert

Some fundamental and practical aspects of 'CHEMFETs'

H.H. van den Vlekkert

Design: John + Rolf '88
Photography: Hans
Lithography: Danny
Printing: Print Productions bv
The Netherlands

Many things we do naturally become difficult only when we try to make them into intellectual subjects. It is possible to know so much about a subject that you become totally ignorant.

Frank Herbert
in *Chapterhouse: Dune*

To Jannie, Roy and Spetter.

IMPRIMATUR POUR LA THÈSE

Some fundamental and practical aspects of "CHEMFETs"

de Monsieur Hendrik van den Vlekkert

UNIVERSITÉ DE NEUCHATEL

FACULTÉ DES SCIENCES

La Faculté des sciences de l'Université de Neuchâtel,
sur le rapport des membres du jury,

Messieurs N. de Rooij, M. Degrauwe,
P. Bergveld (Twente) et W. Göpel (Tübingen)

autorise l'impression de la présente thèse.

Neuchâtel, le 18 mai 1988

Le doyen:

F. Persoz

UNIVERSITÉ DE NEUCHÂTEL
INSTITUT DE MICROTECHNIQUE

Some fundamental and practical aspects of 'CHEMFETs'

THÈSE

PRÉSENTÉE À LA FACULTÉ DES SCIENCES
POUR OBTENIR LE GRADE DE DOCTEUR ÉS SCIENCES

PAR

Hendrik H. van den Vlekkert

Preface

When I became involved in the world of sensors,
I discovered soon that for the development of an useful sensor knowledge
of different fields is necessary. Because this knowledge
can hardly be concentrated in one person, collaboration with others is
of the upmost importance. During the preparation of this thesis
I therefore sought and found help. From this place I want to thank all those
people for their advice and help and I hope that someday
I can return the favor.
Furthermore I wish to acknowledge the FSRM (Fondation Suisse pour la
Recherche en Microtechnique) for its financial support.
The cooperation with the University of Geneva, Section de Médicine Dentaire,
the University of Tübingen, Institut für physikalische und
theoretiche Chemie and the CSEM (Centre Suisse d'Electronique et
Microtechnique), Neuchâtel, was greatly appreciated.

Table of contents

Chapter 1 Introduction

Introduction

The interest in chemically sensitive electronic devices has increased sharply in the last decades, as can be seen from the increasing number of publications and conferences dealing with this subject. One of the most widely used devices is the silicon based field effect transistor, first introduced by Bergveld in 1970 [1]. He called his device an Ion Sensitive Field Effect Transistor (ISFET). Since then a whole new family of sensors was developed, based on this transducer [2]. Comprehensive and critical reviews dealing with the development of field-effect chemical sensors were published by Sibbald [3,4], Janata and Huber [5], and Kelly and Owen [6]. An important area for the application of such sensors is the biomedical field. In this area, however, the requirements for reliability, biocompatability, sensitivity, selectivity, stability, lifetime and response time are very high [7]. Only very few sensors have proved their feasibility, until now, for such a clinical application. Some of the main problems, which have hampered the large scale utilization of ISFETs, are short lifetime, due to poor packaging, drift, temperature sensitivity and lack of selectivity. In this work these problems will be discussed and some solutions will be proposed. A more extensive introduction to each problem will be given in each chapter in order to be able to read each chapter separately.

Outline

In Chapter 2 the design, fabrication and characterization of a pH sensitive ISFET, with alumina as pH sensitive layer will be discussed. A method will be outlined to achieve reliable pH measurements.
In Chapter 3 it is shown that ISFETs can fulfill the specific requirements for biomedical application when carefully designed.
In Chapters 4 and 5 attention will be given to the drift and temperature behavior of the ISFETs.
In Chapter 6 a method will be outlined to improve and simplify the encapsulation of ISFETs. The described encapsulation technique is based on the anodic bonding of glass to silicon. Also a pCl-ISFET will be presented.
Finally in Chapter 7 the transformation of the sensitivity of pH sensitive ISFETs with solvent polymeric membranes will be discussed.

References

1. Bergveld,P., *IEEE Trans.Biomed.Eng.* **BME-17,** 70 (1970).
2. Bergveld,P., *Sensors Actuators* 8, 109 (1985).
3. Sibbald,A., *IEE Proc.1* **130,** 233 (1983).
4. Sibbald,A., *J.Molecular Electronics,* **Vol 2,** 51 (1987).
5. Janata,J., Huber,R.J., *in* Ion Selective electrodes in Analytical Chemistry, (H.Freiser, Ed.,Plenum Press), Vol. 2, p.107, 1980.
6. Kelly,R.G., Owen,A.E., *IEE Proc.1* **132,** 227 (1985).
7. Oesch,U., Ammann,D., Simon,W., *Clinical Chem.* **32,** 1448 (1986).

Chapter 2 The design, fabrication and characterization of pH-sensitive ISFETs

accepted for publication in:

Analusis:

Design, fabrication and characterization of pH-sensitive ISFETs
H.H.van den Vlekkert, N.F.de Rooij

parts of this Chapter were presented at:

SSC-ASMT'85 , 59 congress,
1985 Interlaken, Switzerland

Miniaturized silicon sensors for biomedical applications
Ch.Arnoux, B. Kloeck, H.H.van den Vlekkert, N.F.de Rooij
(Proc.SSC-ASMT'85, Interlaken, Switzerland, 1985 p. 39)

2nd International Meeting on Chemical Sensors
1986, Bordeaux, France

A practical approach to the application of ISFETs as accurate ion-sensors
H.H.van den Vlekkert, Ch.Arnoux, Ph.Lomazzi, N.F.de Rooij
(Proc. 2nd Int. Meeting on Chemical Sensors, Bordeaux, France, 1986 p.462)

Abstract

Miniaturized silicon sensors show great promise for biomedical applications, in particular for invasive applications. The possibility of integrating the sensing elements with on-chip signal processing electronics and eventually actuators may lead to fully integrated miniaturized closed-loop systems.
The physics and technology of miniaturized silicon sensors is discussed using a pH sensitive field effect transistor (pH-ISFET). The characteristics and accuracy of a pH-ISFET, fabricated with standard CMOS technology and using alumina as pH sensitive material, are presented. The behaviour of the pH-ISFET, operated in the constant current mode, is based on the application of a Taylor expansion of the reference electrode to source voltage (V_G), limited to second order terms. By using the obtained algorithm, the pH of a solution under investigation can be calculated from V_G, provided that all coefficients are known. With this method a residual standard deviation of 0.01 pH is observed between a pH-ISFET and a conventional glass electrode.

Introduction

Miniaturized silicon sensors have received considerable interest during the last decades, stimulated by the enormous computing and information processing capabilities of the integrated solid state technology [1]. This technology offers the advantages of miniaturization and mass production and therefore low cost sensors. The biomedical field is an especially important area for the application of miniaturized sensors [2,3]. An example of such a miniaturized sensor suitable for biomedical applications is the ion sensitive field effect transistor (ISFET). Placed in the tip of indwelling catheters, their feasibility for monitoring parameters and blood electrolytes has been demonstrated [4,5,6].
The ISFET can be considered to be an IGFET (insulated gate field effect transistor) with the metal gate replaced by a reference electrode, electrolyte solution and an ion selective material deposited over the gate insulator, as is shown in Fig. 1.
Two main types of ion selective materials are used:

a) inorganic insulators such as Si_3N_4, Al_2O_3 and Ta_2O_5 as pH sensitive materials [7,8] or aluminosilicates as pNa or pK sensitive materials [8,9].
b) ion selective membranes (polymeric as well as solid state type [6,10]).

ISFETs feature the following specific advantages: small size, high to low impedance conversion, rugged solid state structure, the possibility ot obtaining multi-ion sensors and integration of signal processing capabilities.
However the drift and temperature sensitivity of ISFETs can easily result in incorrect ion activity determinations, especially for the ion activity determinations in physiological ranges where a high accuracy is necessary (Table 1, adapted from [11]).

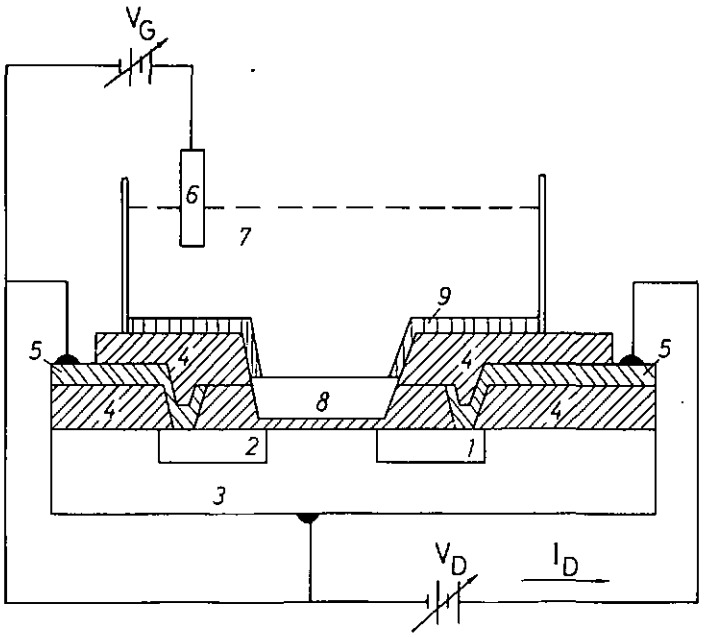

Fig. 1: *Schematic diagram of an ISFET (adapted from [15])*

1) drain
2) source
3) bulk
4) insulator
5) metal
6) reference electrode
7) solution
8) ion-selective material
9) encapsulant

Table 1: *Demands towards potentiometric ion activity determinations based on the physiological ranges.*

Ion I^{z+}	Concentration range (mMol/l)	EMF range[a] (mV)	Tolerable standard deviation[b] (mV)
Na^+	135-150	2.4	0.12
K^+	3.5-5.0	9.1	0.46
Ca^{2+}[c]	1.0-1.2	2.4	0.12
H^+	4.3×10^{-5}- 5.6×10^{-5}	6.8	0.35

a) Calculated on the basis of the Nernst equation according to the corresponding activity ranges.
b) For a five fold subdivision of the given physiological range with a 95% confidence limit.
c) Free ionized Ca^{2+}.

Other problems which so far have hampered the large scale introduction of ISFETs for clinical applications are unsatisfactory encapsulation, the lack of a reliable on chip reference electrode and unwanted threshold voltage shift due to electrostatic discharge across the insulator. Solutions have already been proposed to solve these technological problems [12,13,14].
In this Chapter pH sensitive ISFETs are characterized and a method will be outlined to obtain accurate pH data from the output of these pH sensitive ISFETs by using a correction method for the drift and temperature effects. This method is verified on pH-ISFETs, fabricated using a standard CMOS process, which may allow in a later phase the integration of circuitry for the execution of the outlined compensation procedure.

Theory

ISFETs can be operated either in the unsaturated region or in the saturated region [15]. For an n-channel device the drain current I_D in the unsaturated region ($V_D < V_G - V_T$) is given approximately by:

$$I_D = \mu_n \frac{W}{L} C_{ins} \left(V_G - V_T - \frac{1}{2}V_D\right) V_D \qquad (1)$$

where μ_n denotes the electron mobility, W the channel width, L the channel length, C_{ins} the insulator capacitance per unit area, V_G the reference electrode (gate) to source voltage relative to ground, V_T the threshold voltage and V_D the drain to source voltage. Source and substrate are short-circuited. In the case of pH-ISFETs using inorganic oxides as pH sensitive material, for instance Al_2O_3, the threshold voltage V_T is given by [16]:

$$V_T = E_{ref} - \Psi_o + \chi - \frac{1}{q}\Phi^{Si} - \frac{Q_{ins}}{C_{ins}} + 2\phi^F - \frac{Q_{inv}}{C_{ins}} \qquad (2)$$

Here E_{ref} denotes the reference electrode potential relative to vacuum, Ψ_o the potential difference between the insulator surface and the bulk of the solution, χ the surface dipole potential at the insulator/solution interface. Φ^{Si} represents the silicon work function, q the unit charge, Q_{ins} is the charge inside the insulator which is assumed to be located at the insulator/silicon interface per unit area, Q_{inv} the charge per unit area in the silicon surface at inversion and Φ^F the Fermi potential. Comparing Equation (2) with the threshold voltage expression for an IGFET we see that the metal work function Φ^M has been replaced by E_{ref}, Ψ_o and χ. For V_T^{MOST}, the threshold voltage for an IGFET, this results in:

$$V_T^{MOST} = V_T - E_{ref} + \Psi_o - \chi + \frac{\Phi^M}{q} \qquad (3)$$

In the case of inorganic oxides such as SiO_2 or Al_2O_3 the potential difference Ψ_o is given by [16]:

$$\Psi_o = 2.303 \frac{kT}{q} \frac{\beta}{\beta+1} (pH_{pzc} - pH) \qquad (4)$$

where k denotes the Boltzmann constant, T the absolute temperature, β the sensitivity parameter and pH_{pzc} the pH at the point of zero charge of the oxide material. In β all the constants of the surface reactions and of the electrical double layer are lumped together. Equation (4) is only valid if $q\Psi_0/kT<\beta$ [16]. The preferred mode of operation of an ISFET is the constant current mode with constant V_D, using a feed-back circuit which compensates for induced changes in I_D by adjusting V_G. For the linear range this results in:

$$V_G = \frac{I_D}{\frac{W}{L}\mu_n C_{ins} V_D} + E_{ref} - \Psi_o + \chi - \frac{1}{q}\Phi^{Si} - \frac{Q_{ins}}{C_{ins}} + 2\phi^{F} - \frac{Q_{inv}}{C_{ins}} + \frac{1}{2}V_D \qquad (5)$$

V_G is considered to be dependent on pH, temperature T and time of exposure to the electrolyte solution t. V_G can be developed in a Taylor series at the point (pH_o,T_o,t_o) resulting in:

$$\begin{aligned} V_G = {} & V_G^o + \left(\frac{\partial V_G}{\partial pH}\right)_{T,t}(pH-pH_o) + \left(\frac{\partial V_G}{\partial T}\right)_{pH,t}(T-T_o) + \left(\frac{\partial V_G}{\partial t}\right)_{pH,T}(t-t_o) \\ & + \frac{1}{2}\left(\frac{\partial^2 V_G}{\partial pH^2}\right)_{T,t}(pH-pH_o)^2 + \frac{1}{2}\left(\frac{\partial^2 V_G}{\partial T^2}\right)_{pH,t}(T-T_o)^2 + \frac{1}{2}\left(\frac{\partial^2 V_G}{\partial t^2}\right)_{pH,T}(t-t_o)^2 \\ & + \frac{1}{2}\left(\frac{\partial^2 V_G}{\partial pH \partial T}\right)_{t}(T-T_o)(pH-pH_o) + \frac{1}{2}\left(\frac{\partial^2 V_G}{\partial T \partial pH}\right)_{t}(pH-pH_o)(T-T_o) \\ & + \frac{1}{2}\left(\frac{\partial^2 V_G}{\partial pH \partial t}\right)_{T}(t-t_o)(pH-pH_o) + \frac{1}{2}\left(\frac{\partial^2 V_G}{\partial t \partial pH}\right)_{T}(pH-pH_o)(t-t_o) \\ & + \frac{1}{2}\left(\frac{\partial^2 V_G}{\partial T \partial t}\right)_{pH}(t-t_o)(T-T_o) + \frac{1}{2}\left(\frac{\partial^2 V_G}{\partial t \partial T}\right)_{pH}(T-T_o)(t-t_o) \end{aligned} \qquad (6)$$

Taken into account are only the first and second order terms and V_G^o denotes the V_G for the pH value of the calibration buffer pH_o, at temperature T_o and time t_o or $V_G^o = V_G\ (pH_o,T_o,t_o)$.
Expressions for the partial differentials of V_G with respect to pH ,T and t can be derived from Equation (5), with the partial differentials of I_D equal to zero.
For the first order terms this will result in:

pH-sensitivity

$$\frac{\partial V_G}{\partial pH} = -\frac{\partial \Psi_o}{\partial pH} = 2.303\ \frac{kT}{q}\frac{\beta}{\beta+1} \tag{7}$$

Temperature sensitivity

$$\frac{\partial V_G}{\partial T} = \frac{\partial V_T}{\partial T} - \frac{I_D\, b}{\mu_{n_o}\frac{W}{L}C_{ins}T_o V_D} \tag{8}$$

In Equation (8) μ^o_n is the electron mobility at the temperature T_o. Equation (8) can be easily found using the empirical relationship $\mu = aT^b$ for the electron mobility where a and b are constants independent of temperature [17,18]. Equation (8) can be rewritten as follows:

$$\frac{\partial V_G}{\partial T} = \frac{\partial V_T^{MOST}}{\partial T} + \frac{\partial E_{ref}}{\partial T} - \frac{\partial \Psi_o}{\partial T} - \frac{I_D\, b}{\mu_{n_o}\frac{W}{L}C_{ins}T_o V_D} \tag{9}$$

where V_T^{MOST} accounts for the solid state part of the sensor. The term $\partial V_T^{MOST}/\partial T$ is given by the following expression [17,18]:

$$\frac{\partial V_T^{MOST}}{\partial T} = \left(2 - \frac{Q_{inv}}{2C_{ins}\phi_F}\right)\frac{\partial \phi_F}{\partial T} \text{ and } \frac{\partial \phi_F}{\partial T} = -\frac{1}{T}\left(\frac{E_{go}}{2q} - \phi_F\right) \tag{10}$$

with E_{go} the energy bandgap of silicon at 0 K.

Drift behaviour

In a first approximation the drift can be related to changes with time of the interface potential difference and the dipole potential (denoted as chemical drift) as well as with changes in the solid state part of the sensor. Assuming that E_{ref} is stable this results in:

$$\frac{\partial V_G}{\partial t} = \frac{\partial V_T^{MOST}}{\partial t} - \frac{\partial \Psi_o}{\partial t} + \frac{\partial \chi}{\partial t} \tag{11}$$

Similar expressions for the second order terms will be given later based on the

experimental results of the verification of the first order terms.
Another parameter, besides hysteresis, can influence the accuracy of an ISFET namely the selectivity of the pH sensitive layer for hydrogen ions. An extensive treatment of the influence of other ions on the response of an ISFET is given in reference [16]. Because of the good selectivity of alumina for hydrogen ions over cat-ions as will be shown later, it is not necessary to include this influence in the above mentioned derivations.

Experimental

ISFET fabrication:

Two different types of n-channel ISFETs have been realized.
The first type has a very simple fabrication process as is shown in Fig. 2a [19a]. A photograph of the ISFET and corresponding MAOSFET is shown in Fig. 2b.
A boron doped oxide layer is deposited by chemical vapour deposition (CVD) on a p-type wafer (3-5 Ohmcm) and then removed from the source and drain regions (step 1). Then a phosphorous doped oxide layer is deposited on the entire wafer also by CVD. This step is followed by an etch process, which removes the doped oxide layer on the area where the gate oxide has to be grown.

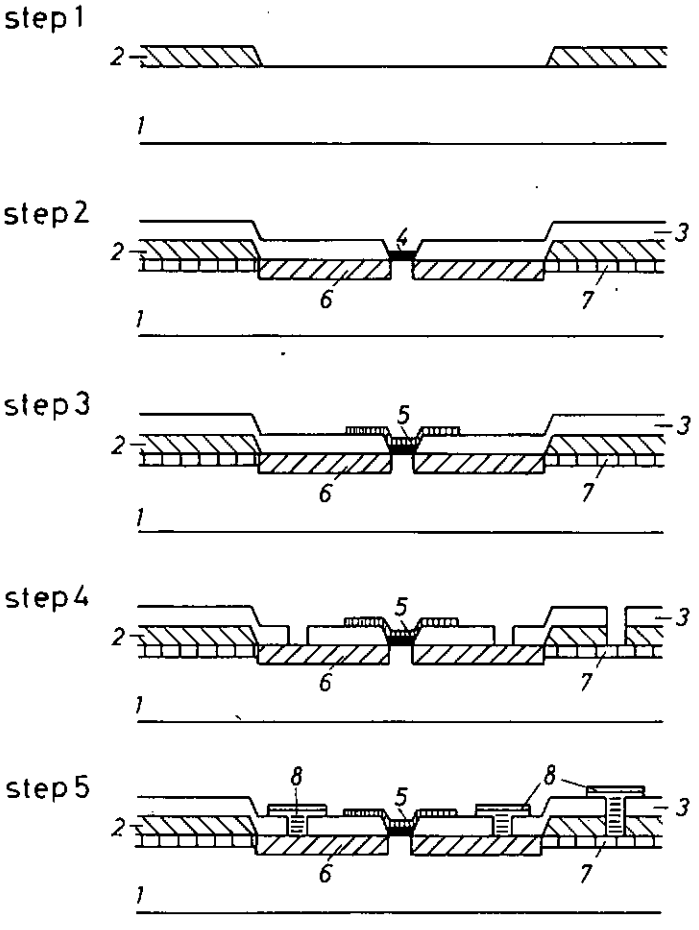

Fig. 2a: *Fabrication process of an ISFET.*

1) p-type silicon
2) boron doped SiO_2
3) phosphorous doped SiO_2
4) thermally grown SiO_2
5) alumina
6) drain and source (phosphorous)
7) channel stop (boron)
8) aluminium (drain, source and substrate contact)

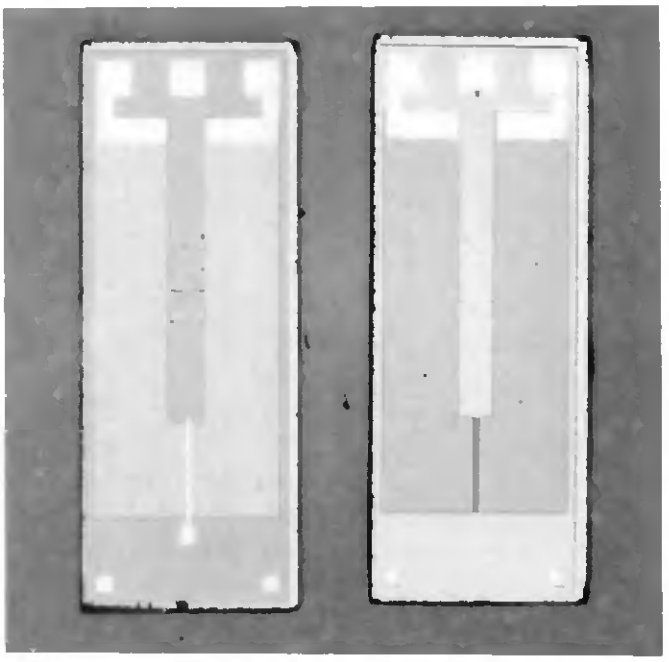

Fig. 2b: *Photograph of the ISFET and MAOSFET (type 1)*

A thick gate oxide is then grown (typically 900Å) and during this step the source and drain regions are diffused simultaneously into the silicon (step 2). Then an alumina layer as pH sensitive layer is deposited (also by CVD typically 600Å). A contact window is defined in the Al_2O_3 layer using an undoped SiO_2 layer, deposited by CVD, as masking material (step 3). Then the contacts are detined in the doped oxide layers (step 4) and after the metallization with aluminium the last mask defines the contact pads (step 5). Simultaneously, several ISFET gates are covered with aluminium, thereby forming IGFETs. When excluding the alumina layer ISFETs and IGFETs with SiO_2 as pH sensitive layer can also be obtained.
The second type was fabricated using an adjusted low power p-well polysilicon gate CMOS process with 6 µm channel length developed at CSEM, Neuchâtel, Switzerland, as reported elsewhere [19b]. The gate insulator consists of thermally grown SiO_2 with the Al_2O_3 layer as pH sensitive material on top. A temperature sensitive resistor is integrated on the same chip.
The tirst design enabled us to make relatively easy ISFETs and IGFETs with different insulators. The second design showed the compatibility of an ISFET production process with a normal CMOS process and gave the possibility to perform the experiments where an on chip temperature sensor was necessary. After dicing the wafer into individual chips, they were mounted on standard printed circuit boards. After wire bonding, the chips were covered with an epoxy (Shell Epon 825) in order to insulate the various electrical connections. Only the pH sensitive gate area remained uncovered.

ISFET characterization:
The ISFETs were then connected to a specially developed amplitier system, which operates the devices at constant drain current and constant drain to source voltage. The V_G was the experimentally determined quantity. Also the temperature sensor was measured by this system. The outputs of this control system were fed to a recorder (SE120) and/or to a micro computer (HP216). In Fig. 3 the I_D - V_G characteristics of the n-channel ISFETs and corresponding

IGFETs are shown. The characteristics were recorded with a HP4145. The characteristics show a perfect fit between ISFET and IGFET behaviour except for the positive shift in threshold voltage (≈ 0.7 V) which can be explained by replacing the metal gate with a reference electrode and a solution [16]. The difference in transconductance and threshold voltage between the two types can be explained by differences in gate geometry and in substrate doping. The nonlinearity of the I_D-V_G curves as function of V_D in the unsaturated region can be ascribed to the relatively high resistance values of the source and drain diffusions [20].
Every coefficient of Equation (6) was evaluated as function of pH, temperature and time. A conventional glass electrode (Metrohm 6.0102.002) and a temperature sensor (Metrohm 6.0726.100) were used as a reference system. The glass electrode and ISFET were measured against the same reference electrode (Metrohm 6.1103.000). In this manner deviations caused by the reference electrode, e.g. changes in liquid junction potential, were eliminated. In order to investigate the reproducibility, the ISFETs were tested over a period of several months. In between measurements they were stored dry at room temperature.

Determination of the first order terms:
pH-sensitivity
A representative result for the pH sensitivity is shown in Fig. 4 where V_G is plotted against pH. The pH of a Tris/HCl buffer was varied between pH 3 and 12 by adding acid or base. The devices and the solution were kept at constant temperature by using a thermostatted titration vessel. Subsequent measurements showed no change in pH sensitivity within the experimental error (±0.5 mV/pH) due to possible calibration errors of the reference system i.e. the glass electrode.

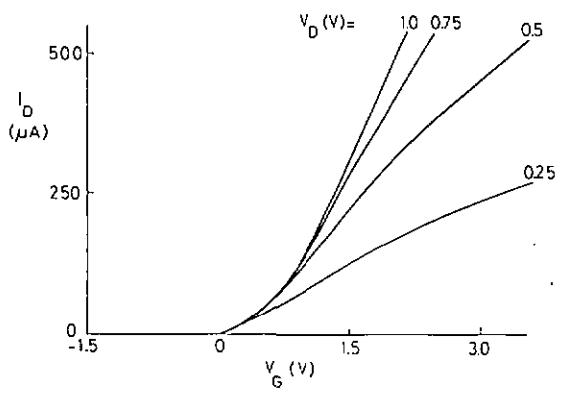

Fig. 3:
The I_D-V_G characteristics of the n-channel ISFETs and an IGFET as function of V_D.
a) ISFET type 1 using a Tris/HCl buffer and an Ag/AgCl double junction reference electrode

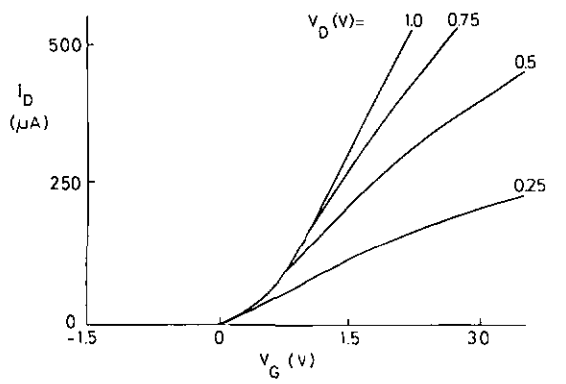

b) IGFET type 2

c) ISFET type 2 using a Tris/HCl buffer and an Ag/AgCl double junction reference electrode

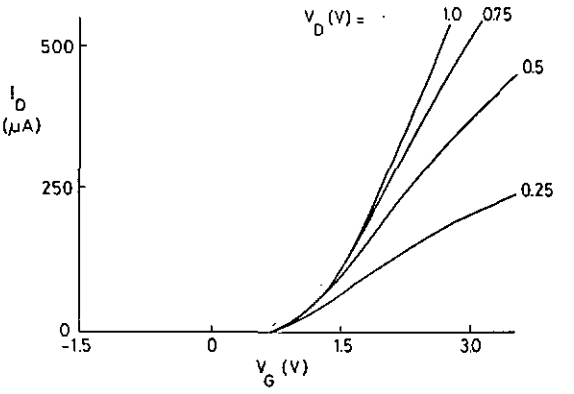

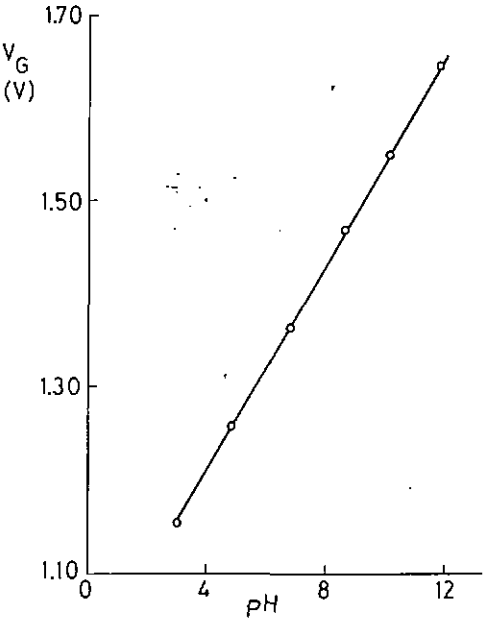

Fig. 4:
pH response of an ISFET at 25°C.
The pH was adjusted by adding 0.5M HCl resp. 0.5M NaOH to a buffer containing 0.616M Tris and 0.5M HCl
($V_D = 1.0$ V, $I_D = 100$ μA)
Slope = 55.2 mV/pH, $n = 45$ and $r^2 = 0.999$

Temperature sensitivity

Values for the temperature sensitivity were determined over a temperature interval 15-35°C as function of the drain current in a given buffer (Tris/HCl). Since the pH value of buffers change with temperature, the measured value of the change in V_G with temperature is given by:

$$\left(\frac{\partial V_G}{\partial T}\right)_m = \frac{\partial V_G}{\partial T} + \left(\frac{\partial V_G}{\partial pH}\right)\left(\frac{\partial pH}{\partial T}\right) \qquad (12)$$

where $\partial pH/\partial T$ denotes the change in the pH value of the buffer with temperature. Experimental data for $(\partial V_G/\partial T)_m$ are plotted against I_D in Fig. 5 . No change in the $(\partial V_G/\partial T)_m$ could be detected during subsequent measurements. In the same manner the temperature sensitivity of IGFETs was investigated.

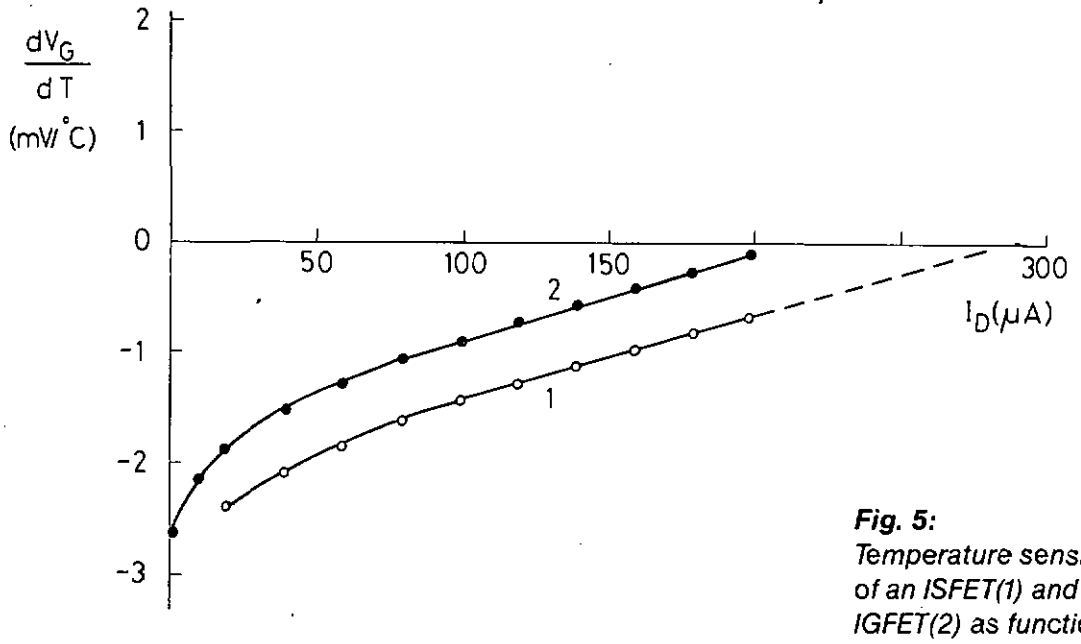

Fig. 5:
Temperature sensitivity of an ISFET(1) and an IGFET(2) as function of I_D.
(V_D = 1.0 V, Tris/HCl buffer pH = 7.6, temperature range 15-35°C)

From Fig. 5 it can be seen that a linear relationship exists between $(\partial V_G/\partial T)_m$ and I_D in accordance with Equations (8) and (10), when the devices are operated in the unsaturated regions.

Drift behaviour

The dependence of V_G on time was measured during the first exposure of the device to a Tris/HCl buffer as well as during subsequent exposures. Representative results are shown in Fig. 6 where V_G is plotted against time.

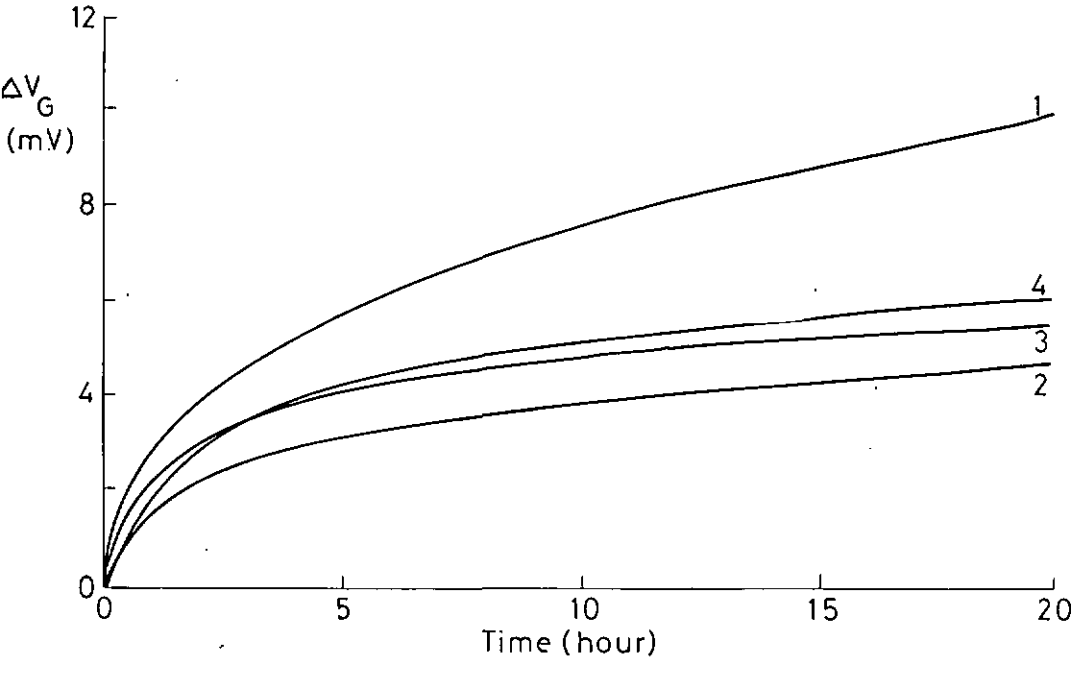

Fig. 6:
Drift behaviour of an ISFET at 25°C in a Tris/HCl buffer (V_D = 0.5 V, I_D = 100 μA)
Time between measurements:
1 and 2 : 1 week
1 and 3 : 2 weeks
1 and 4 : 18 weeks

During the first exposure the total drift is much larger than the drift observed during subsequent exposures. In addition the drift during subsequent measurements is quite reproducible. Also after the first hours of the measurement the drift can be considered linear over a certain period of time. The drift during the first exposure may be explained by a combined effect of chemical drift and solid state drift. After the first exposure the oxide surface seems to be conditioned and mainly solid state drift remains. To investigate the drift behaviour further, similar experiments were carried out with IGFETs with Al_2O_3 and SiO_2 as insulator materials. The results are shown in Fig. 7.

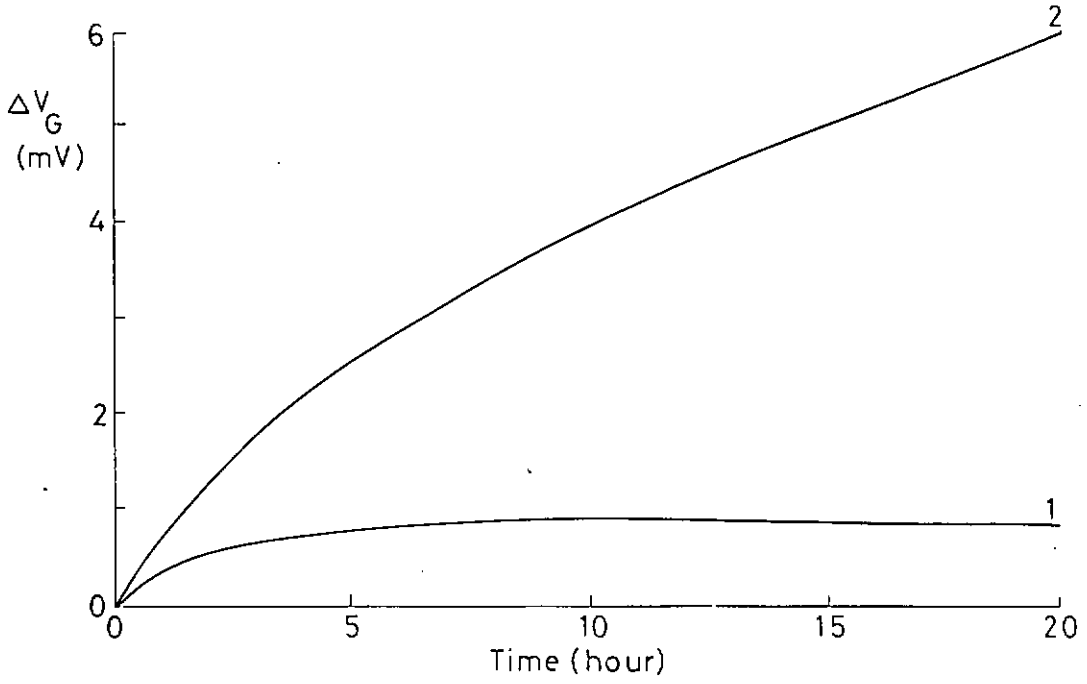

Fig. 7: *Drift behaviour of IGFET's at 25°C ($V_D = 0.5$ V, $I_D = 100$ μA)*
1) IGFET with SiO_2 as insulator material
2) IGFET with Al_2O_3/SiO_2 as insulator material

It is found that for the IGFETs no initial decrease can be detected during subsequent tests. Furthermore it can be seen that the SiO_2 IGFET does not drift and that the Al_2O_3/SiO_2 IGFET has the same drift pattern as the ISFET (Table 2). It should be noted that a SiO_2 ISFET has a very large drift due to hydratation of the SiO_2 layer [21].

Determination of the second order terms:
Because of the linear behaviour under certain limited conditions, the terms $(\partial^2 V_G/\partial T^2)$, $(\partial^2 V_G/\partial pH^2)$ and $(\partial^2 V_G/\partial t^2)$ can be set equal to zero. The pH sensitivity was measured at different temperatures as described before. The results are shown in Fig. 8 where the pH sensitivity is shown as function of temperature. The slope is now $(\partial^2 V_G/\partial T \partial pH)$ and is equal to 0.23 mV/pH°C.

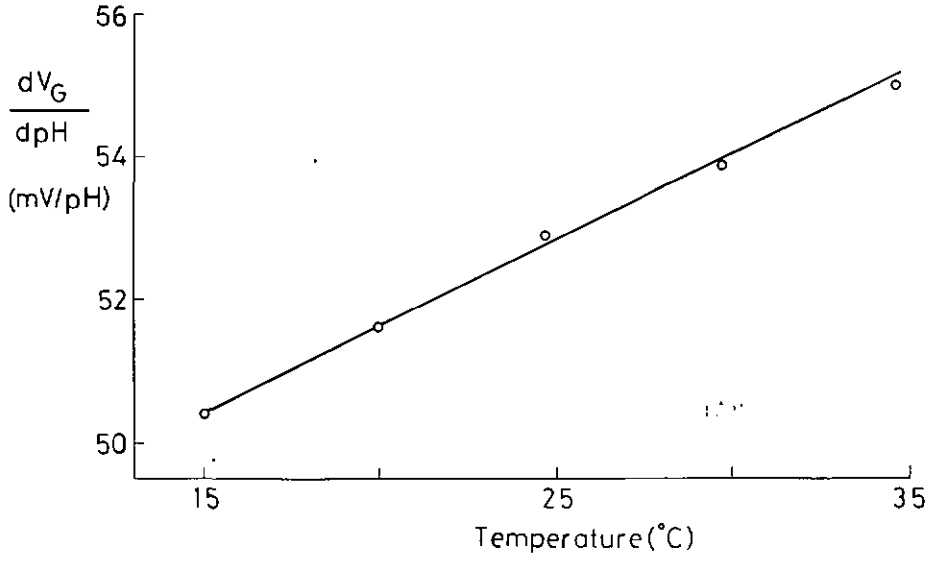

Fig. 8: *pH sensitivity of an ISFET as function of temperature.*
The pH was adjusted by adding a 0.5M HCl resp. a 0.5M NaOH solution to a Tris/HCl buffer. ($V_D = 0.5$ *V,* $I_D = 100$ *μA)*
Slope = 0.23 mV/pH°C.

The term $(\partial^2 V_G/\partial pH \partial T)$ was determined by measuring $(\partial V_G/\partial T)_m$ at constant I_D and constant V_D in different buffer solutions (Merck) with known $(\partial pH/\partial T)$. With Equation (12) the real $(\partial V_G/\partial T)$ can now be obtained and from this term $(\partial^2 V_G/\partial pH \partial T)$ was calculated as 0.23 mV/pH°C.
The drift behaviour was measured in several buffers (Merck pH = 5 and 9) but no change in drift rate could be detected. As shown before no change in pH sensitivity could be detected with time. Furthermore, the drift rate was measured by changing the temperature between 15 and 35°C in a Tris/HCl buffer. The change in drift rate with temperature is very small and is proportional to the normal drift rate at 25°C. Typical values are 0.2 mV/h at 25°C between 4th and 16th hour of the measurement and 0.025mV/h°C for $(\partial^2 V_G/\partial T \partial t)$.
No change with time could be observed for a change of temperature sensitivity, probably due to the determination limit (± 0.05 mV/°C).
A summary of the results is given in Table 2. No differences were observed between the two types of ISFETs for pH sensitivity and drift behaviour. The temperature sensitivity differed of course as can be seen from Equation (8).
In order to evaluate the validity of Equation (6) the following experiment was carried out. The outputs of the ISFET control system are periodically read by the microcomputer which calculates the pH according to Equation (6). The calculated pH is then compared with that given by the glass electrode. The results are presented in Fig. 9 where the drift compensation is shown and in Fig. 10 where the effect of pH and temperature is shown, the drift correction is, of course, included.
The effect of high potassium, sodium, calcium and lithium concentrations on the pH sensitivity is shown in Fig. 11 from which it can be seen that alumina has an excellent selectivity for hydrogen ions. The sensitivity was measured by titration of a 0.99 M MCl + 0.01 M MOH solution with HCl. Hysteresis was measured by determining the difference in V_G at pH = 7 going alternatively to pH 5 and 9 : the hysteresis was less then 1 mV at pH = 7.

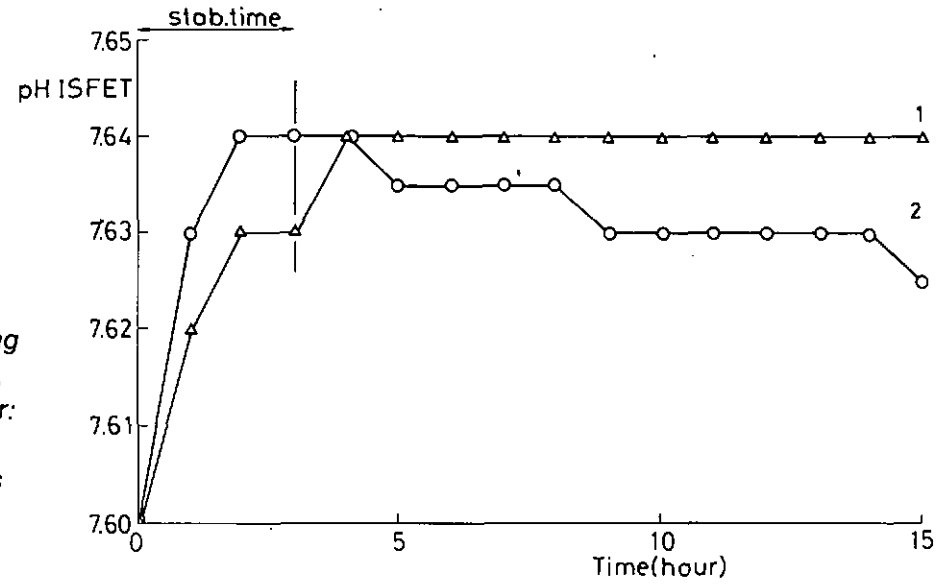

Fig. 9:
pH calculated from V_G for two ISFETs according to Eq. (6). Temp. 25°C, pH of the Tris/HCl buffer: 7.60 ± 0.005 as measured by the glass electrode.

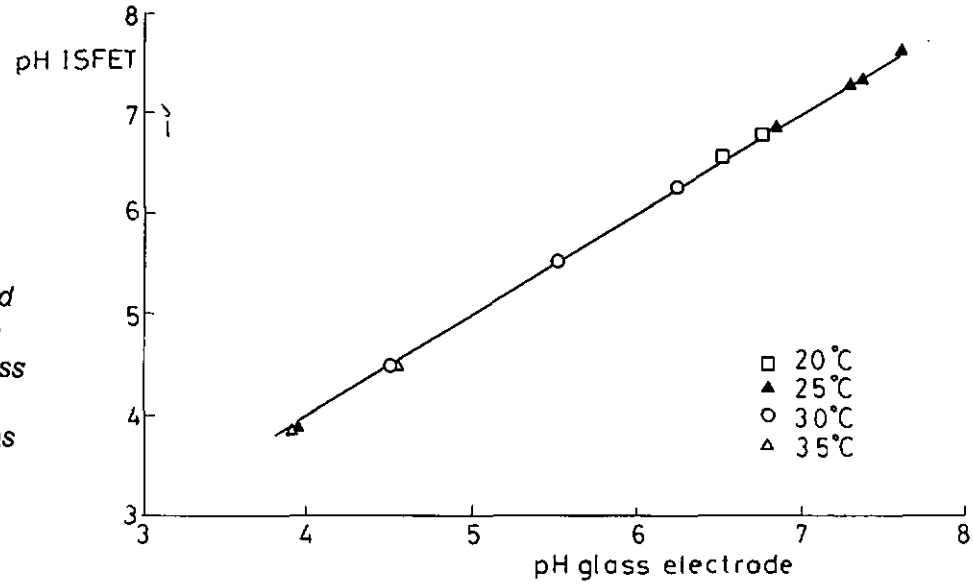

Fig. 10:
Comparison between pH-ISFET as calculated according to Equation (6) and the pH of a glass electrode. Measurement time was four hours. Slope = 1.006, n = 12.

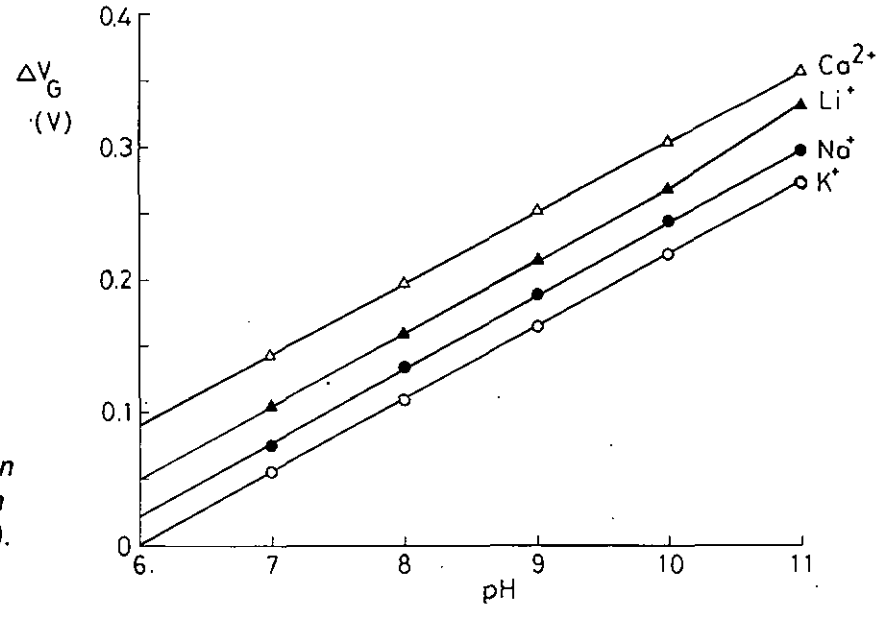

Fig. 11:
The effect of cations on the pH sensitivity of an ISFET(off-set arbitrary).

Table 2: *pH-ISFET and IGFET characteristics ($V_D = 0.5$ V, $I_D = 100$ μA)*

Coefficient	Value	Conditions
$\partial V_G/\partial pH$	53-57 mV/pH	Temp. 25°C pH 2-10
$\partial V_G/\partial T$	± 2 mV/°C	Tris/HCl Temp. range 15-35°C
*$\partial V_G/\partial t$	0.1-0.2 mV/h	Temp. 25°C Tris/HCl
*$\partial V_G/\partial t$	0.1-0.2 mV/h	IGFET with Al_2O_3/SiO_2
*$\partial V_G/\partial t$	10 μV/h	IGFET with SiO_2
$\partial^2 V_G/\partial T \partial PH$	0.20 - 0.25 mV/pH°C	Temp. range 15-35°C pH 3-10
$\partial^2 V_G/\partial pH \partial T$	0.20 - 0.25 mV/pH°C	Temp. range 15-35°C pH 3-10
$\partial^2 V_G/\partial T \partial t$	0.01 - 0.04 mV/h°C	Temp. range 15-35°C Tris/HCl

*drift rate was measured between 5th and 15th hour of third measurement

Discussion of the results

The various characteristics of the pH sensor can be summarized as follows: the pH sensitivity, observed in the pH range pH 3 to 12, has a value of approximately 55 mV/pH at 25°C, with a reproducibility of 0.5 mV/pH for a single ISFET, which is in the same order of magnitude as reported elsewhere [7,22]. Furthermore with Equation (7) and with pH_{pzc} assumed to be around pH = 8 [23], ß can be calculated and is equal fo ≈ 14. This high value of ß explains the high linearity and negligible sensitivity reduction around pH_{pzc}, as was pointed out by Bousse [16].

The femperature sensitivity depends nof only on the drain current but also on

the temperature dependence of the pH of the solution. By choosing a correct I_D the temperature dependence can be set below 1mV/°C. With its reproducibility of ± 0.05 mV/°C in combination with a reliable temperature sensor (accuracy ± 0.1 °C), accurate measurements are possible using Equation (6). From the temperature measurements b and $(\partial V_T^{MOST}/\partial T)$ can also be determined: b = -1 and $(\partial V_T^{MOST}/\partial T)$ = -2.6 mV/°C. These values are in agreement with those reported elsewhere [18,24] and therefore it can be concluded that Equations (8),(9) and (12) are valid.
The drift behaviour of an ISFET is mainly determined by the solid state part of the sensor after initial aging as can be seen from Fig. 6. After initial aging the drift reproducibility during subsequent exposures is within 0.1mV/h when using a linear approximation of the drift curve over short periods of time. The reproducibility is demonstrated in Fig. 9 where ISFET 1 is correct compensated and ISFET 2 somewhat undercompensated. This drift behaviour is comparable to that of the corresponding IGFET. Similar observations were reported by Ligtenberg [25]; he even extended the linear approximation with a logarithmic curve fitting method thereby reducing the initial stabilization period. Furthermore the drift behaviour of the IGFET indicates that the drift is mainly caused by the Al_2O_3 layer. Equation (11) can therefore be reduced to:

$$\frac{\partial V_G}{\partial t} = - \frac{\partial Q_{ins}}{C_{ins}\partial t} \tag{13}$$

A more detailed discussion of this drift phenomenon will be given in Chapter 4. For the second order terms the above discussed results confirm the observations : there is no pH dependence of the drift with time:

$$\frac{\partial^2 V_G}{\partial pH \partial t} = \frac{\partial}{\partial pH}\left(- \frac{\partial Q_{ins}}{C_{ins}\partial t}\right) = 0 \tag{14}$$

and there is no time dependence of the pH sensitivity, at least after initial aging $(\partial^2 V_G/\partial t \partial pH) = 0$.
Based on the assumption that the drift is caused by hydrogen tunneling, the temperature dependence of the drift should not exist or only be very small [26]. Our measurements show this clearly and they are supported by experiments on the drift behaviour of MIS capacitors where only a very small activation energy for the drift was found [25].

For the last second order terms straightforward derivations can be made based on Equations (7) and (9) resulting in

$$\frac{\partial^2 V_G}{\partial pH \partial T} = \frac{\partial}{\partial T}\left(2.303 \frac{kT}{q} \frac{\beta}{\beta+1}\right) = 2.303 \frac{k}{q}\left(\frac{\beta}{\beta+1} + \frac{T}{(\beta+1)^2} \frac{\partial \beta}{\partial T}\right) \tag{15}$$

and

$$\frac{\partial^2 V_G}{\partial T \partial pH} = \frac{\partial}{\partial pH} \cdot \frac{\partial \Psi_o}{\partial T} = 2.303 \frac{k}{q}\left(\frac{\beta}{\beta+1} + \frac{T}{(\beta+1)^2} \frac{\partial \beta}{\partial T}\right) \tag{16}$$

From the measured values of $(\partial^2 V_G/\partial pH \partial T)$ and $(\partial^2 V_G/\partial T \partial pH)$ which are both equal to 0.23 mV/pH°C it can be seen that the term $\partial\beta/\partial T$ is not negligible. A further examination of the data will give information on the enthalpies of the surface ionisation reactions of the Al_2O_3 surface (Chapter 5).
After the introduction of the above mentioned values into Equation (6) a very high accuracy of pH measurements can be achieved. The mean deviation between a glass electrode and a pH-ISFET is 0.01 pH (s.d. $= \pm 0.025$ over a pH range of pH 4 to pH 8, temperature range of 20 to 35 °C and a measurement time of 4 hours). These data are comparable to those mentioned by De Rooij [19] who reported an accuracy of $\pm$ 0.05 pH for similar conditions but using a more simple correction formula [27].

Conclusions

The function of an ISFET can be described by applying the theory of an IGFET in combination with the site-binding theory. Together with the data for the hysteresis and selectivity it has been demonstrated that the pH sensitive ISFET has a sufficient high accuracy for biomedical applications. For modified pH-ISFETs, similar equations as Equation (6) can be derived and, provided the same reproducibility and magnitude of the coefficients are found, a similar accuracy can be expected. Taking into consideration the physiological ranges and the required accuracy for intravascular applications, a potassium sensitive ISFET should be possible, but a sodium or calcium sensitive ISFET appears to be doubtful.

References

1. Middelhoek,S., *Ed. Sensors Actuators*, 1981-1986.
2. Ko,W.H., *IEEE Trans.Biomed.Eng.* **BME-33 no 2,** 153 (1986).
3. Nylander,C., *J.of Physics E, Scientific Instruments* **18 no** 9, 736 (1985).
4. Schepel,S.J., De Rooij,N.F., Koning,G., Oeseburg,B., Zijlstra,W.G., *Med. Eng. & Comp.* **22,** 6 (1984).
5. Kohama,A., Nakamura,Y., Nakamura,M., Yano,M., Shibatani,K., *Crit. Care Med.* **12 no 11,** 940 (1984).
6. McKinley,B.A., Houtchens,B.A., Janata,J., *IEEE Trans. Electron Devices* **ED-26,** 173 (1984).
7. Abe,H., Esahi,M., Matsuo,T., *IEEE Trans. Electron Devices* **ED-26,** 1939 (1979).
8. Akiyama,T., Ujihara,Y., Okabe,Y., Sugano,T., Niki,E., *IEEE Trans. Electron Devices* **ED-29,** 1936 (1982).
9. Esahi,M., Matsuo,T., *IEEE Trans. Biomed. Eng.* **BME-25,** 184 (1978).
10. Sibbald,A., *IEE Proceedings* **130,** 233 (1983).
11. Meier,P.C., Ammann,D., Osswald,H.F., Simon,W., *Med. Progr. Technol.* **5,** 1 (1977).
12. Decroux,M., Van den Vlekkert,H.H., De Rooij,N.F., *in* Proc. of the 2nd. Int. Meeting on Chemical Sensors, Bordeaux p.403,1986.
13. Smith,R.L., Scott,D.C., *IEEE. Trans. Biom.Eng.* **BME-33,** 83 (1986).
14. Smith,R.L., Huber,R.J., Janata,J., *Sensors Actuators* **5,** 127 (1984).
15. Janata,J., Huber,R.J., *in* Ion-Selective Electrodes in Analytical Chemistry (H Freiser, Ed.,Plenum Press), Vol. 2, p.107, 1980.
16. Bousse,L., *Thesis,* University of Twente, The Netherlands, 1982.
17. Leistiko.L., *Physica Scripta* **18,** 445 (1978).
18. Vadasz,L., Grove,A.S., *IEEE Trans. Electron Devices* **ED-13,** 1966 (1966).

19a. Bergveld,P., De Rooij,N.F., Nederlands Tijdschrift voor Natuurkunde, **A46 no 1,** 46 (1980).

19b. De Rooij,N.F., Haemmerli,A., *in* Proc. of the 6th General Conf. of the European Physical Society, Prague, p. 597, 1984.

20 Janata,J., Huber,R.J., *Ion-Selective Electrodes Rev.* **1,** 31 (1979).

21. Bousse,L., Bergveld,P., *Sensors Actuators* **6,** 65 (1984).
22. Dost,L., Van den Vlekkert,H.H., Koning,G., Feijen,J., *in* Proc. of the 4th. European Conf. on Biomaterials, Leuven, p.234, 1983.
23. Parks,G.A., *Chem. Reviews* 65, 177 (1965).
24. Sze,S.M., in Physics of Semiconductor Devices , 2nd ed., Wiley and Sons, p.452, 1984.
25. Ligtenberg,H.C.G., *Thesis,* University of Twente, The Netherlands, 1987.
26. Decroux,M., personal communications.
27. Van den Vlekkert,H.H., De Rooij,N.F., *Dutch patent application* no 8302964.

Chapter 3 Biomedical applications of ion-sensitive field effect transistors.

published in
Sensors and Actuators Vol. 14, No 2, pp.165-176 (1988)
A pH-ISFET and an integrated pH-pressure sensor with back-side contacts
H.H.van den Vlekkert, B.Kloeck, D.Prongue, J.Berthoud, B.Hu, N.F.de Rooij, E.Gilli, Ph.de Crousaz

presented at:
Transducers '87
1987, Tokyo, Japan
A pH-ISFET and an integrated pH-pressure sensor with back-side contacts
H.H.van den Vlekkert, B.Kloeck, D.Prongue, J.Berthoud, B.Hu, N.F.de Rooij, E.Gilli, Ph.de Crousaz
(Proc. Transducers '87, Tokyo, Japan, 1987 p.726)

Abstract

Solid state sensors are used more and more in the biomedical field for research as well as for monitoring devices. However these sensors are often not designed for a specific application which may inhibit a large scale application of these sensors. Specific sensors, however, can be fabricated when technologies for different sensor designs are integrated. As an example for such an approach, a pH-ISFET for dental plaque pH measurements and a combined pH-pressure sensor for oesophageal studies are presented. Both sensors show improved properties compared to systems which are frequently used for these investigations.

Introduction

Over the past years much attention has been paid to the application of solid state sensors in the biomedical field for research purposes as well as for monitoring devices [1,2]. However each application has its special requirements with respect to e.g. sensor characteristics, dimensions and encapsulation.
In this chapter it will be shown that technologies used for different sensor designs can be combined to fabricate sensors which are more suitable for the environment where they have to be used than present available sensors. In part 1, a pH-sensitive ISFET for the measurement of dental plaque pH will be discussed. In part 2, a combined pH-pressure sensor will be presented for oesophageal studies.

Part 1: pH-ISFET for dental plaque pH measurements

Introduction

Dental caries develops in susceptible teeth covered by dental plaque and in contact with dietary carbohydrates [3,4,5,6]. Efforts to reduce caries incidence include enamel protection, plaque elimination and diet modification. The intraoral cariogenicity test [7], when performed with human instead of bovine enamel, and intraoral plaque pH telemetry [8] seem the best methods available at present to evaluate in-vivo whether certain foods or food components are safe for teeth. Currently the intraoral plaque pH is normally measured by micro glass electrodes [8], initially developed by Graf and Mühlemann [9].
However these electrodes are fragile and have a slow response to pH changes. Both problems can be solved, as was shown previously by Igarashi *et al.* [10], by using a pH sensitive ISFET developed by Esashi and Matsuo [11]. Moreover, the surface of the sensor should be at the same level as the surface of the fragment of human enamel into which the sensor is built, especially when the interproximal plaque has to be investigated. This requirement can be fulfilled by the glass electrode but hardly with the afore-mentioned ISFET because of the encapsulation of the bonding wires which considerably increases the distance between the active part of the sensor and the surface of the human enamel. A solution for this problem is an ISFET with back-side contacts.
Over the years several techniques have been developed to create holes in a silicon wafer, e.g.:
1) spark erosion [12]
2) ion beam milling [13]
3) diffused Al column with thermal gradient to form conductive parts [14]
4) laser drilled holes [15]
The most simple method, however, which can even be used on wafer level, is the anisotropically etching of the silicon substrate with e.g. potassium hydroxide to form holes in the substrate leaving a thin membrane whose thickness can be controlled [16]. Electrical contact to the source and drain regions,

formed on the top side of the chip, can be made by diffusion of the drain/ source dopant through this thin silicon membrane.

Experimental

Fabrication process:

On a double side polished wafer (p-type 3-5 Ohmcm, orientation (100) and 380 μm thick) an oxide layer is grown of about 1.5 μm. Then the openings of the drain and source back-side contacts are made. The remaining oxide acts as a masking layer during the etching of the holes. The holes in the silicon are etched in a 40% KOH solution at 60°C. The water is etched until less then 10 μm of silicon is left, leaving a diaphragm of about 80 μm x 80 μm at the bottom of the hole. The etching is stopped by calculating the time needed for a specified depth. Unfortunately, the etch rate changes with time. But by careful operation this method allows thickness control of about 1 μm. Furt hermore this diaphragm varies in thickness according to the taper of the wafer, therefore the wafers are selected beforehand on a taper of less then 3 μm which leads to a diaphragm thickness between 6 and 10 μm over one wafer and from one wafer to another. The back-side openings are now enlarged and a phosphorous doped silicon dioxide layer is deposited by chemical vapor deposition (CVD). The increased dimension enhances a good step coverage of the CVD layer. After diffusion of the phosphorous into the silicon (junction depth about 8 μm), all oxide layers are etched away. Now a boron doped silicon dioxide layer is deposited on both sides of the wafer (channel stopper). The drain and source areas are now opened and a phosphorous doped silicon dioxide layer is deposited. After opening the gate area the gate oxide is grown (900 Å) and simultaneously the drain and source areas are formed together with the channel stopper at both sides of the wafer and the feed-through contacts are formed. Alumina is then deposited by CVD (600 Å) as pH sensitive layer. After opening the contact windows on the back-side, aluminum contacts are formed by lift-off and source and substrate are directly connected. Furthermore some MAOSFETs are made for on wafer testing. A diagram of the sensor is shown in Fig.1. The overall dimensions are 1.5 mm x 1.5 mm. Photographs of both sides of the sensor are shown in Fig.2.

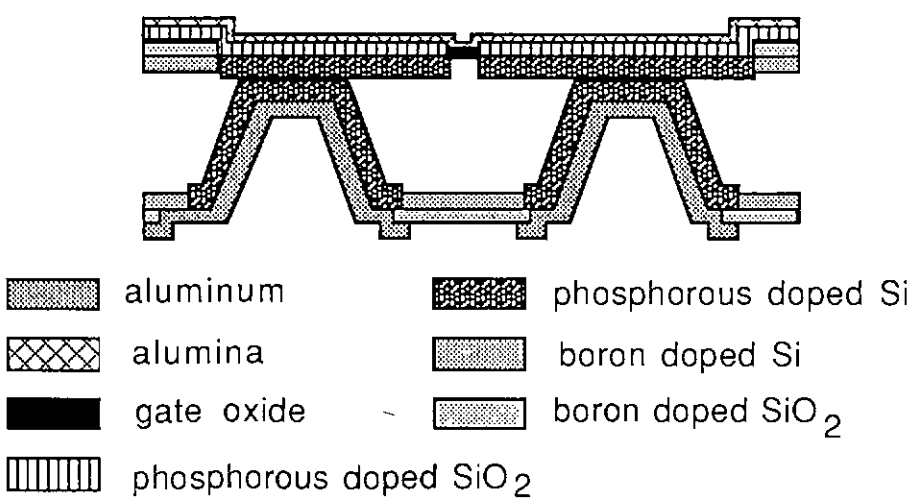

***Fig. 1:** Diagram of the sensor*

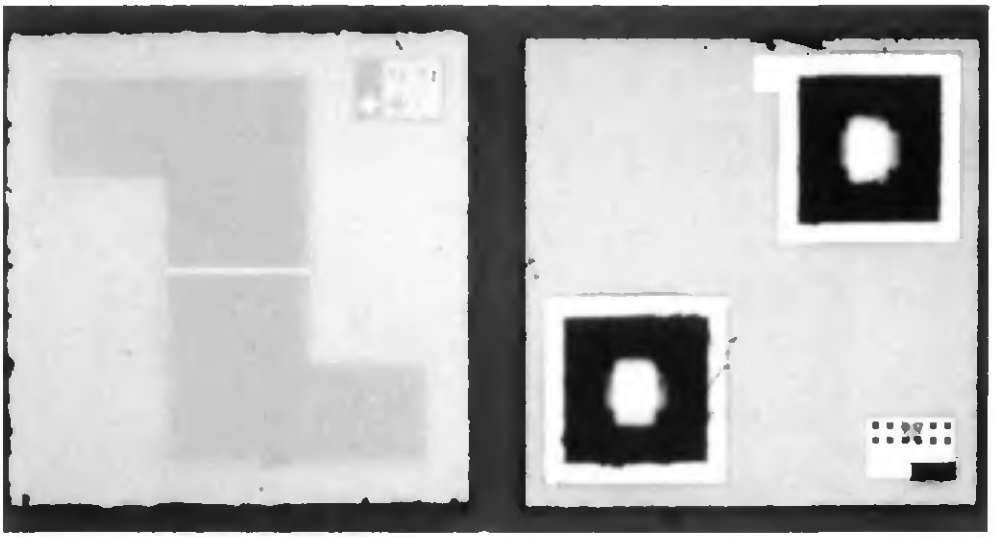

Fig. 2: *Top side (left) and back-side (right) of the sensor*

One of the major problems during the fabrication of the sensors was the photoresist deposition in the vicinity of the holes. By adjusting the spin speed during the photoresist deposition and by depositing two resist layers a reasonable patterning could be achieved, even around the holes. By reducing the thickness of the wafer to 300 μm the size of the holes could be reduced from 600 μm x 600 μm to 480 μm x 480 μm. Keeping the dimensions of the other masks the same, the photoresist deposition problems are decreased even further and excellent patterning is obtained as can be seen in Fig.2.

Characterization

After dicing the wafer, the sensor was mounted in a plexiglass holder. Then the contact wires were glued into the contact holes with a conductive epoxy. After the final isolation with epoxy the sensor characteristics were measured. Typical I_D-V_G curves are shown in Fig.3. In addition the pH-ISFETs were tested on drift behavior and pH sensitivity as was described elsewhere [17]. For the in-vivo dental plaque pH measurements the same encapsulation technique was used but instead of the plexiglass holder a piece of human enamel was used which could be mounted in a prosthesis. The first stage of the encapsulation is shown in Fig.4. The final assembly for the in-vivo test is shown in Fig.5 where it can be seen that the surface of the ISFET is nearly parallel with the human enamel. The results of typical in-vivo experiments are shown in Fig.6. The ISFET's were measured against a normal skin reference electrode mounted on the arm of the subject. A one point calibration was carried out in-vivo upon removal of the dental plaque after the experiment with a buffer pH 7 (Merck).

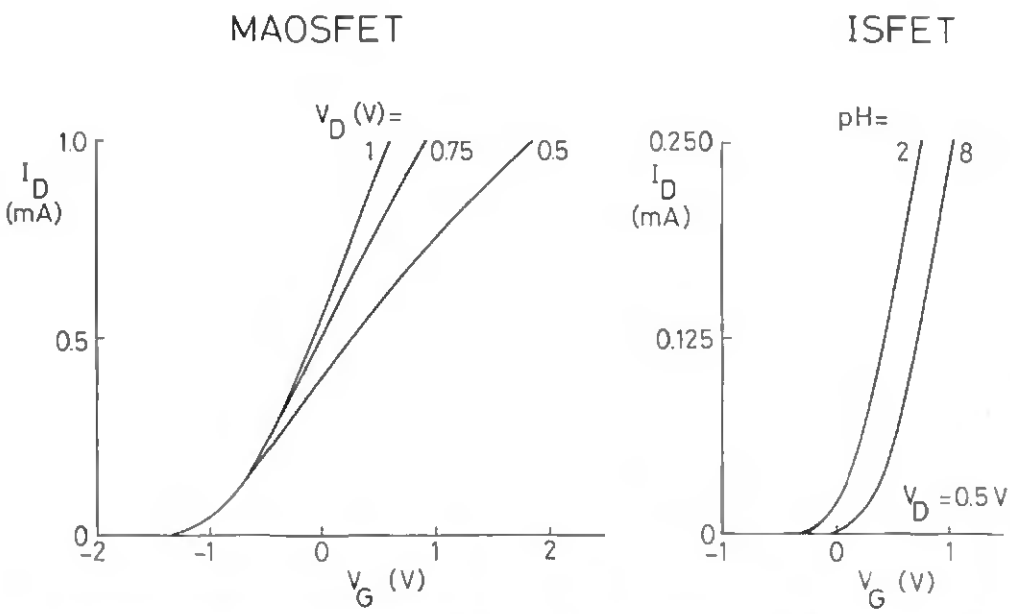

Fig. 3:
I_D-V_G characteristics of a back-side contacted MAOSFET and ISFET in different buffers.

Fig. 4:
Epoxy encapsulated pH-ISFET with back-side contacts

Fig. 5:
A back-side contacted pH-ISFET mounted in a partial denture

Results and discussion:

The in-vitro characteristics of the pH sensor are comparable to those for standard pH sensitive ISFETs with alumina as pH sensitive layer [17,18,19, Chapter 2]: a drift rate of less than 0.5 mV/h and a pH sensitivity of about 55 mV/pH. This means that under normal in-vivo testing conditions: (maximum test time 2 hours and a pH range from 3 to 8) an accuracy of 0.1 pH unit can be obtained, with a one point calibration. This implicates that for the interdental plaque pH measurements no compensation has to be carried out for the output signal of the ISFET amplifier as was described before [17, Chapter 2]. The first in-vivo results were satisfactory. The responses observed for the sucrose, sorbitol and urea rinses and paraffin chewing are similar to those reported before [8,9]. By the same token the life time of the sensor which depends mainly on the quality of the encapsulation has proven to be adequate (several weeks in the mouth). At the moment test sequences are being developed for the investigation of different foods and food components.

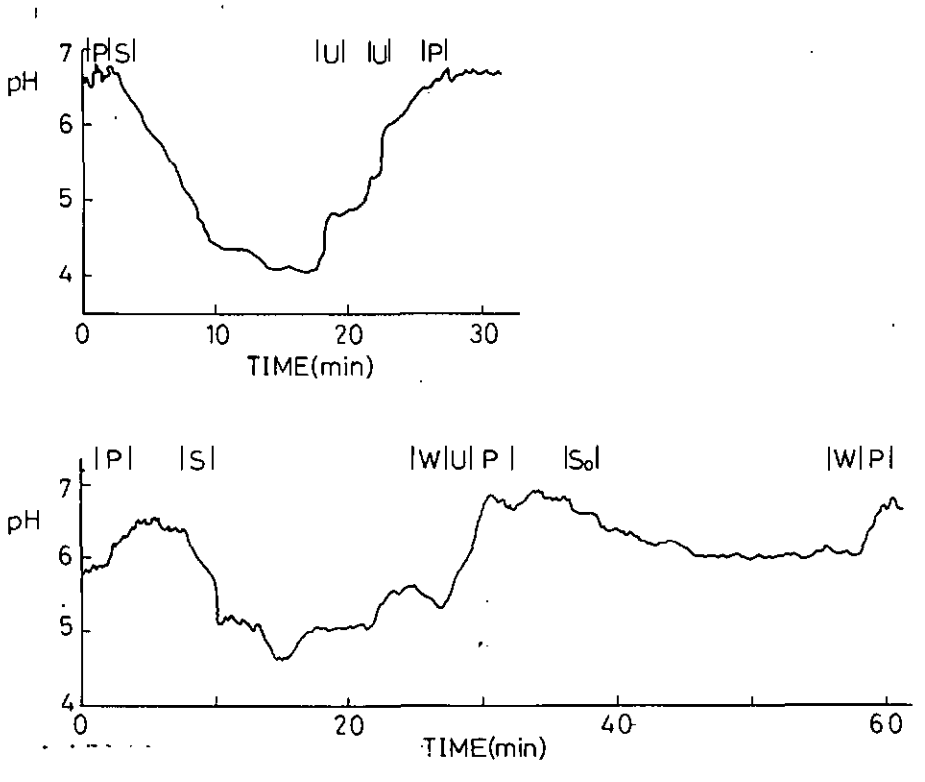

Fig. 6: *Two pH recordings of different 3-day interdental plaque pH*
P = paraffin chewing
S = rinse with 15 ml 10% sucrose
So = rinse with 15 ml 10% sorbitol
U = rinse with 15 ml 3% urea

Part 2: Combined pH-pressure sensor for oesophageal studies

Introduction

For the investigation of the oesophageal function oesophageal manometry and pH studies are of great value. Pressure measurements enable studies of the tonus of the upper and lower oesophageal peristalsis and the competence of the hiatal canal through which the oesophagus passes on its way to the stomach [20,21]. For the investigation of the gastro-oesophageal reflux [22,23] and of the oesophageal acid clearing capacity [24] the studies of pH can provide useful information. An optimal diagnosis could be obtained when both pressure and pH could be measured simultaneously and at different

sites. Another requirement is that the diameter of the sensor is as small as possible.
The first combined pressure-pH catheter used a pH glass electrode and a perfused multilumen catheter with external pressure transducer with a diameter of about 6 mm [25]. A similar catheter, with an antimony pH electrode, had a reduced diameter of 3 mm [26]. A more elegant solution was found by Huang and Wise [27] who developed a chip which combines a capacitive pressure transducer and a pH-ISFET. However this chip has some disadvantages: the necessity of on-chip signal processing circuitry for the pressure transducer, a rather large chip size (2.7 mm x 4.4 mm) and a pH sensitive layer on the FET (silicon nitride) which has a rather large drift in pH sensitivity as well as in absolute potential [18,28]. To circumvent these drawbacks a piezoresistive pressure transducer and an ISFET with alumina as pH sensitive material on the same chip were developed with dimensions of 1.5 mm x 4.0 mm.

Experimental

Fabrication:

The pressure sensor part consists of four diffused piezoresistors, disposed at the edges of a thin membrane and connected in a Wheatstone bridge configuration. The output voltage is proportional to the pressure on the membrane and to the applied voltage. For practical use of pressure sensors the output of the sensor should be standardized. Therefore it is important that the sensing element varies as little as possible from one sensor to another. Apart from the reproducibility of the four piezoresistors the sensitivity across one water depends mainly on the membrane thickness. The method discussed in Part 1 to fabricate thin silicon membranes is therefore not very suitable. A more reliable method to control the membrane thickness is the electrochemical etch-stop [29-32]. The principle of this method is that an epitaxial layer of n-type silicon is deposited on a p-type silicon substrate. The p-type substrate is etched and the etching can now be stopped at the epi-layer/substrate interface by applying a passivating potential to the epi-layer, positive with regard to the etch solution. The substrate epi-layer p/n junction is inversely biased and the substrate is electrically isolated from the epi-layer. No potential being imposed on the substrate, it will be at open circuit conditions and etched. When the etch front reaches the p/n junction, the applied potential passivates the n-type surface that becomes exposed to the etch solution and etching is stopped. The thickness of the remaining silicon membranes is thus defined exactly by the thickness of the epitaxial layer and not influenced by the taper of the wafer. The most effective way to execute this etch-stop method was developed by Kloeck *et al.* [33] who used the so-called four electrode method schematically shown in Fig.7.
In this set-up the working electrode is connected to the substrate, to impose a potential at which it is optimally etched. The etch rate depends on the applied potential as was described by Smith *et al.* [34]. Hereby the substrate potential becomes independent of the epi-layer potential. The reference electrode is used to measure and control exactly the substrate/solution (Si/KOH) potential and the counter electrode provides the current. The positive pole of the additional voltage supply is connected to the epi-layer to keep it at a passivating potential; the negative pole of this supply contacts the substrate, to take care of any current going through or by-passing the inversely biased p/n junction, preventing this current from interfering with etch behaviour of the p-substrate. Depending on the substrate/epitaxial layer interface, the additional voltage supply will deliver more or less current through the reversely

biased p/n junction. As soon as the junction is reached, the current increases to deliver the charge that is needed to form the passivating oxide. When the etch-stop process is finished, the current is again constant, since a new equilibrium state is established at the $Si/Si_xO_y/KOH$ interface [33].

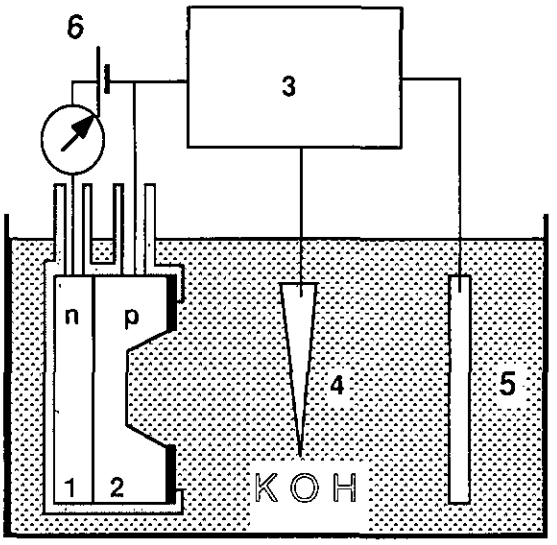

Fig. 7: *Four electrode set-up for electrochemical etch stop.*
1) n-type silicon epitaxial layer
2) p-type silicon substrate
3) three electrode potentiostat
4) calomel reference electrode
5) platinum counter electrode
6) additional voltage supply

The fabrication sequence to produce the combined sensor, including the four electrode method to fabricate the membranes for the pressure sensor is as follows:

1) dry oxidation (2000 Å)
2) patterning epi-layer (for ISFET back-contacts) (back)
3) etching epi-layer (40% KOH 60°C)
4) wet oxidation (1.4-1.8 μm)
5) fabrication of n^{++} contact on the epi-layer by means of CVD of a phosphorous doped SiO_2 layer (back)
6) opening of the ISFET back-contacts (back)
7) metallizaton of the n^{++} contact and the ISFET contacts(back)
8) opening of the pressure membrane area (top)
9) electrochemically etching of the substrate to form the "pressure" membrane (top).
10) removing metallization and etching of the ISFET contact holes till less then 10 μm is left (back)
11) patterning deep diffusion (back)
12) deposition of P-doped SiO_2 (CVD)(back)
13) diffusion of P into Si (8 μm) (back)
14) etching all oxides, reoxidation (2000 Å)
15) patterning resistors (back)
16) deposition B-doped SiO_2 (CVD)(back)

17) patterning channel stopper (back/top)
18) deposition B-doped SiO_2 (CVD)(back/top)
19) patterning drain/source regions(top)
20) deposition P-doped SiO_2 (top)
21) opening gate (top)
22) oxidation of the gate and diffusion of the boron to form the resistors and the channel stoppers and of phosphorous to form the drain/source areas.
23) deposition of alumina as pH sensitive layer (top)
24) definition of the contacts for the resistors and the ISFET drain/source/substrate contacts (back)
25) metallization of the contacts (back)
26) patterning of the contacts (back)

A cross section is shown in Fig.8 whereas in Fig.9 a photograph is shown of the finished sensor.

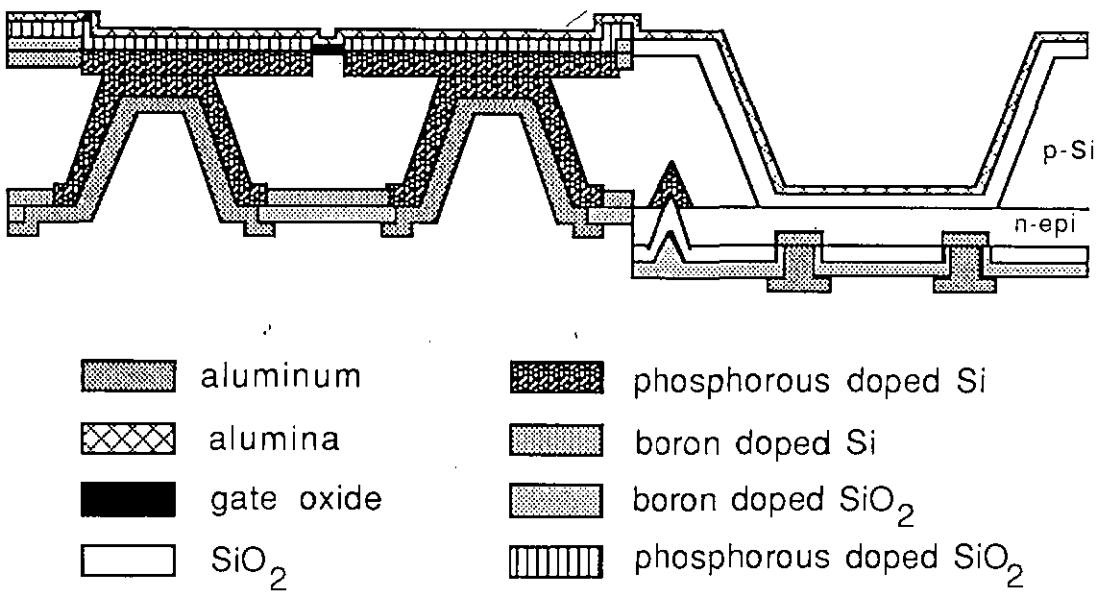

Fig. 8: *Schematic design of the combined pressure-pH sensor*

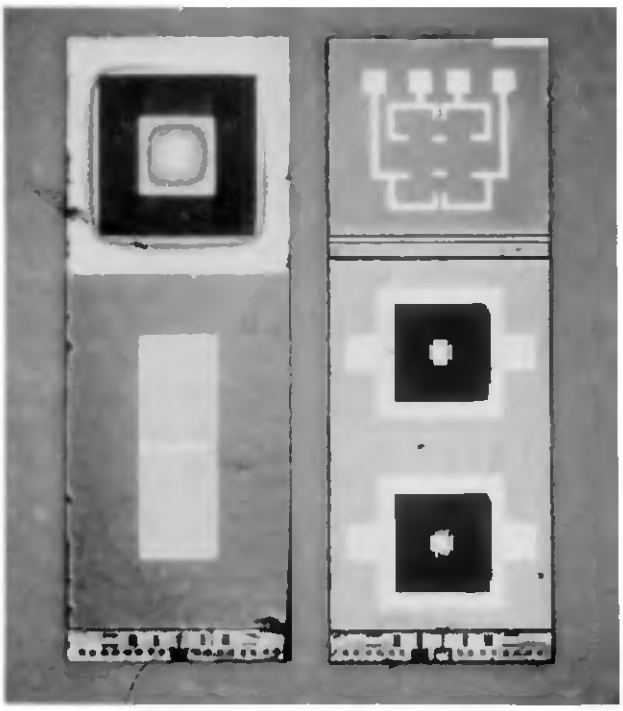

Fig. 9: *Top-side(left) and back-side(right) of the combined pressure-pH sensor.*

Characterization

In order to verify the etch-stop the membrane thicknesses over one wafer were measured mechanically with an inductive pin having a precision of 0.1 μm. The pressure sensitivity was measured on wafer to eliminate occasional encapsulation problems. A typical measurement is shown in Fig.10. The pH-ISFET was tested as was described in Part 1.

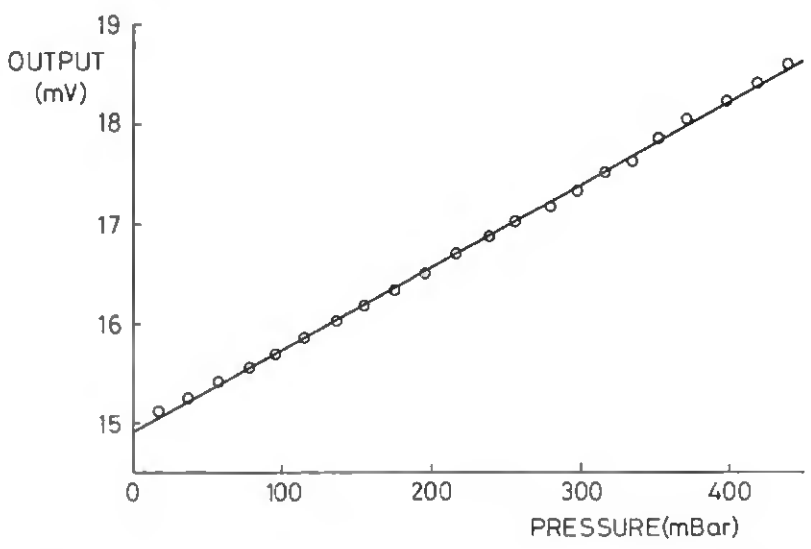

Fig. 10: *Pressure sensitivity of a combined pressure-pH sensor. slope: 8.4 mV/V/bar, offset = 14.9 mV.*

Results and discussion

Over one wafer the membrane thickness was 13.9 μm with a standard variation of 0.4 μm (n = 50) which is comparable to those found for similar pressure transducers [33]. The measured pressure sensitivity of 8 mV/V/bar is in agreement with a computer simulation with SENSIM [35]: 7.5 mV/V/bar. This sensitivity can be improved by decreasing the thickness of the epitaxial layer. The output of the pressure sensors varied considerably over one wafer due to differences in resistance values of the piezoresistors (1 to 2 kOhm) although no significant difference could be observed between these resistors on one sensor. These differences were mainly caused by the production method of the resistors. When using the ion implantation technique for the formation of the doped areas the production process could be simplified and the variation over one wafer of the pressure sensitivity could be reduced to less then 10% [33]. The pH-ISFET characteristics were the same as described in Part 1. Therefore a high accuracy can be obtained which can even be improved by using the compensation method described in Chapter 2 and reference [17].

Conclusions

It is shown that the integration of technologies used for different sensor designs can result in application specific sensors. The pH-ISFET with back-side contacts and the pH-pressure sensor show for their specific applications improved properties compared to conventional sensors used for these special applications.

The pH sensitive ISFET with back-side contacts has a sufficiently high accuracy and life time for the measurement of dental plaque pH. The first in-vivo results are in excellent agreement with similar experiments. The easy encapsulation and the one point calibration has been proven to be very helpful when these sensors are used on a regular basis. The effect of the position of the sensitive area relative to the human enamel into which it is mounted is at the moment under investigation.

The small dimensions of the combined pH-pressure sensor allow a catheter diameter of 2 mm. The excellent reproducibility of the pressure membrane when combined with ion-implanted resistors will result in high reproducibility of the pressure sensor output. The combination on one chip will reduce the encapsulation costs and more measuring sites are feasible.

References

1. Ko,W.H., *IEEE Trans. Biomed. Eng.* **BME-33 no 2,** 153 (1986)
2. Engels,J.M.L., Kuypers,M.H., *J.Phys..E: Sci.Instrum.* **16,** 987 (1983).
3. Kite,O.W., Shaw,J.H., Sognnaes,R.F., *J.Nutr.* **42,** 89 (1950).
4. Haldi,J., Wynn, W., Shaw,J.H., Sognnaes,R.F., *J.Nutr.* **49,** 295 (1953).
5. Bowen,W.H., Amsbaugh,S.M., Monell-Torens,S., Brunell,J., Kuzmiak-Jones,H., Cole,M.F., *J.Am.Dent. Ass.* **100,** 677 (1980).
6. Orland,F.J., Blayney,J.R., Harrison,R.W., Reyniers,J.A., Trexler,P.C., Wagner,M., Gordon,H.A., Luckey,T.D., *J.Dent. Res.* 33, 147 (1954).
7. Bodden,R., Koulourides,T.,Keller,S., Manson-Hing,I., *J. Dent Res.* 53: spec.iss., 205 (1974).
8. Imfeld,T.N., *in* Monographs in Oral Science **Vol. 11,** (H.M.Myers ed. Karger A.G. Basel), 1983.
9. Graf,H., Mühlemann,H., *Helv.Odont.Acta* **10,** 94 (1966).
10. Igarashi,K., Kamiyama,K., Yamada,T., *Archs. Oral.Biol.* **26,** 203(1981).
11. Esashi,M., Matsuo,T., *IEEE Biomed.Eng.* **BME-25,** 184 (1978).
12. Van Osenbrugge,C., *Philipps Tech. Rev.* **30,** 195 (1969).
13. Bollinger,D.,Fink,R., *Solid State Technol.* **25,** 79 (1980).
14. Anthony,T., Cline,H., *J.Appl.Phys.* **49,** 2777 (1978).
15. Ehrlich,D.et.al., *IEEE Trans.Components, Hybrids, Manuf. Technol.,* **CHMT-5 no 4,** 520 (1982).
16. Petersen,K.E., *Proc.of the IEEE* **70 no 5,** 420 (1982).
17. Van den Vlekkert,H.H., Arnoux,Ch., Lomazzi,Ph., De Rooij,N.F., *in* Proc. 2nd. Int.Meeting on Chemical Sensors, Bordeaux, p. 462, 1986.
18. Abe,H., Esashi,M., Matsuo,T., *IEEE Trans.Electron Devices* **ED-26 no 12,** 1939 (1979).
19. Ligtenberg,H.C.G., Van den Vlekkert,H.H., Koning,G., *in* Sensors and Actuators (P.Bergveld, Ed., Kluwer,Deventer) p. 123, 1984.
20. Kramer,P., Ingelfinger,F.J., *Am.J.Med.* **7,** 168 (1949).
21. Ellis,F.H., *Ann. Thorac.Surg.* **12,** 446 (1971).
22. Dodds,W.J., *Arch.Int.Med.* **136,** 515 (1976).
23. DeMeester,T.R., Wang,I.C., Wernely,J.A., Pellegrini,C.A., Little,A.G., Klementschitsch,P., Johnson,L.F., Skinner,D.B., *J.Thorac. and Cardiovas.Surg.* **79,** 656 (1980).
24. Booth,D.J., Kemmerer,W.T., Skinner,D.B., *Arch.Surg.* **96,** 731 (1968).
25. Orringer,M.B., Lee,R., Sloan,H., *Ann.Thoracic.Surg.* **26,** 581 (1978).
26. Ask,P., Edwall,G., Tibbling,G., *Med.&Biol.Eng.&Comp.* **19,** 443 (1981).
27. Huang,J.C.-M., Wise,K.D., *Int.Elec.Dev.Meeting Tech.Digest* p.316, 1982.
28. Chauvet,F., Amari,A., *Sensors Actuators* **6,** 255 (1984).
29. Waggener,H.A., *Bell Systems Tech.Journal* **49 no 3,** 473 (1970).
30. Hirata,M., Suwazono,S., Tanigawa,H., *in* Proc.Transducers '85, Philadelphia, USA, p.287, 1985.
31. Kim,S.-C., Wise,K.D., *IEEE Trans.Electron Devices* **ED-30 no 7,** 802 (1983).
32. Sarro,P.M., Van Herwaarden,A.W., *J.Electrochem.Soc.* **133 no 8,** 1724 (1986).
33. Kloeck,B., De Rooij,N.F., *in* Proc. Transducers '87, Tokyo, Japan, p.116, 1987.
34. Smith,R.L., Kloeck,B., De Rooij,N.F., Collins,S.D., to be published.
35. Lee,K.W., Wise,K.D., *IEEE Trans.Electron Devices* **ED-29,** 64 (1982).

Chapter 4 Drift phenomena of Al_2O_3

Abstract

One of the main problems, which so far have prevented the commercialization of pH-ISFETs, is their drift behavior. Until now different materials have been used as pH sensitive layer, from which alumina seems to be a very suitable material with regard to stability and, for biomedical applications, blood compatibility
In this chapter a method will be outlined by which the drift rate of alumina can be reduced from 0.1 - 0.2 mV/h to ~50 μV/h. This reduction in drift rate implicates that the accuracy of pH-ISFETs is improved to within 0.01 pH over a measuring period of at least 5 hours. Although no conclusive data are yet available, the origin of the drift of alumina can probably be attributed to diffusion of positive charges (probably hydrogen or aluminum ions) at the grain boundaries of the alumina.

Introduction

One of the main problems encountered with ISFETs is their base line drift. This base line drift influences the accuracy of the measurement and can therefore prevent the application of ISFETs, especially in the biomedical field where a very high accuracy is demanded and recalibrations have to be avoided.
Over the past years many different materials were investigated as pH sensitive layers. However, comparative data on base line drift are scarce and are difficult to compare due to different fabrication methods, measuring techniques and definition of base line drift.
Abe *et al.* [1] have compared the properties of SiO_2, Si_3N_4 and Al_2O_3. They found that SiO_2 was not stable at all and that Al_2O_3 has a better stability than Si_3N_4; Si_3N_4 has a drift rate of about 0.6 mV/h and Al_2O_3 of about 0.3 mV/h, after 10 hours stabilisation.
Akiyama *et al.* [2] reported a long term drift rate of 8-20 mV/h for SiO_2 in an alkaline solution but they did not give data for their Al_2O_3 and Ta_2O_5 layers. Matsuo *et al.* [3] compared SiO_2, Si_3N_4, Al_2O_3 and Ta_2O_5 where they found for Si_3N_4 a drift rate of 1 mV/h and for Al_2O_3 and Ta_2O_5 a drift rate of 0.1-0.2 mV/h, after 1000 min of operation in pH 7. The best results to date have been reported by Klein and Kuisl [4] for Ta_2O_5 who found drift rates of less than 0.1 mV/day. Although Al_2O_3 and Ta_2O_5 seem to be the most suitable materials for the fabrication of pH-ISFETs, Si_3N_4 is the most widely used. Chauvet *et al.* [5] have recently reported the influence of fabrication methods on the drift behaviour of Si_3N_4. They reported an improved drift behaviour when the NH_3/SiH_2Cl_2 ratio is optimized during the Si_3N_4 deposition. The best value they give is 0.05 pH/day (about 0.1 mV/h). The variation of the drift rates for Si_3N_4, as reported in the literature, can therefore probably be ascribed to the differences in fabrication. The data for Al_2O_3 seem to be the most independent of fabrication and measurement techniques.
The mechanism of the drift is not very clear and probably different for each material. The drift behaviour for SiO_2 can be described by the theory of buried sites at the periphery of the electrolyte interface as far as chemical drift is concerned [6].
In a recent study, Ligtenberg [7] showed that the drift of ISFETs with alumina as pH sensitive layer was caused by solid state effects that are present both in the ISFET and MAOSFET (metal-alumina-silicondioxide-field-effect-transistor) structure. He investigated therefore further MAOS capacitor structures which were subjected to bias temperature time stress experiments (BTTS) [8]. Based on the results of these experiments he claimed that the drift phenomenon in alumina ISFETs can be attributed to solid state bulk polarization of the alumina layer.

In a similar study Arnoux *et al.* [9] confirmed that the base line drift of ISFETs is mainly a solid state effect due to the alumina layer. The drift of MAOS capacitors was also investigated with repetitive bias temperature time stress measurements. The results of their experiments showed that the baseline drift is a linear function ot the stress voltage, is proportional to the logarithm of time and is slightly thermally activated with a small activation energy (E_a=167meV). These results are in perfect agreement with those found by Ligtenberg for his measurements. Besides these measurements they analysed the structure of the Al_2O_3 layer. They showed that this layer was polycrystalline with a structure of γ-Al_2O_3 and that the grain size was 30-50 nm. The γ-structure ot Al_2O_3 is formed by a face centered cubic closed-packed lattice(spinel structure) of oxygen atoms where aluminum ions do not completely fill up all the interstitial spaces. The baseline drift of the flatband voltage was then interpreted as a diffusion of positive charges through the Al_2O_3 layer. The small activation energy is consistent with this theory. In the alumina layer, hydrogen, which is used during the fabrication process [10], could therefore be responsible tor the drift. To verify this assumption they varied the hydrogen concentration during the Al_2O_3 deposition and the same BTTS measurements were carried out. The long term drift showed a linear dependence on the $[H_2]/[AlBr_3]$ ratio. Another possible explanation of the long term instability of these layers is given by Senturia [11]. He reported a remarkable spiral peel effect in a CVD aluminum oxide layer, which can be explained by a chemical attack of the intertace between the film and the substrate through a pinhole defect which leads to a crack. This crack is then followed by the spiralling ribbon-shaped peeling of the film as it debonds from the surface.
Although a considerable amount of research was undertaken to analyse the drift problem of alumina, until now this has not resulted in a reduced drift rate of the ISFETs with such a layer. In this chapter a method will be presented on how to reduce the drift rate of alumina without pretending that the origin of this decrease is fully understood.

Experimental

The ISFETs, used during the drift measurements, are described in chapter 2 (type 1) and chapter 6. At first glance the only important difference between these two designs is the encapsulation method. Type 1 is encapsulated with epoxy (EP), and the ISFET in chapter 6 is encapsulated with glass (GL). MAOSFETs (M) of both types were also tested; these were always encapsulated with epoxy.
The sensors were measured with a specially designed electronic control system which operates the device at constant drain current (I_D) and constant drain to source voltage (V_D) and measures the reterence electrode to source potential (V_G) (see also chapter 2).

In order to be able to compare the different sensors, the following conditions were maintained tor all experiments:

For MAOSFETs:
- Temperature = 25 °C ± 0.1 °C
- V_D = 0.5 V, I_D = 100 μA.
- Drift rate is defined as the drift rate between 5th and 15th hour of the measurement.({V_G at 15th h -V_G at 5th }/10)
- Each sensor was repeatedly measured with an interval of at least 1 week, and was stored in ambient atmosphere.

and for ISFETs the additional conditions:
- Tris/HCl solution: pH ≅ 7.60 (controlled with a pH-glass electrode and, when necessary, the data were corrected for changes in pH).
- Ag/AgCl double junction reference electrode, with as inner solution saturated KCl and as outer solution Tris/HCl was used.

Results and discussion

The results are summarized in Table 1. Also included are some measurements performed on pCl-ISFETs (described in detail in chapter 6).
As can be seen from Table 1 there is no significant difference in drift rates between ISFETs and MAOSFETs of type 1 (EP and M-EP), which is comparable to the results reported previously [7,9,Ch.2]. Furthermore the absolute value of the drift rate, between 0.1 and 0.2 mV/h of the second and third measurement, is comparable to those reported by e.g. Matsuo [3].
For the glass encapsulated sensors there is no difference in drift rate between the MAOSFETs, ISFETs and pCl-ISFETs, which confirms once more that the drift is not related to the insulator/electrolyte interface (AgCl/electrolyte or Al_2O_3/electrolyte). However there is a remarkable difference in amplitude of the drift rate between the two sensor types. The drift rate is reduced with a factor 3 to 4 for the glass encapsulated devices. It should be noted that at a drift rate of less then 0.1 mV/h, the accuracy of the drift measurements decreases rapidly because of the increasing importance of small changes in temperature, pH and reference electrode potential of the solution. A change, for example, of 0.01 pH of the solution, with a sensitivity of 50 mV/pH for the ISFET, is over a period of 10 hours already a change of 0.05 mV/h in the calculated drift rate.

Table 1: *Drift measurements of ISFETs and MAOSFETs.*

Type	drift rate (mV/h)		
measurement*	1	2	3
M-EP	0.25	0.18	0.13
M-EP	0.35	0.30	0.21
M-EP	0.26	0.19	0.10
M-EP	-	0.37	0.19
M-EP	0.23	0.38	0.23
EP	0.24	0.15	0.04
EP	0.45	0.21	0.12
EP	0.45	0.16	0.06
EP	0.31	0.10	0.13
EP	0.30	0.11	0.16
EP	0.30	0.20	0.19
M-GL	0.05	0.05	0.02
M-GL	0.03	0.04	0.03
GL	0.10	0.05	0.07
GL	0.36	0.08	0.06
GL	0.10	0.02	0.05
GL	0.35	0.10	
GL	0.10	0.09	
GL-AgCl-ISFET	0.11	0.05	0.04
GL-AgCl-ISFET	0.07	0.05	

*Time interval between measurements is one week.

Apart from the drift rate, another difference was noted between the epoxy and glass encapsulated sensors: the difference in threshold voltage (V_T) between the MAOSFETs and ISFETs. For the epoxy encapsulated sensors the difference was about 1 V which is comparable to the value given by Bousse [12]. However for the glass encapsulated sensors the difference was much greater: 1.8 V. This shift indicates that the alumina layer is not identical for the different sensors.

An explanation for the observed differences could be that the deposition

circumstances for both layers were not identical. Normally, however, no differences in drift behaviour from different depositions have been observed. The method of encapsulation seems not to play a role either, because previous changes in encapsulation methods did not yield a difference in drift behavior (chapter 2 and 3).
The only remaining difference between the two different sensor types is the method of fabrication during which the alumina layer is submitted to different anneal steps and covered with metals. In Type 1 ISFETs, the alumina layer is temporarily covered with aluminum (for the fabrication of the contacts and metal gate for the MAOSFETs) which is etched away. In order to get good contacts the aluminum is afterwards annealed at 450 °C under nitrogen during 15 min.
The sensors which are glass encapsulated have aluminum on top of the alumina, which is annealed two times before it is etched away. The first anneal is equal to the type 1 anneal for the aluminum contacts (450 °C under nitrogen during 15 min). The second one takes place during the anodic bonding: 10 min at 400 °C under ambient atmosphere (during which 600 V is applied for 30 seconds (chapter 6). After the anodic bonding the aluminum layer is etched away in a phosphoric acid/nitric acid/acetic acid mixture at 55 to 60 °C (whereas the aluminum for type 1 is etched at 42 °C). For the pCl-ISFET the alumina layer is covered with aluminum, which is etched away (similar as for type 1), and then covered with a Ti/Ag/Ti/Al layer. This layer is then annealed during the anodic bonding (10 min at 400 °C under ambient atmosphere).
In order to investigate the effect of the different annealing and etching steps the MAOSFETs of type 1 were either transformed into ISFETs by the same etching procedure (ETCH), as used for glass encapsulated sensors or were subjected to the additional anneal before their transformation into ISFETs (ANNEAL/ETCH). The results of the drift tests on these devices are summarized in Table 2.

Table 2: *Drift measurements of MAOSFETs, transformed into ISFETs, of Type 1*

Type	drift rate (mV/h)		
measurement*	1	2	3
ETCH	0.30	0.10	0.15
ETCH	0.85	0.16	0.10
ANNEAL/ETCH	0.07	-	-
ANNEAL/ETCH	1.85	0.06	0.01
ANNEAL/ETCH	0.10	0.05	0.07

*Time interval between measurements is one week

Furthermore the change in threshold voltage for both types is not 1 V (see difference MAOSFET/ISFET type 1) but also about 1.8 V. It should be noted that there was no significant shift in threshold voltage for the MAOSFETs themselves upon this anneal (less then 100 mV). The large differences in drift rates for the first measurements can be explained by the etching procedure. A large over etch has the same effect as aging [Ch.2]. Some MAOSFETs of the second type were also tested without having had the anneal of 10 min at 400 °C under ambient atmosphere. They had a drift rate three times higher, compared to the same sensors with this anneal.

In order to investigate if there was a change in composition of the alumina layer due to the different annealing steps, Auger and SIMS techniques were used. However no difference in layer composition was observed. In Table 3 all results are summarized.

Table 3: *Summary of the results*

Production step on gate area	EP (Ch.2 type 1)		GL (Ch.6)	
	MAOSFET	ISFET	MAOSFET	ISFET
gate oxidation	x	x	x	x
alumina deposition	x	x	x	x
CVD SiO_2	x	x	x	x
etch CVD SiO_2	x	x	x	x
aluminum deposition	x	x	x	x
etch aluminum	-	x	-	-
anneal 450°,15 min,N_2	x	x	x	x
encapsulation epoxy	x	x	x	-
mean drift rate	0.23	0.13	0.11	-
mean V_T	-1.1	-0.1	-0.75	-0.75
etch aluminum	x*	-	-	-
mean drift rate	0.13	-	-	-
mean V_T	0.7	-	-	-
anodic bonding	-	-	-	x
anneal 400°C,10min,ambient	x*	-	x*	x
encapsulation epoxy	-	-	x	-
mean V_T	-1.1	-	-0.75	-0.35
mean drift rate	-	-	0.04	-
etch aluminum	x	-	-	x
encapsulation epoxy	x	-	-	-
mean drift rate	0.05	-	-	0.06
mean V_T	0.7	-	-	1.05

mean drift rate:
mean value of all 2nd and 3th measurements (mV/h)
mean V_T : mean value of V_G at $I_D = 1$ μA (V).
(for ISFETs in Tris/HCl with pH = 7.6)

x = executed
– = not executed
* = new MAOSFETs (after first anneal)

The following conclusions can be drawn from Table 3:
1) there is no difference between MAOSFET and ISFET drift rates of the same type
2) the metal anneal at 450 °C under nitrogen has no influence on the drift rate
3) the anneal of 10 min at 400 °C under ambient atmosphere reduces the drift rate with a factor 3 to 4
4) there is an increased shift in V_T upon annealing with aluminum on the gate for the ISFETs
5) No substantial change in chemical composition of the alumina layer is observed upon annealing

From the above results it can be seen that the drift is a solid state effect and that the threshold voltage shift is due to changes of the solution/insulator interface. Based on the equation for the drift rate, derived in chapter 2, the reduction of the drift rate, upon the anneal treatment, has to be explained by a reduction of mobile positive charges in the insulator layer. However the nature of these positive charges is not clear.

In contrast to our results and those of Arnoux [9], Ligtenberg [7] found that O_2, N_2 and H_2 anneal at 900 °C did not have benificial effects on the drift rate and that the ISFET drift should depend on V_G. From his point of view a positive V_G should then result in a negative drift, which is not confirmed by our results. Arnoux suggested that hydrogen, trapped in the alumina layer during deposition, could be responsible for the drift. However it seems unlikely that the anneal at 400 °C during 10 minutes reduces the hydrogen content in the alumina layer. As a hypothesis however, claiming that the hydrogen transport takes place mainly at the grain boundaries of the alumina, a modification of these boundaries, especially at the surface, could easily result in a diminished rate of diffusion and thereby cause a reduction of the drift rate. Although no alteration of the alumina layer, covered with aluminum, could be observed upon annealing (under ambient atmosphere at 400 °C, 10 min), the formation of TiO_x was observed upon annealing of alumina covered with titanium (process for the pCl-ISFETs, Ch.6), indicating that changes of the alumina layer can occur during the anneal. Furthermore the effect of hydrogen content, during fabrication of the alumina layer, on the drift rate, as found by Arnoux, could then be explained by a change of the grain boundaries.
For the increased shift in threshold voltage upon annealing, the explanation should be sought in variation of the potential difference between the insulator and the bulk of the solution Ψ_o and the surface dipole potential at the solution/insulator interface χ. A variation of Ψ_o seems unlikely because no change in pH-sensitivity was observed. The term χ is an unknown quantity and has been subject to much discussion in the literature, based on very little experimental evidence, and that mainly of the silicon dioxide/electrolyte interface, as was discussed by Bousse [12].

Conclusions

It has been shown that the drift rate of pH sensitive ISFETs, with alumina as pH sensitive layer, can be reduced, by a simple anneal treatment, to a very low level, typical about 50 μV/h. Measurements over at least 5 hours are now possible, within an accuracy of 0.01 pH unit, without the neccesity for correction for the drift rate. It should be noted that the drift rate values approach the accuracy of the measurement set-up, especially for the pH-ISFETs.

A possible explanation for the drift could be the diffusion of hydrogen at the grain boundaries of the alumina layer. To verify this hypothesis a more detailed research of the alumina layer and the influence of the anneal treatment is neccesary and could lead to even lower drift rates and a better understanding of the surface properties of the alumina layer.

References

1. Abe,H., Esashi,M., Matsuo,T., *IEEE Trans. Electron Devices* **ED-26,** 1939 (1979).
2. Akiyama, T., Ujihara,Y., Okabe,Y., Sugano,T., Niki,E., *IEEE Trans. Electron Devices* **ED-29,** 1936 (1982).
3. Matsuo,T., Esashi,M., *Sensors Actuators* **1,** 77 (1981).
4. Klein,M., Kuisl,M., *VDI-Berichte* **509,** 275 (1984).
5. Chauvet,F., Amari,A., Martinez,A., *Sensors Actuators* **6,** 255 (1984).
6. Bousse,L., Bergveld,P., *Sensors Actuators* **6,** 65 (1984).
7. Ligtenberg,H.C.G., *Thesis* University of Twente, The Netherlands,1987.
8. Snow,E.H., Deal.B.E., *J.Elecrochem.Soc* **113,** p.263 (1966).
9. Arnoux,Ch., Buser,R., Decroux,M., Van den Vlekkert,H.H., De Rooij,N.F., *in* Proc. Transducers '87, Tokyo, Japan, p.751, 1987.
10. Stephany,F., *Thesis* RWTH-Aachen FRG, 1979.
11. Senturia,S.D., *in* Proc. Transducers '87, Tokyo, Japan, p.11, 1987.
12. Bousse,L., *Thesis* University of Twente, The Netherlands, 1982.

Chapter 5 The temperature dependence of the surface potential at the Al_2O_3/electrolyte interface

accepted for publication in :
J. Colloid and Interface Science

The temperature dependence of the surface potential at the Al_2O_3/electrolyte interface

H.H.van den Vlekkert, L.Bousse, N.F.de Rooij

Abstract

Electrolyte/insulator/silicon structures can be used to measure the variations of surface potential at the insulator/electrolyte interface. We have used this method to measure the temperature dependence of the surface potential Ψ_o at the γ-Al_2O_3 electrolyte interface. By applying the surface site dissociation model, this measurement can be interpreted in terms of enthalpy changes of the ionization reactions of OH surface sites. As this theory predicts, it is found that $\partial\Psi_o/\partial T$ varies linearly with pH. From the slope and the intercept of this experimental line, the following enthalpies can be deduced:
$\Delta H_{a1} = +34.8 \pm 2.0$ kJ/mole, for the dissociation of a proton from an SOH_2^+ site, and $\Delta H_{a2} = +54.0 \pm 2.0$ kJ/mole for the dissociation of a proton from an SOH site. These results imply that proton dissociaton on Al_2O_3 surfaces is endothermic, and are in reasonable agreement with those obtained by Griffiths and Furstenau with a colloidal suspension.

Introduction

Measurements on electrolyte/insulator/silicon (EIS) structures open up the possibility of measuring the variations of the surface potential at the insulator/electrolyte interface. The possible applications of such measurements to colloid science were first pointed out by Schenck [1]. The devices most commonly used are the ion-sensitive field-effect transistors (ISFETs) originally described by Bergveld [2,3]. It is also possible to use electrolyte/insulator/silicon (EIS) capacitors (which are simpler to fabricate) for these measurements [4,5,6].
In all these devices the variations of the flat-band voltage or of the threshold voltage are determined; this is equal to the variations of Ψ_o in a given experimental arrangement [7]. This method of measuring Ψ_o can be used in principle for all oxides, including those which are good insulators. Conceptually, these measurements can be viewed as an extension of the case in which the oxide itself is semiconducting, as occurs for instance with TiO_2. Variations of the flat-band potential of TiO_2 will also be equal to variations of Ψ_o. In an EIS device, however, the presence of the silicon substrate relieves the oxide itself of the requirement to be a semiconductor. Measurement of the surface potential on oxide surfaces have been obtained for SiO_2 [1,8,9,10], Si_3N_4 [11,12], Al_2O_3 [11,9,13], Ta_2O_5 [11] and ZrO_2 [14].
A theoretical model for predicting the surface potential Ψ_o, based on the surface site dissociation and complexation concepts, has been developed [8,9,13]. Experimental data in agreement with this theory have been found for SiO_2 [8,9,13] and especially for Al_2O_3 [13]. In particular, it has been found that the surface chemical parameters pH_{pzc} (pH at the point of zero charge) and ΔpK (separation of the surface acidity constants) determined on the basis of Ψ_o/pH measurements are within the range of those found with surface charge measurements on colloidal suspensions [9,13]. The surface potential Ψ_o, however, is much less sensitive to surface complexation with counter ions than the surface charge σ_o [13,15].
This chapter presents measurements of the temperature dependence of the surface potential at the γ-Al_2O_3/electrolyte interface. The importance of this investigation is two-fold. First, ion-sensitive field-effect transistors which measure surface potential can be used as miniature and robust pH sensors. An example of such an application is the clinical measurement of blood acidity [16]. In this and other applications, high accuracy is essential, and the temperature dependence of the sensor must be known and understood in order to apply a suitable correction as is shown in chapter 2. Second, it will be shown that $\partial\Psi_o/\partial T$ is related to the enthalpies of the surface ionization reactions of

the Al_2O_3 surface. Knowledge of $\partial\Psi_o/\partial T$ enables calculation of these enthalpies. The values found in this way can be compared with those measured directly by calorimetry of colloid suspensions. Such a comparison leads to another link between the study of oxide surface chemistry with EIS structures and with colloidal suspensions. Knowledge of the surface enthalpies provides additional data to clarity our present knowledge ot the reactions occurring on oxide surfaces in aqueous solutions.

Relation between $\partial\Psi_o/\partial T$ and the surface dissociation enthalpies

Following Levine and Smith [17], Davis *et al.* [18], and Smit [19], we can write the surface proton dissociation reactions as follows, in the notation used by James *et al.* [20]:

$$SOH_2^+ \rightleftharpoons SOH + H_s^+ \qquad K_{a1} = \frac{\{H^+\}[SOH]}{[SOH^+]} \exp\left(-\frac{q\Psi_0}{kT}\right) \tag{1}$$

$$SOH \rightleftharpoons SO^- + H_s^+ \qquad K_{a2} = \frac{\{H^+\}[SO^-]}{[SOH]} \exp\left(-\frac{q\Psi_0}{kT}\right) \tag{2}$$

where $\{H^+\}$ is the H^+ activity in the bulk solution, and quantities in square brackets are numbers of surface sites per unit area. The activity coefficients for the surface sites are assumed to be constant and are incorporated in the equilibrium coefficients, as was discussed by Smit and Holten [19]. Healy and White [21] have given a derivation of these equations, showing under which assumptions they are valid.
These reactions give rise to surface potential Ψ_o, which can be calculated to be given by [9,15]:

$$2.303\,(pH_{pzc} - pH) = \frac{q\Psi_o}{kT} + \sinh^{-1}\left(\frac{q\Psi_o}{\beta kT}\right) \tag{3}$$

where $pH_{pzc} = 1/2(pK_{a1}+pK_{a2})$ is the pH at the point of zero charge, and β is a dimensionless pH sensitivity parameter, given by:

$$\beta = \frac{2q^2N_s}{C_{DL}kT}\left(\frac{K_{a2}}{K_{a1}}\right)^{1/2} \tag{4}$$

where N_s is the surface density, and C_{DL} is the linearized double layer capacitance [15]. Equation (3) is an approximation valid for surfaces, such as oxides, where the site density is high enough to ensure that the surface charge is never close to its maximum value in the aqueous pH range. It is assumed that $\Delta pK = pK_{a2} - pK_{a1}$ is large enough to ensure that $K_{a2}/K_{a1} << 1$. It has been shown that the formation of surface complexes between charged sites and counter ions has only a small effect on the Ψ_o/pH relation, due to the very large capacitances associated with these complexes [13,15].
Around the point of zero charge, the relation of Equation (3) can be linearized to yield:

$$\Psi_o = \frac{\beta}{\beta+1} \frac{2.303\ kT}{q} (pH_{pzc} - pH) \qquad (5)$$

This is an approximation valid in the region around the point of zero charge where $(q\Psi_o/kT) < \beta$. When the oxide is Al_2O_3, β is expected to lie around 5 [9], and pH_{pzc} is close to 8. Therefore Equation (5) is expected to be valid roughly from pH 6 to 10, with some deviation outside that range. The temperature dependence of Ψ_o as given in Equation (5) can be calculated as:

$$\frac{\partial \Psi_o}{\partial T} = \frac{2.303\ k}{q} \frac{\beta}{\beta+1} \left[\left(1 + \frac{T}{\beta(\beta+1)} \frac{\partial \beta}{\partial T} \right) (pH_{pzc} - pH) + T \frac{\partial pH_{pzc}}{\partial T} \right] \qquad (6)$$

To calculate the derivatives relative to temperature of pH_{pzc} and β, the temperature dependence of the surface dissociation equilibrium constants is needed. From standard thermodynamics it follows that:

$$\frac{1}{K_{ai}} \frac{\partial K_{ai}}{\partial T} = \frac{\Delta H_{ai}}{RT^2} \quad \text{for } i = 1,2 \qquad (7)$$

in which ΔH_{ai} is the enthalpy change for reaction i. We will make the assumption that ΔH_{ai} is constant in the pH range around pH_{pzc} where Equation (5) is valid. Note that, as can be verified from Equation (7), the choice of the units for the activities, and therefore the choice of the standard state, does not affect the enthalpy obtained in Equation (7). It follows immediately that :

$$2.303 \frac{\partial pH_{pzc}}{\partial T} = - \frac{\Delta H_{a1} + \Delta H_{a2}}{2RT^2} \qquad (8)$$

In order to find $\partial\beta/\partial T$, we will neglect the temperature dependence of C_{DL} and N_s. The site density is expected to be fixed essentially by the oxide lattice parameters, and the double layer capacitance by geometric factors. In both cases, a linear temperature dependence should result, which will be negligible compared to the exponential dependence implied by Equation (7). Under those conditions it follows that:

$$\frac{\partial\beta}{\partial T} = \frac{\beta}{T}\left(\frac{\Delta H_{a2} - \Delta H_{a1}}{2RT} - 1\right) \tag{9}$$

The results of Equations (8) and (9) can be substituted into Equation (6) to yield the final result:

$$\frac{\partial\Psi_o}{\partial T} = \frac{\partial^2\Psi_o}{\partial pH\partial T}(pH - pH_{pzc}) - \frac{k}{q}\frac{\beta}{\beta+1}\frac{\Delta H_{a1} + \Delta H_{a2}}{2RT} \tag{10}$$

where the second derivative of Ψ_o relative to pH and temperature is given by:

$$\frac{\partial^2\Psi_o}{\partial pH\partial T} = -\frac{2.303\,k}{q}\frac{\beta}{\beta+1}\left[1 + \frac{1}{\beta+1}\left(\frac{\Delta H_{a2} - \Delta H_{a1}}{2RT} - 1\right)\right] \tag{11}$$

These equations show that the measurement of the second derivative $\partial^2\Psi_o/\partial pH\partial T$ yields the difference of enthalpy changes of the two ionization reactions. The constant term in the pH-dependence of $\partial\Psi_o/\partial T$ yields the sum of these enthalpy changes. Therefore, knowledge of the variation of $\partial\Psi_o/\partial T$ with pH enables ΔH_{a1} and ΔH_{a2} to be calculated individually.

Measurement of insulator surface potentials with EIS structures

The dependence of the flat-band voltage or the threshold voltage of an EIS structure on Ψ_o has been analyzed in [7] and [9], where it has been shown that the expression of the flat-band voltage of an EIS structure is given by:

$$V_{FB}(EIS) = E_{ref} - \Psi_o - \frac{\Phi^{Si}}{q} + \chi - Q_{ins}/C_{ins} \tag{12}$$

where E_{ref} is the reference electrode potential relative to vacuum [7], Φ^{Si} is the work function of silicon, q is the absolute value of the charge of an electron, C_{ins} is the insulator capacitance, and Q_{ins} is the charge inside the insulator

which is assumed to be located at the insulator/silicon interface. The term χ represents the sum of a number of dipole potentials which are small and can be neglected; the potential due to the water dipoles at the insulator electrolyte interfaces is not negligible, but is included in Ψ_o. Similarly, the flat-band voltage of a metal/insulator/silicon (MIS) structure is given by:

$$V_{FB}(MIS) = \frac{1}{q}(\Phi^M - \Phi^{Si}) + \chi'' - Q_{ins}/C_{ins} \qquad (13)$$

where Φ^M is the work function of the metal used in the MIS structure, and χ' is a collection of dipole potentials associated with the oxide/metal and the oxide/silicon interfaces. The last terms on the right hand side of the last two equations are the same if the MIS and EIS structures are made identically, except for the presence of a metal gate in one case. Both EIS and MIS structures can be used to make field effect transistors (FETs), whose threshold voltage is related to the flat-band voltage by:

$$V_T = V_{FB} + 2\phi^F - Q_{inv}/C_{ins} \qquad (14)$$

where Φ^F is the potential of the Fermi level relative to the mid gap level, and Q_{inv} is the charge per unit area in the silicon surface at inversion. Equation (12) is the basis for using EIS capacitors or ISFETs to measure changes in Ψ_o. Note that only variations of Ψ_o can be measured, because the other terms in Equation (12) are not independently known with sufficient accuracy.
By taking the difference between Equations (12) and (13) we find that:

$$V_{FB}(EIS) - V_{FB}(MIS) = V_T(EIS) - V_T(MIS) = E_{ref} - \Psi_o - \frac{\Phi^M}{q} + (\chi - \chi') \qquad (15)$$

Taking the partial derivative relative to temperature of this equation results in:

$$\frac{\partial V_T(EIS)}{\partial T} - \frac{\partial V_T(MIS)}{\partial T} = -\frac{\partial \Psi_o}{\partial T} + \frac{\partial E_{ref}}{\partial T} \qquad (16)$$

in which it is assumed that the temperature dependence of both Φ^M/q and of $(\chi - \chi')$ are negligible. The difference of dipole potentials contains contributions from both the M/SiO_2 and the electrolyte/SiO_2 interfaces, all of which are probably very small [7] and should not contribute any appreciable temperature dependence over a small temperature range. The problem of the temperature dependence of the metal work function is a more complex subject. The magnitude of this temperature dependence is still an open question, both from

the experimental and theoretical point of view. In particular, for aluminum, the metal which we have used, $\partial\Phi^M/\partial T$ is not known. There is considerable evidence, however, that the temperature dependence is in the order of k (Boltzmann's constant) at the most, i.e. less than 0.09 mV/°C [22,23,24]. Cardona and Ley [23] calculate that for aluminum the two main contributions to $\partial\Phi^{Al}/\partial T$ cancel approximately. For metals whose work functions can be measured with thermionic emission, experimental determinations are possible, and the values listed in [24] are generally in the order of 0.1 mV/°C or less. For tungsten, for instance, $\partial\Phi^W/\partial T = 0.015$ to 0.06 mV/°C has been found [24]. Since the temperature dependence of Ψ_o will be found to be of the order of 1 mV/°C, it is justified to neglect the effect of $\partial\Phi^{Al}/\partial T$.
The variations of threshold voltage of an ISFET are usually determined by a feedback circuit in which the gate to source voltage is adjusted to keep the drain current constant, while the drain to source voltage remains fixed. In first order field effect transistor theory this current is given by :

$$I_D = k\left(V_G - V_T - \frac{V_D}{2}\right)V_D \qquad (17)$$

assuming both the source and substrate to be grounded. The parameter k in this equation is the product of the carrier mobility in the silicon surface, the width over length ratio of the transistor, and the insulator capacitance. Taking the temperature derivative of this equation with V_D constant, we obtain:

$$\frac{\partial V_G}{\partial T} = \frac{\partial V_T}{\partial T} + \frac{I_D}{V_D}\frac{\partial}{\partial T}(k^{-1}) \qquad (18)$$

The last term in this equation can be found by measuring the dependence of $\partial V_G/\partial T$ on I_D. By taking measurements at various drain currents and extrapolating to $I_D = 0$ it is then possible to determine $\partial V_T/\partial T$ for both an ISFET or an Al-gate FET. Alternatively, since in Equation (18) the last term is the same for the ISFET and the identical Al-gate FET, we can write that:

$$\frac{\partial}{\partial T}\{V_G(EIS) - V_G(MIS)\} = \frac{\partial}{\partial T}\{V_T(EIS) - V_T(MIS)\} = \frac{\partial}{\partial T}\{\Delta V_T\} = -\frac{\partial \Psi_0}{\partial T} + \frac{\partial E_{ref}}{\partial T} \qquad (19)$$

This can be measured at a variety of values of I_D and averaged. In practice, when the temperature dependence of the threshold voltage is measured, two effects contribute: the explicit temperature dependence of the surface potential, and the contribution due to the change in the pH of the buffer solution. Thus, the measured quantity is:

$$\left(\frac{d\Delta V}{dT}\right)_m = \frac{\partial \Delta V_T}{\partial T} + \frac{\partial \Delta V_T}{\partial pH}\frac{\partial pH}{\partial T} \qquad (20)$$

in which $\partial\Delta V_T/\partial pH$ is the pH sensitivity of the ISFET. By measuring both this pH sensitivity and the temperature dependence of the buffer pH, Equation (20) can be used to correct for the influence of the variability of the buffer pH.

Experimental

The ion selective field effect transistors used were individual n-type field effect devices on silicon substrates. These devices have been reported before [25] (see also chapter 2) and are similar to those used by Bousse *et al.* [9,13]. The pH sensitive insulator consisted of a 600Å layer of Al_2O_3, deposited by chemical vapour deposition at 900°C using the reaction between $AlBr_3$, NO and H_2. This method of depositing thin films of Al_2O_3 has been reported earlier by Balk and Stephany [26]. The material deposited under these conditions was determined to have the structure of γ-Al_2O_3, with a grain size of around 400Å [27] (see also chapter 4). On the same wafer, both ISFETs and aluminum gate FETs were fabricated. The Al-gate FETs were identical except that a layer of aluminum was deposited and patterned to form the gate electrode. After the wafer was scribed, both types of devices were mounted on standard printed circuit board material, bonded, and encapsulated with epoxy resin. Only in the case of the ISFETs was the gate area left open to the electrolyte solution.
The variations of the threshold voltage of the ISFETs were measured with the drain and source follower amplifier circuit described by Bergveld [28]. The output from this circuit provided readings accurate to within 0.1 mV.

The solution pH was measured with a glass electrode (Metrohm 6.0102.002) and a separate double junction reference electrode (Metrohm 6.0726.100). The pH buffers used were Taorell buffers [29], a Tris/HCl buffer, and ready-made buffers supplied by Merck. The temperature dependence of the buffer was given by the supplier in the case of the Merck buffers; for the others it was measured comparing the glass electrode potentials, calibrated with the Merck buffers, at two temperatures.

The ISFET, glass electrode, and reference electrode were introduced in a thermostatted titration vessel. The temperature of the electrolyte was monitored with a temperature sensor (Metrohm 6.1103.000). The reference electrode served a dual function. It was the gate electrode of the ISFET, and also the reference electrode for the pH measurements with the glass electrode. Since it was a double junction electrode, it was possible to keep only the tip of the outer glass frit immersed in the solution, in order to hold the temperature of the reference electrode as constant as possible.
The outer filling solution was similar to the electrolyte being used, to minimize the potential of the liquid over which the temperature gradient occurs. The inner liquid junction has a constant potential, since it is no longer subject to temperature variations. We verified that no change in cell potential with electrolyte temperature could be observed in a cell consisting of the reference electrode, and a calomel electrode which was kept at 25°C and placed in the solution for only a few moments. This confirms that the precautions described above had the effect of eliminating any temperature dependence of the reference electrode potential.

Results

The pH sensitivity of the ISFET was determined at various temperatures by titrating a Tris/HCl solution in the pH range 6 to 8 while recording the ISFET response. The resulting temperature dependence of the slope of the ISFET response $\partial\Psi_o/\partial pH$ is shown in Fig. 1.

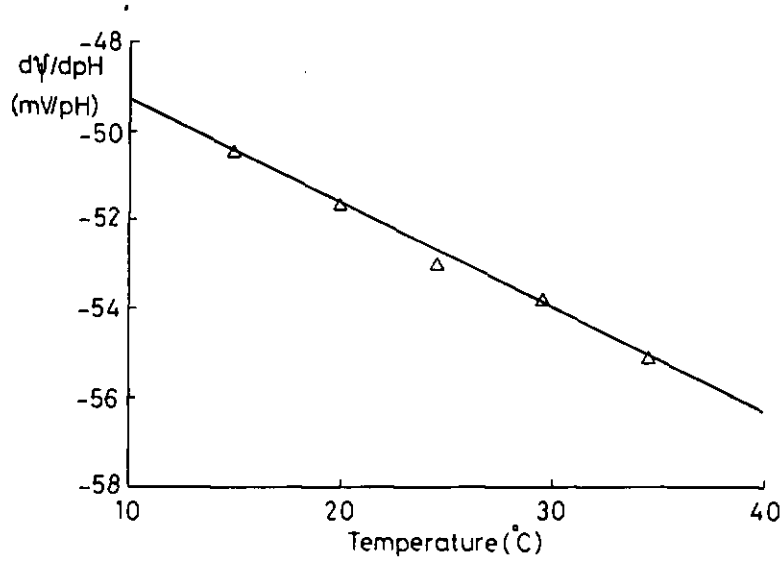

Fig. 1: *The slope of the pH response of an Al_2O_3-gate as a function of temperature.*
slope = -0.234 mV/(pH°C)

From this data, it can be deduced that at 25 °C the slope is equal to -52.8 mV/pH. According to Equation (5), this corresponds to a value of ß of 8.31. From the slope of the regression line in Fig.1 it also follows that:

$$\frac{\partial^2 \Psi_o}{\partial T \partial pH} = -(0.234 \pm 0.11)\ \text{mV/(pH°C)} \qquad (21)$$

This and subsequent error limits will refer to one standard derivation of the statistical distribution of the measurement.
The temperature dependence of the threshold voltage was determined in eight different buffer solutions, with pH values ranging from 4 to 9 (see Table 1). Every measurement consisted of recording the ISFET responsa, at 20 and 30 °C, and at various drain currents. The same measurement was also done on an identical Al-gate FET. This led to plots of dV_G/dT against drain current such as those shown in Fig. 2.

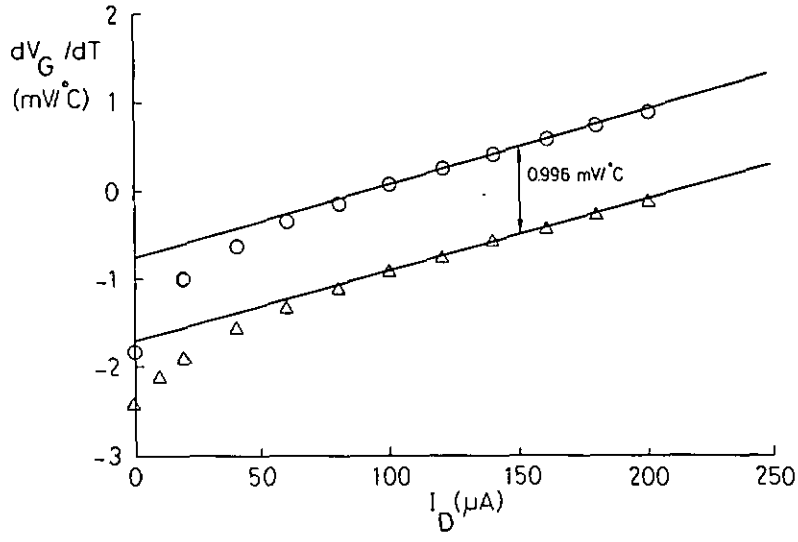

Fig. 2: *Experimental data for the temperature dependence of the gate voltage as a function of drain current, for both an ISFET (o) and an aluminum-gate FET (Δ) The curves are regression lines based on the points between 80 and 200μA. The difference between two lines leads to a value of $(d\Delta V_T/dT)_m$ at the pH value used. The drain voltage was 1 V, and the buffer was a Teorell buffer with pH = 6.635.*

As predicted by Equation (18), this plot is linear, except at low drain currents (where the first order theory no longer applies). Also Fig. 2 confirms that the behavior of both types of FETs is identical except for a shift. The value of this shift was found by calculating the regression line of the linear part of the two curves, and taking the differences between the regression lines in the middle of the linear range. The desired values of $\partial\Psi_o/\partial T$ were calculated by using Equation (20), with an ISFET pH sensitivity ot -52.8 mV/pH (Table 1). When comparing Fig. 2 and Fig. 5 in chapter 2 the influence of the temperature on the pH of different solutions becomes evident

Table 1: *Overview of the experimental results obtained in various buffers. Each $(d\Delta V_T/dT)_m$ value is obtained from the difference of two regression lines of the dV_G/dT vs. I_D curves as is shown in Fig. 2.*

pH (at 25 °C)	V_D (V)	$(d\Delta V_T/dT)_m$ (mV/°C)	$\partial pH/\partial T$ ($pH°C^{-1}$) ($\times 10^{-3}$)	$-\partial\Psi_o/\partial T$ (mV/°C)
Teorell buffers				
5.595	1.0	0.958	+1.05	0.902
6.635	1.0	0.996	-1.08	1.053
7.600	1.0	0.982	-4.21	1.205
8.425	1.0	1.008	-9.28	1.498
Teorell buffers				
5.595	0.5	1.001	+1.05	0.945
6.635	0.5	1.042	-1.08	1.099
7.600	0.5	1.002	-4.21	1.224
8.425	0.5	1.072	-9.28	1.562
Merck buffers				
4.005	1.0	0.344	+1.04	0.289
5.000	1.0	0.737	0	0.73
8.955	1.0	1.027	-9.18	1.512
Tris/HCl buffer				
7.701	1.0	-0.179	-28.27	1.314

The 12 different points for $\partial\Psi_o/\partial T$ found in this way are plotted as a function of pH in Fig.3.

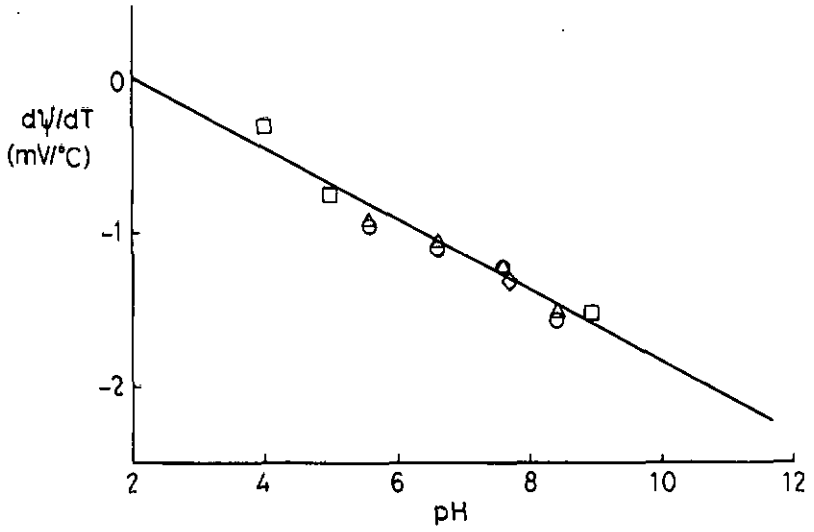

Fig. 3: *The temperature dependence of the surface potential of an Al_2O_3 surface, as a function of pH.*
Δ : Teorell buffers with $V_D = 1.0$ V
O : Teorell buffers with $V_D = 0.5$ V
□ : Merck buffers
◇ : Tris/HCl buffer

As Equation (10) predicted, the plot is a straight line. The equation of the regression line which passes through these points is

$$\frac{\partial \Psi_o}{\partial T} = -(0.231 \pm 0.017)(pH - 8) - (1.38 \pm 0.033)\ mV/°C \qquad (22)$$

where it is assumed that $pH_{pzc} = 8$ [13]. The slope of this line yields a second measurement of $\partial^2\Psi_o/\partial pH\partial T$. As expected, this value agrees with the one found previously, although the error limits on the two results show that the closeness of the agreement is fortuitous. This amounts to verifying experimentally that the second derivative of the surface potential relative to pH and temperature does not depend on the order in which the differentiations are carried out.
The numbers from the previous equations, together with the value of β, can then be.substituted in to Equations (10) and (11) to yield the following values:

$$\Delta H_{a2} - \Delta H_{a1} = (7.8 \pm 1.4)RT = (19.3 \pm 3.4)\ kJ/mole \qquad (23)$$

$$\Delta H_{a2} + \Delta H_{a1} = (35.8 \pm 0.9)RT = (88.8 \pm 2.1)\ kJ/mole \qquad (24)$$

These equations can be solved to find the following individual reaction enthalpies:

$$\Delta H_{a1} = (14.0 \pm 0.8)RT = 34.8 \pm 2.0 \text{ kJ/mole} \quad (25)$$

$$\Delta H_{a2} = (21.8 \pm 0.8)RT = 54.0 \pm 2.0 \text{ kJ/mole} \quad (26)$$

It should be noted that the error limits given above do not take into account possible systematic errors, such as the influence of the temperature dependence of the work function of aluminum.

Discussion It is desirable to compare the values found above by other means, preferably direct calorimetry on a colloidal suspension. Griffiths and Furstenau [30] have measured the heat of immersion of an Al_2O_3 dispersion. Using the location of the point of zero charge, and a theoretical estimate of the entropy change involved in reactions (1) and (2), they arrived at:

$$\Delta H_{a2} + \Delta H_{a1} = (87.57 \pm 6.27) \text{ kJ/mole} \quad (27)$$

This number is uncertain because it is partly based on an estimation of the entropy change involved. Nevertheless, it agrees closely with the value we have reported above. By fitting the measured pH dependence of the heat of immersion with a theoretical model, Griffiths and Furstenau also attempted to find individual values for the two ionization enthalpies. They report ΔH_{a1} = 46 kJ/mole and ΔH_{a2} = 41 kJ/mole, although this separation is subject to even more uncertainty due to scatter of the data and the curve fitting which is required. Therefore, although the order of magnitude is the same, we disagree with Griffiths and Furstenau about which of the two ionization enthalpies is the larger one.

More recently, results of calorimetric titrations on dispersions of other oxides have been reported. For TiO_2, Davis *et al.* [31] found that the enthalpy for the release of one proton at the pH_{pzc} is -35 to -40 kJ/mole, i.e. the reaction is exothermic. Foissy's [32] measurements on TiO_2 show an enthalpy of -20 to -30 kJ/mole. Although these authors agree on the sign and order of magnitude of the enthalpy, the variation in the reported value for TiO_2 is considerable. Davis *et.al.* [31] report a peak of the proton release enthalpy around pH_{pzc} which is not seen by Foissy. These disagreements are probably indicative of the experimental difficulties involved in microcalorimetric measurements. Davis *et al.* [31] also report that for goethite (FeOOH), contrary to TiO_2, the enthalpy change is endothermic. This result has been confirmed by Zeltner *et al.* [33], who report an endothermic proton desorption heat of around 40 kJ/mole at the point of zero charge of goethite. It appears, therefore, that the proton release enthalpy of an oxide depends strongly on the nature of the oxide.

We have not yet discussed an important aspect of the reactions occurring on an oxide surface, namely the formation of surface complexes of charged sites with oppositely charged counter-ions. Many studies of the oxide/electrolyte interface have suggested that most of the charged sites do form complexes,

and that they are much more numerous than noncomplexed charged sites [18,34,35]. In other words, most of the protons released from an oxide surface actually come from the ion exchange reaction (in the case of pH values above the pH_{pzc}):

$$SOH + Na^+ \rightleftharpoons SO^-Na^+ + H^+ \qquad (28)$$

which is the sum of Equation (2) and the formation reaction of a surface charge complex. Such ion-exchange reactions are therefore a major source of the surface charge generated by the titration of a colloidal suspension. The ion exchange process has little effect on the surface potential Ψ_o, however [13,15]. This is due to the large capacitance associated with a complex such as SO^-Na^+, which implies that very little surface potential is generated by reaction (28). Therefore, the assumption we have made that the measured temperature dependence does not involve the formation of surface complexes is justified. In the case of calorimetric measurements discussed above, the possibility exists that complex formation does affect the measured results significantly, especially at some distance from the point of zero charge. The enthalpy values reported by various authors [31,32,33] could have a more complex origin than merely ionization reactions (1) and (2). Depending on the pH, part or all of the measured enthalpy will be that of reaction (28). The increased influence of complex formation at pH values away from pH_{pzc} is a possible explanation for the tendency of the experimental enthalpies reported in [31] and [33] to show a peak at the pH_{pzc}.

Conclusions

From Equation (22) we can deduce that the temperature dependence of Ψ_o is known with an error of less than 0.1 mV/°C in the pH range covered here. This amounts to less than 0.01 pH units for the temperature variations of 5 °C. We conclude that it is possible to sufficiently compensate for the temperature dependence of an ISFET for biological applications, where high accuracy is required. Note however that we have eliminated the influence of the reference electrode in our set-up, which is not possible in practical applications. In general, the temperature dependence caused by the reference electrode must also be taken into account.

Our results for the surface ionization enthalpies of Al_2O_3 agree reasonably well with the only colloid calorimetry measurements which are available for that material, especially when seen in light of the dispersion of results reported on other oxide colloids. We can therefore safely conclude that both surface ionization reactions on Al_2O_3 are endothermic, with an enthalpy change of around 40 kJ/mole.

More precise colloidal calorimetry measurements on Al_2O_3 would be desirable, however, to ascertain the influence of the formation of surface complexes with counter ions on the results. It is to be hoped that it will become possible to separate the enthalpy changes, due exclusively to proton adsorption/desorption, from those caused by the subsequent complex formation. If that can be combined with knowledge of the equilibrium constants of these reactions [15], then information about entropy changes might be deduced. Thus it appears that measurements as those reported here, together with calorimetric measurements on colloids can generate new thermodynamic data about the reactions occurring at oxide surfaces, and thereby improving the understanding of the electrolyte/oxide interface.

References

1. Schenck,J.F., *J.Colloid Interface Sci.* **61,** 569 (1979).
2. Bergveld,P., *IEEE Trans. Biomed.Eng.* **BME-17,** 70 (1970).
3. Bergveld,P., *IEEE Trans. Biomed.Eng.* **BME-19,** 342 (1972).
4. De Rooij, N.F., Bergveld,P., *Thin Solid Films* **71,** 327 (1980).
5. Cichos,C., Geidel,T., *Colloid polymer Sci.* 256, 1140 (1978).
6. Cichos,C., Geidel,T., *Colloid polymer Sci.* **261,** 947, (1983).
7. Bousse,L., *J. Chem. Phys.* **76,** 5128 (1982).
8. Siu,W.M., Cobbold,R.S.C., *IEEE Trans. Electron Devices* **ED-26,** 1805 (1979).
9. Bousse,L., De Rooij, N.F., Bergveld,P., *IEEE Trans. Electron Devices* **ED-30,** 1263 (1983).
10. Fung,C.D., Cheung,P.W., Ko,W.H., *IEEE Trans. Electron Devices* **ED-33,** 8 (1986).
11. Matsuo,T., Esashi,M., *Sensors and Actuators* **1,** 77 (1981).
12. Harame,D., Bousse,L., Schott,J., Meindl,J.D., *IEEE Trans. Electron Devices,* to be published.
13. Bousse,L., De Rooij, N.F., Bergveld,P., *Surface Science* **135,** 479 (1983).
14. Sobczynska,D., Torbicz,W., *Sensors Actuators* **6,** 93 (1984).
15. Bousse,L., Meindl,J.D., *in* Geochemical processes at mineral surfaces, (J.A. Davis and K.F. Hayes Eds.), p. 79. ACS Symposium Series,Vol. 323, American Chemical Society, 1986.
16. Schepel,S.J., De Rooij,N.F., Koning,G., Oeseburg,B., Zijlstra,W.G., *Med. Biol.Eng. & Comp.* **22,** 6 (1984).
17. Levine,S.,Smith,A.L., *Disc. Faraday Soc.* **52,** 290, (1971).
18. Davis,J.A., James,R.O., Leckie,J.O., *J.Colloid Interface Sci.* **63,** 480 (1978).
19. Smit,W., Holten,C.L.M., *J.Colloid Interface Sci.* **78,** 1 (1980).
20. James,R.O., Parks,G.A., *in* Surface and Colloid Science, Vol. 12 (E. Matijevic Ed., Plenum Press), p.119,1982.
21. Healy,T.W., White,L.R., *Advan. Colloid Interface Sci.* **9,** 303 (1978).
22. Herring,C., Nichols,M.H., *Rev. Mod. Physics* **21,** 185 (1949).
23. Cardona,M., Ley,L., *in* Photoemission in Solids I, p. 42, Springer, Berlin, 1978.
24. Haas,G.A., *in* The AIP Handbook of Physics, Third Edition, p. 9-172. The American Institute of Physics, 1972.
25. Van den Vlekkert,H.H., Arnoux,C., Lomazzi,P., De Rooij,N.F., *in* Proc. of the 2nd Int. Meeting on Chemical Sensors, Bordeaux p.462, 1986.
26. Balk,P., Stephany,F., *J. Electrochem. Soc.* **118,** 1634 (1971).
27. Arnoux,C., Van den Vlekkert,H.H., Buser,R., de Rooij,N.F., *in* Transducers '87, Tokyo, Japan, p. 751, 1987.
28. Bergveld,P., *Sensors Actuators* **5,** 13 (1984).
29. Teorell,T., Stenhagen,E., *Biochemischer Zeitung* **299,** 416 (1938).
30. Griffiths,D.A., Furstenau,D.W., *J.Colloid Interface Sci.* **80,** 271 (1981).
31. Davis,J.A., Lewis,E.A., Cook,A.D., Mehr,S., *in* Digest of the 190th National Meeting, Division of Environmental Chemistry, Chicago, American Chemical Society, p. 308, 1985.
32. Foissy,A., *Thesis,* Université de Franche-Comté (France), 1985.
33. Zeltner,W.A., Yost,E.C., Machesky,M.J.L., Tejedor-Tejedor, M.I.,Anderson,M.A., *in* Geochemical processes at mineral surfaces (J.A. Davis and K.F. Hayes Eds.), p. 79. ACS Symposium Series, Vol. 323, American Chemical Society, 1986.
34. Smit,W., Holten,C.L.M., Stein,H.N., de Goeij,J.J.M., Theelen,H.M.J., *J.Colloid Interface Sci.* **63,** 120 (1978).
35. Foissy,A., MPandou,A., Lamarche,J.M., Jaffrezic-Renault,N., *Colloids Surf.* 5, 363, (1982).

Chapter 6 Glass encapsulation of chemical solid state sensors

parts of this chapter were presented at:
2nd Int. Meeting on Chemical Sensors
1986, Bordeaux, France

Glass encapsulation of Chemfets:
a simultaneous solution for Chemfet packaging
and ion-selective membrane fixation
M.Decroux, H.H. van den Vlekkert, N.F.de Rooij
(Proc. 2nd Int. Meeting on Chemical Sensors, Bordeaux, France, 1986 p.406)

Transducers '87
1987, Tokyo, Japan

Glass encapsulation of chemical solid state sensors based on anodic bonding
H.H. van den Vlekkert, M.Decroux, N.F.de Rooij
(Proc. Transducers '87, Tokyo, Japan, 1987 p.730)

Abstract

One of the main factors which prevents the use of chemical sensors on a large scale is their unreliable performance due to poor packaging. In this chapter the possibility of glass encapsulation of chemical sensors will be discussed. The results of the influence of the electrostatic bonding of glass (anodic bonding) to MOS devices and a planar silver/silverchloride electrode, on top of a p-type buried conductor, suggest a need for a special fabrication process for CHEMFETs. Such a process, necessary to maintain the quality of the electric components integrated into the silicon substrate during the anodic bonding of glass, is proposed here.
To evaluate the validity of this fabrication process a pH-sensitive and a pCl-sensitive ISFET are realized. These ISFETs are anodically bonded with glass. Both types of ISFETs show satisfactory properties with respect to sensitivity and drift. No breakdown of the glass seal could be observed during use over several weeks.

Introduction

A main problem which prevents the large scale use of chemical sensors, based on FET-technology, is the unreliable performance due to poor packaging. Especially when multi-ion sensors are required the packaging poses a major problem. Until now the encapsulation of ISFETs and related devices has been mainly realised by the utilisation of different types of epoxies. However, these epoxies only allow a restricted operational lifetime because they are all permeable to water and they adhere poorly to the sensor chip. Another disadvantage is that they are applied by hand, resulting in low yield, time consuming procedures, low reliability and high costs.

Several approaches to improve the encapsulation have been proposed:
1) sidewall and backside protection of the sensor chip by inorganic oxides, obtained by CVD procedures [1].
2) location of the bonding pads on the backside of the sensor [2,3,4].
3) reverse biasing of a p-well in an n-type substrate [5].
4) application of polyimides [6].
5) silicon on sapphire [7].

However, the proposed methods only offer partial solutions of the problem. The first step to a complete solution of the encapsulation problem could be the use of glass to silicon electrostatic bonding, which method is already successfully used for physical sensors, e.g. silicon pressure transducers and solar cells [8,9]. The following improvements can be obtained with this method:
1) excellent sealing properties
2) high resistance against chemical attack
3) compatibility with ion-selective membrane deposition
4) wafer level processing

The encapsulation problem of the sidewalls and backside of the sensor can be solved by embedding the active devices in a well and then reverse biasing the well/substrate [5]. The contact wires can then be adequately isolated by placing them either on the backside of the sensor or using aluminum contacts on the glass plates in combination with tape automatic bonding [10].
The ability to bond anodically silicon with glass has been demonstrated by Pomerantz in 1968 [11]. The schematic set-up for electrostatic bonding is shown in Fig. 1.

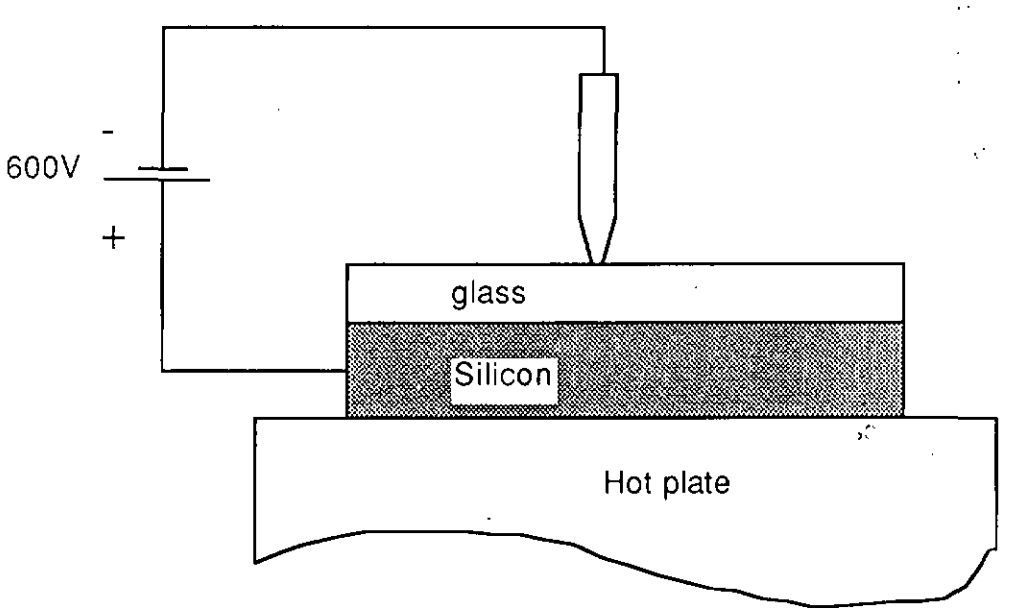

Fig. 1: *Schematic set-up of anodic bonding process*

To achieve the bonding between a glass plate and a silicon substrate, a high negative dc voltage with respect to the substrate (200-1000 V) and temperatures of 180-500°C are required. At the silicon/glass interface a large electrical field is built up, caused by the migration in the glass of alkali ions (normally sodium) away from this interface. The extremely high field which now builds up at the glass/silicon interface transports oxygen out of the glass to bond with the silicon surface [12].

As a consequence of the extreme conditions of the bonding process the electric components integrated into the silicon substrate can be damaged [13,14]. A further problem can be the difference in the thermal expansion coefficient of the glass and the substrate. Other important factors which can influence or even inhibit the bond are the surface roughness and the presence of dust particles [15]. A step of more than 1000 Å can inhibit already a complete bonding. The latter problems can be overcome by a suitable choice of the glass, careful sensor design and clean working conditions.

The damage of the electric components is a much more serious problem. To protect these components, a polysilicon layer can be deposited on top of the structure. When this layer is grounded, it screens the huge field developed at the polysilicon/glass interface and thereby avoids the degradation of the silicon/silicondioxide interface [16]. However for a chemical sensor the sensing area has to be open to the outside world. Since the electrical field is concentrated at the polysilicon/glass interface, it would be expected that the field inside the glass hole would be low enough to avoid damage of the sensing part. This was investigated by measuring the C-V characteristics of MOS capacitors before and after the bonding with glass which had holes of different diameters. However, in all cases an important shift of the flat band voltage and a large increase of the density of the interface states was observed after the anodic bonding, indicating a degradation of the silicon/silicon dioxide interface. This degradation of the silicon/silicon dioxide interface could only be prevented by discharging the floating electrode of the capacitor [17]. Therefore, the protection of the floating electrode depends on the nature of the devices. A protection of the sensing part via a diode connected to the sub-

strate seems possible. At an elevated temperature this diode starts conducting which will short-circuit the sensing part with the substrate and thereby avoids the development of the high field at the silicon/silicon dioxide interface. To test this method a silver/silverchloride electrode on top of a p-type buried conductor is realized (described in part 1), which can be anodically bonded to glass. The results are thereafter used to realize glass encapsulated ISFETs (part 2).

Part 1: planar silver/silverchloride electrode

Experimental

Fabrication process:

The basic design of this structure is shown in Fig.2. It consists of a p-type conductor ion-implanted into an n-well. This well is also ion-implanted into the p-type substrate. Because of the necessity to avoid steps, in order to obtain a good bond, photoresist is used as a mask for the ion implantation processes of the conductor and the well. After the deposition of the polysilicon layer and its patterning, an oxidation of this layer is carried out in order to avoid electrical links between adjacent active areas. This thin layer of oxide is removed in the sealing area. In the mean time contact pads are opened. Finally metallization of the contact pads as well as silver deposition is carried out. To achieve a good adhesion between the silicon (silicon dioxide) and the silver an intermediate layer of titanium is used.

To obtain a stable electrochemical interface with the solution the silver layer can be partially converted into silverchloride either chemically [18] or electrochemically [19]. However if this conversion was carried out before the bonding process, degradation of the silverchloride is observed during the bonding of the glass. When the bonding is carried out under ambient atmosphere the silver layer is oxidized thereby inhibiting the conversion of the silver into silverchloride. Bonding under a nitrogen atmosphere gives somewhat better results but still oxidation of the silver surface occurs. It is interesting to note that this oxidation occurs when the voltage is applied and not during the heating process. This confirms that during the bonding oxygen is freed from the glass, as was already indicated before [12]. To protect the silver layer during the bonding two metal layers (titanium and aluminum) were deposited on top of it. The titanium layer acts as a diffusion barrier between the aluminum and the silver which would otherwise alloy with the silver. The aluminum protects the titanium against oxidation which oxide would be difficult to remove. After the bonding the aluminum and titanium layer can be selectively etched, leaving a very clean silver surface which can easily be chloridated.

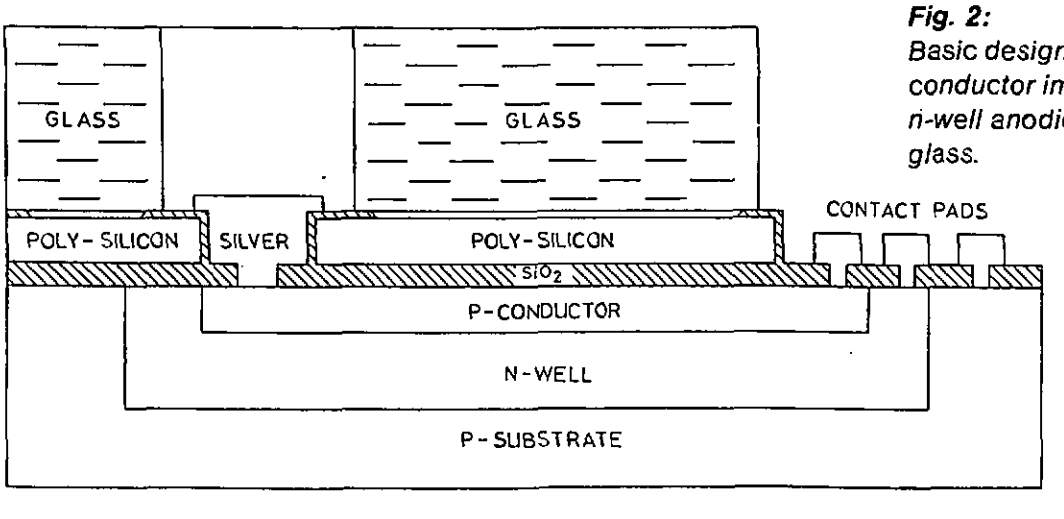

Fig. 2:
Basic design of p-type conductor implanted in an n-well anodically bonded with glass.

Anodic bonding process:
The equipment consists of a high voltage source, 0-2000 V, with adjustable polarity (Heizinger model HNC 2000-10), a temperature controller, 25-600°C, (Digitrade model HTC-I-30-R-C3-0-D), a microscope (Wild M3Z) and a heating plate fixed on a rotable system and an XYZ table. The temperature controller keeps the temperature constant within 1%. The structure to be processed is held on the heating plate by a suction system and the rotable system allows the plate to turn by ± 10°C. A stainless steel tube fixed on the XYZ table allows the glass plate to be held by vacuum and also to transmit the high voltage to the glass. The XYZ table allows motion by ± 10 mm in all directions. The anodic bonding could be carried out in a few seconds at a temperature of 400°C and with an applied voltage of 600 V. A Tempax glass is used as glass material, which has been polished to a thickness between 200 and 300 μm. At the sensing area, holes having a diameter between 300 and 500 μm have been made with an ultrasonic drill.

Results and Discussion

The I-V characteristics of the well-conductor junction before bonding is given in Fig.3. The reverse current of this diode is typically less than 30 pA. When the silicon/silicon dioxide interface is completely protected against the electrical field, a similar characteristic is obtained after the bonding.

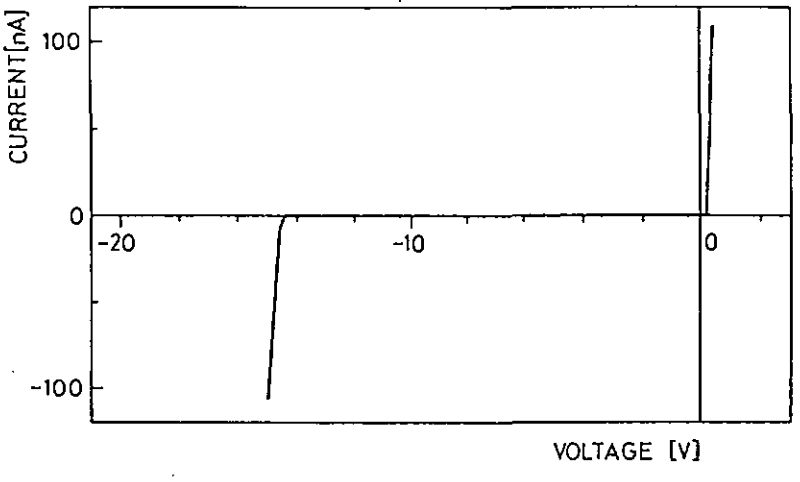

Fig. 3: *I-V characteristics of the diode before the bonding. Normally after the bonding an identical curve is obtained.*

However severe damage of this diode is observed, as demonstrated in Fig.4, when a misalignment or a heavy underetch of the metal sandwich leaves the silicon/silicon dioxide interface unprotected at the junction, schematically demonstrated in Fig.5. The damage created at this interface, as discussed before, increases the generation rate of minority carriers and therefore increases the reverse current of the diode. This explanation is also supported by the square root dependence of this reverse current versus the voltage whereas no shift of the breakdown voltage is observed.

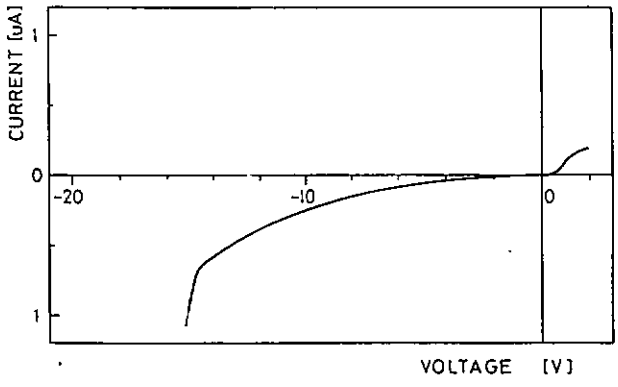

Fig. 4: *I-V characteristic of a diode damaged by anodic bonding.*

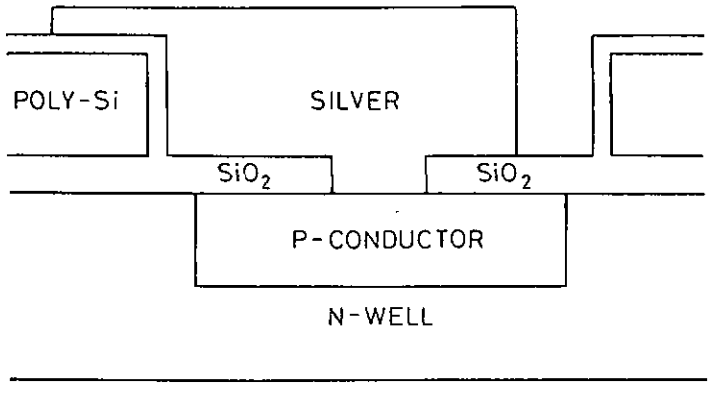

Fig. 5: *Schematic view of the problem caused by misalignment or underetch.*

After the anodic bonding the sensors are mounted on a standard printed circuit board, wire bonded and finally the bond wires are encapsulated with epoxy. The silver could now be chloridated after the etching of the aluminum and titanium layers. The chemical method proved to be the most convenient way to chloridate the silver. Another advantage is that also whole wafers can be chloridated in this way. The sensitivity of these sensors to chloride ions is 58.5 mV/pCl, at 25°C, shown in Fig.6.

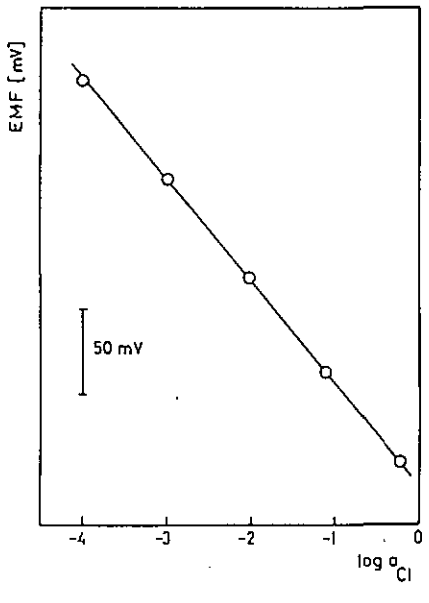

Fig. 6:
Sensitivity to chloride ions of a glass encapsulated sensor.

The observed drift was less than 10 μV/h at 25°C in a 0.1 M KCl solution. The same sensors were also encapsulated with epoxy (no glass encapsulation) and no difference could be observed between these sensors. The sensitivity and drift rates are comparable with those found for other planar structures [20].

Conclusions Glass encapsulation of planar solid state sensors can be achieved with anodic bonding, when proper precautions are taken to protect the sensor against the harsh conditions of the bonding process. Stable, glass encapsulated silver/silverchloride planar electrodes have been fabricated, which can be used for Cl/measurements or as part of a miniaturized reference electrode.

Part 2: pH and pCl sensitive ISFETs

Introduction In the previous section it was demonstrated how to protect a solid state chemical sensor against the harsh conditions of the anodic bonding process. Two protections have to be provided:

1) the part covered by the glass has to be protected by a grounded polysilicon layer.
2) the sensitive area, not covered by the glass, has to be screened from the electrical field developed in the hole. This can be accomplished by covering this area with a metal layer which is connected to a conductor. When this conductor is placed in a well it will be a diode. Under normal conditions this diode will be reverse-biased, however during the anodic bonding it will become conductive and can thereby discharge the metal.

Two other design criteria have to be kept in mind besides the above mentioned:

1) step heights of more then 100 nm have to be avoided
2) the reference electrode to source voltage (operation voltage) has to be larger than -0.5 V, in order to prevent influences of the protection diode, which is in direct contact with the solution during operation.

In our process a pH sensitive and pCl sensitive ISFET are fabricated on the same wafer, which means that the difference in threshold voltage between both types of sensors should be taken into account when determining the process parameters.
For the pCl-ISFET, the expression for the threshold voltage can be given by:

$$V_T = E_{ref} - E^{o}_{Ag/AgCl} + \frac{kT}{q} \ln a_{Cl^-} + \frac{\Phi^{Ti}}{q} - \frac{\Phi^{Si}}{q} - \frac{Q_{ins}}{C_{ins}} + 2\phi^{F} - \frac{Q_{inv}}{C_{ins}} \qquad (1)$$

with E_{ref} = reference electrode potential
$E^{o}_{Ag/AgCl} - (kT/q)\ln a_{Cl^-}$ = the silver/silverchloride electrode potential [19].
Q_{ins} = the charge inside the insulator which is assumed to be located at the insulator/solution interface, per unit area
C_{ins} = the insulator capacitance per unit area
Q_{inv} = the charge per unit areain the silicon surface at inversion
Φ^{F} = the Fermi potential
Φ^{Ti} = the metal work function ot Ti , which is comparable to the metal work function of Al [21].
Φ^{Si} = the silicon work function

When using a silver/silverchloride reference electrode, the term $E_{ref} - E^{\circ}_{Ag/AgCl} + (kT/q)\ln a_{Cl^-}$ becomes very small (depends only on the chloride ion concentration) and Equation 1 reduces to the expression for the threshold voltage of a MAOSFET. Experimentally it was established that if the threshold voltage for a MOSFET is 0 V the threshold voltage for the corresponding MAOSFET will be -1 V. The difference in the threshold voltage between MAOSFETs and ISFETs is around 1V (chapter 2). When the threshold voltage for a MOSFET is e.g. 0 V, this will result in a threshold voltage, for the pH-ISFET, of around 0 V (and an operation voltage (V_G), for $I_D = 100$ μA and $V_D = 0.5$V in pH = 7, of 1 V) and for the pCl-ISFET of around -1 V and an operation voltage of 0 V. By means of the simulation program SUPREM [22], the fabrication parameters on the threshold voltage for the MOSFET were determined. As threshold voltage 0 V was taken, which enables the fabrication of the pH- and pCl-ISFETs simultaneously.

Experimental

The basic design of the structure is shown in Fig. 7.
The processing sequence is as follows:

Step 1: p-well
- a) initial oxidation of n-type wafer(15-35 Ohmcm)
- b) Mask 0: opening of alignment marks
- c) reoxidation
- d) Mask 1: patterning of well
- e) ion implantation of boron (dose = 1E12 at/cm^2, E = 80keV)
- f) diffusion (1400 min N_2, 1150 °C)

Step 2: channel stopper
- a) Mask 2: definition channel stopper
- b) ion implantation boron (dose = 7.5E15 at/cm^2, E = 80keV)

Step 3: source/drain/conductor
- a) Mask 3: defintion active areas
- b) ion implantation phosphorous(dose = 6E15 at/cm^2, E = 100keV)

Step 4: polysilicon (polySi)
- a) Mask 4: opening of the polySi/substrate contact
- b) deposition of polySi: 550 nm

Step 5: gate preparation
- a) Mask 5: opening polySi (sensitive area and contact area)
- b) Mask 6: opening gate area
- c) gate oxidation(1100°C, 30 min, O_2)
- d) diffusion (1100°C, 5 min, N_2)
- e) anneal (450°C, 15 min, N_2/H_2O)

Step 6: alumina
- a) deposition of alumina (CVD) (60 nm)
- b) deposition of SiO_2 (CVD) (etch mask, 400 nm)
- c) Mask 7: removing Al_2O_3 (except on gate) (etch SiO_2, etch Al_2O_3)

Step 7: contact protection diode
- a) Mask 8: opening protection diode
- b) deposition Al/Pt (50 nm each)
- c) lift-off

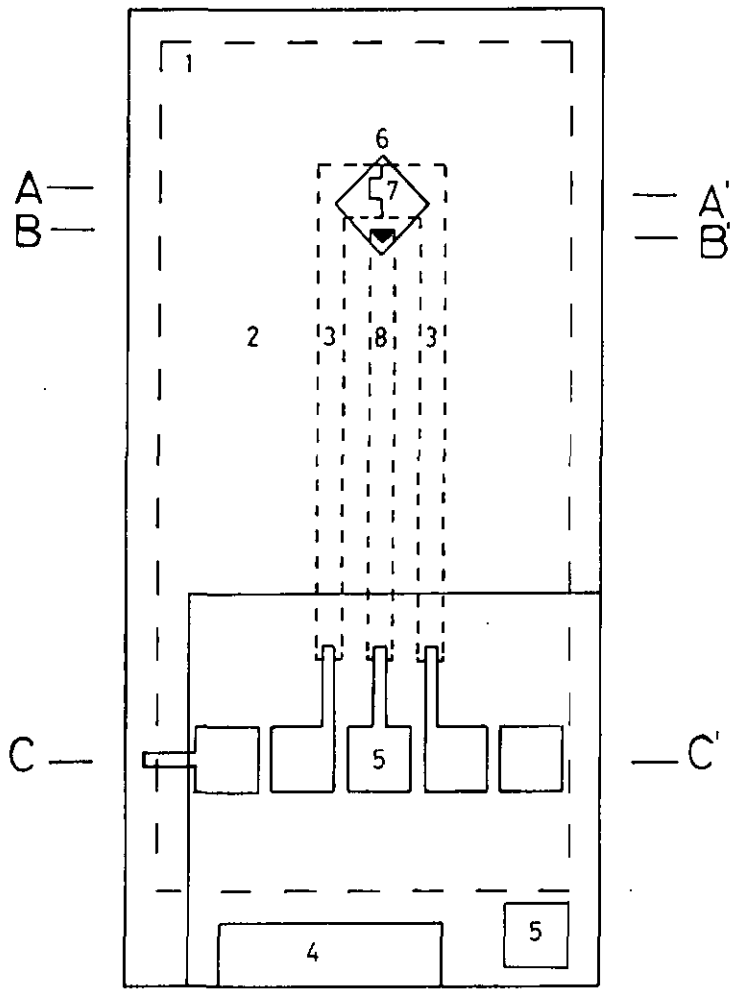

Fig. 7a:
Diagram of the sensor
1) p-well
2) polysilicon
3) drain and source
4) alignment marks
5) contact pads
6) opening in the polysilicon, exposed to the solution after the bonding of glass
7) ISFET gate
8) conductor, with an Al/Pt electrode at the end (triangle), connected to the gate during anodic bonding

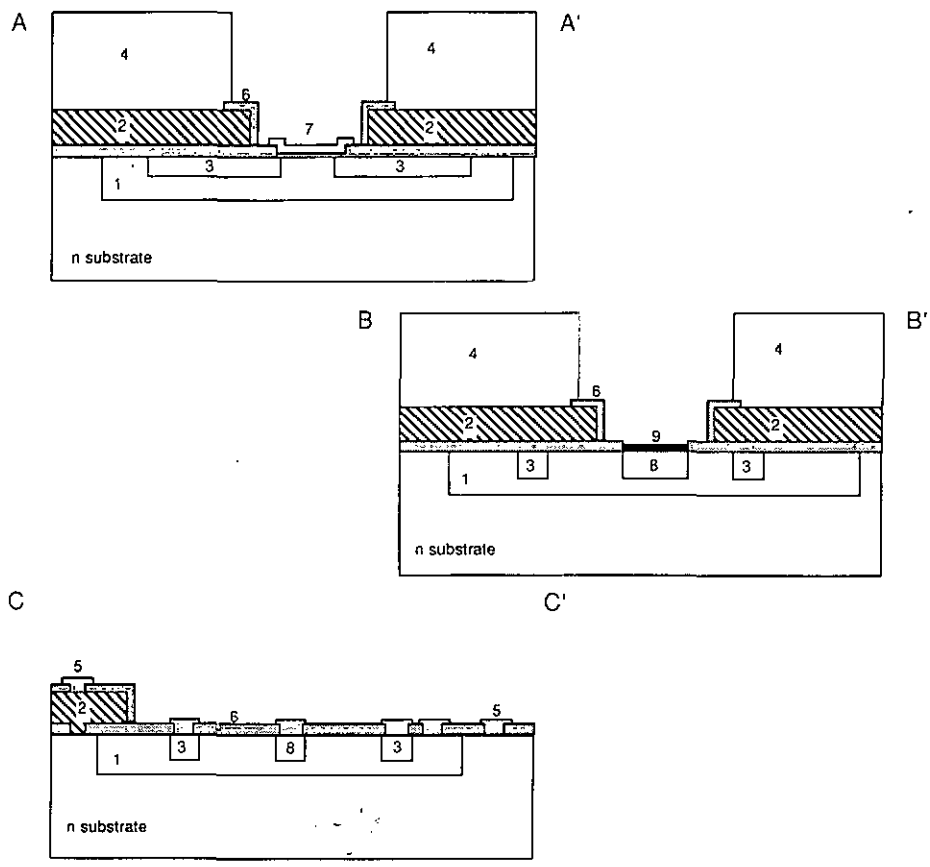

Fig. 7b:
Cross section of the sensor
1) p-well
2) polysilicon
3) drain and source (n-type)
4) glass (anodically bonded to the polysilicon)
5) contact pads (aluminum)
6) silicon dioxide
7) alumina
8) conductor (n-type)
9) Ti/Pt layer

Step 8: contacts and connection gate/protection diode

a) Mask 9: opening contact holes and gate area(the protection layer of SiO_2 on top of the alumina has to be removed, see step 6)
b) deposition of Al (1μm)
c) Mask 10: patterning contacts and connection gate/diode
d) anneal (450°C, 15 min)

Step 9: opening poly Si

a) Mask 11: opening polySi (oxide, which has been formed on the polySi during the gate oxidation, has to be removed)

With an additional step the pCl sensitive ISFETs are fabricated. On the gate area, a Ti/Ag/Ti/Al layer is deposited, instead of the aluminum (between step 8 and 9). A photograph of a dual pH and pCl chip is shown in Fig. 8.

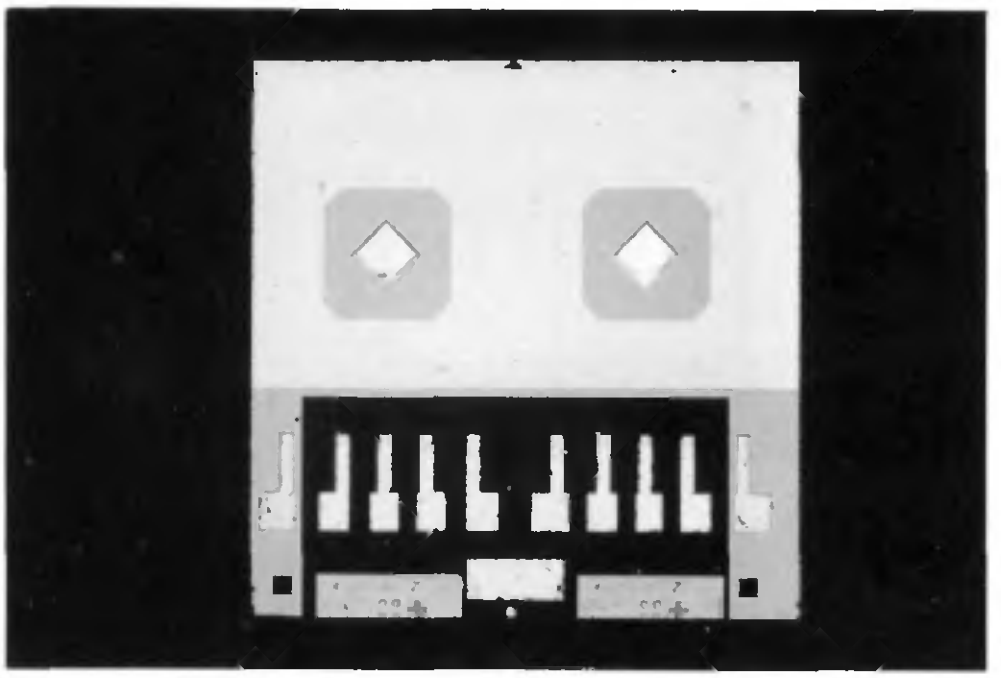

Fig. 8: *A dual pH (right) and pCl (left) sensor, before bonding.*

In order to verify the fabrication process, one wafer was not covered by alumina. The calculated threshold voltage of the MOSFET (-0.01 V) was in good agreement with the measured value: -0.2 V.
After dicing the wafers, the single chips were encapsulated with glass, using the anodic bonding process (part 1). Prior to the bonding the chips were cleaned in an ultrasonic bath with tri-chloroethane, aceton and iso-propanol. The anodic bonding was performed at 400°C at 600 V and was completed in a few seconds. The alignment took several minutes. In order to ascertain a good contact of the Ti layer with the gate, the sensors were kept at 400°C for ten minutes. After the bonding, the protection metal layer on the gate area was etched away or transformed into AgCl as described in part 1. The resulting sensors are shown in Figs. 9 and 10; in Fig. 11 an enlargement of the gate area is shown. The chips were then mounted on standard printed circuit boards and wire bonded. The contact wires were encapsulated with epoxy.

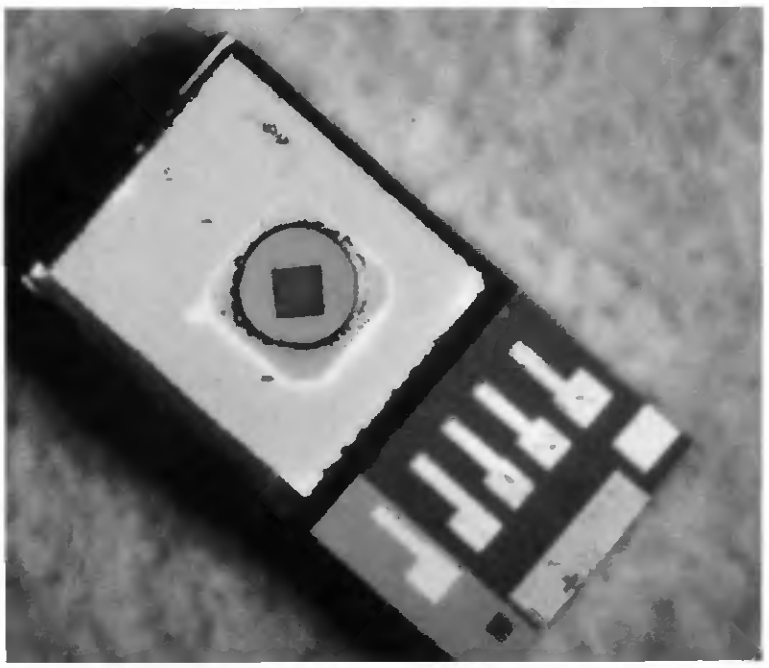

Fig. 9: *A glass encapsulated pCl-ISFET.*

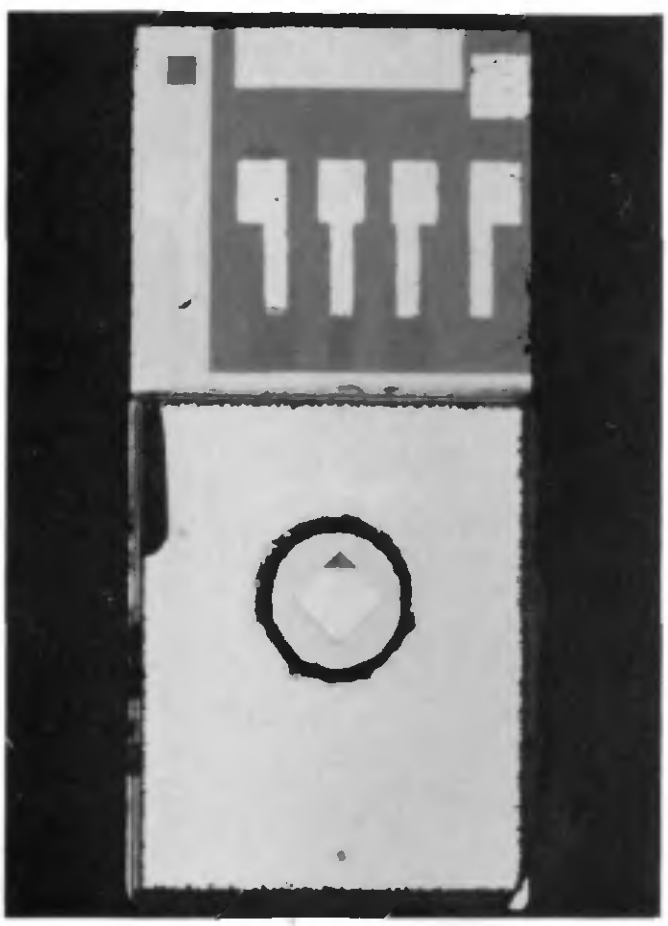

Fig. 10: *A glass encapsulated pH-ISFET.*

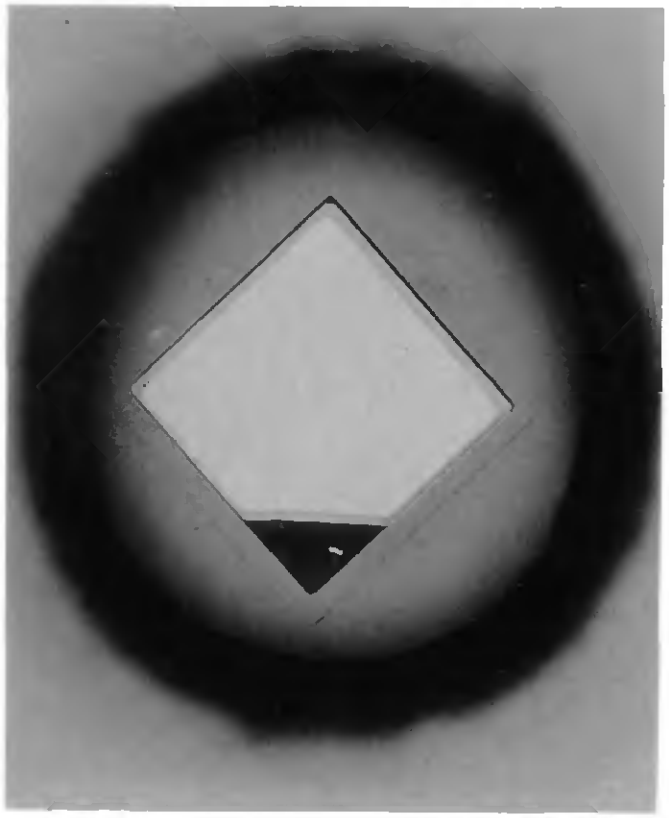

Fig. 11: The gate area of a glass encapsulated pH-ISFET.

Results and discussion

Before and after the bonding, I_D-V_G characteristics of the MAOSFETs were registered. An example is shown in Fig.12, together with the I_D-V_G curve of the pH-ISFET. Upon bonding a mean threshold voltage shift was observed of about 0.4 V. The shift in threshold voltage was sometimes seen when the sensors were only heated. A similar shift was observed on MOS capacitors upon annealing under the same conditions [17]. No other degradations of the sensor characteristics were found.

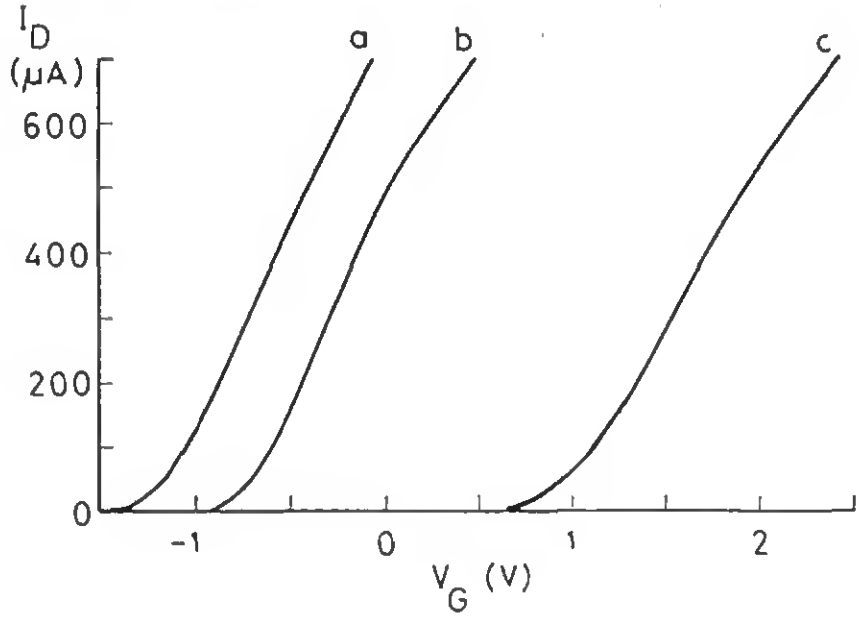

Fig. 12:
I_D-V_G characteristics of a MAOSFET before (a) and after (b) the anodic bonding and of the ISFET in a Tris/HCl solution (c). $V_D = 0.5$ V.

The difference in threshold voltage between a "pH"-MAOSFET and a "pCl"-MAOSFET on the same chip was less then 0.1 V after anodic bonding. The threshold voltage was about -0.35 V. Between wafers differences of up to 0.5 V were found for the initial threshold voltage and on one wafer similar variations were observed.
Upon transforming the "pH"-MAOSFET into a pH-ISFET, a shift in threshold voltage was observed of 1.8 V, instead of the expected shift of only 1 V. This additional shift posed problems for our measuring equipment, which limits the maximum obtainable operational voltage to about 1.8 V, (above this value hydrogen formation can occur in the presence of small leakage currents [23]). Therefore the pH-ISFETs with the lowest threshold voltage were selected (as can be seen from Fig. 12). The pH-ISFETs were then tested on drift behavior and pH-sensitivity.
Upon transforming the "pCl"-MAOSFET into a pCl-ISFET, no significant shift in threshold voltage was observed as was expected. The devices were then also tested on sensitivity and drift behavior. Typical results for both sensors are shown in Fig. 13 and Fig. 14.

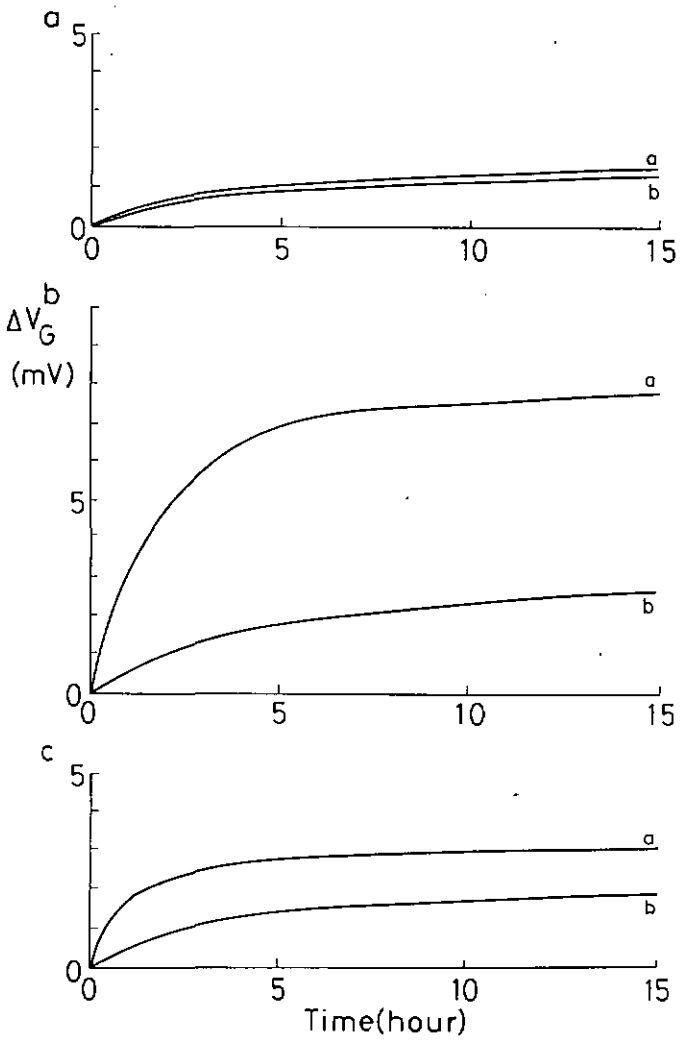

Fig. 13: *Drift measurements*
a) MAOSFET
b) pH-ISFET in a Tris/HCl solution
c) pCl-ISFET in a 0.2 M KCl solution *Time between measurement a and b is one week*

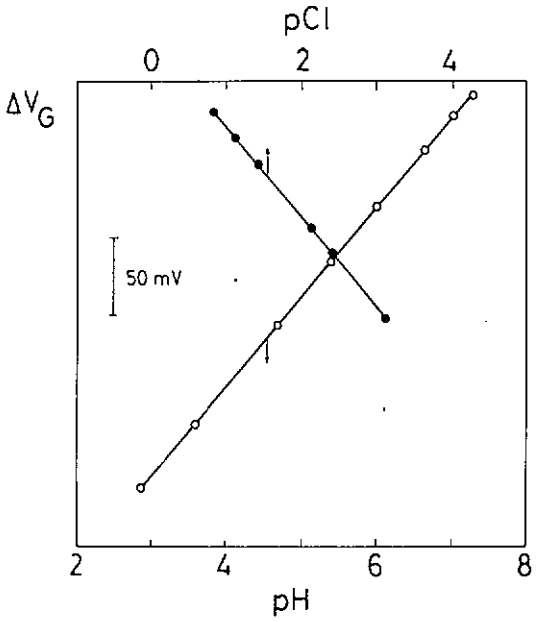

Fig. 14: *pH-sensitivity and pCl sensitivity of glass encapsulated ISFETs*

The sensors had sensitivities of 57 mV/pH and 59 mV/pCl. The drift rates were very low, less than < 0.1 mV/h, and comparable to the MAOSFETs (discussed in chapter 4).
The operational lifetime of the pH-ISFETs was very large. No degradation of the glass encapsulation could be observed over several weeks. (Breakdown was caused by degradation of the epoxy encasulation of the printed circuit boards). In contrast, the pCl-ISFETs had a very large difference in lifetime, varying between several minutes and some weeks. Two effects were responsible for this varying lifetime. One was caused by the protection diode and the other was due to adhesion problems between Ti and Ag.
When the protection diode is illuminated, a photoncurrent is developed which passes through the silver layer and thereby destroys this layer. This effect was even observed on sensors which were stored under ambient conditions. However when reducing the silver layer thickness of 1 μm to 0.7 μm, the connection between the gate area and the protection diode could be broken through an overetch of the Al/Ti protection layer, which is of course a very critical procedure. The sensors, where this process was successful, showed a reasonable lifetime of one to two weeks, after which the Ag/AgCl layer lifted off from the Ti layer. This effect was also observed by Lambrechts *et al.* [24].

Conclusions

It has been shown that the glass encapsulation of chemical solid state sensors with the anodic bonding method is possible. However, a special sensor design is necessary to guarantee the quality of the electric components in the substrate after the bonding. By this method the encapsulation of chemically sensitive solid-state sensors is improved and simplified, even on-wafer encapsulation should be possible. Apart from the problems encountered for the pCl-ISFET and the increased threshold voltage shift for the pH-ISFET both sensors had good properties in regard of sensitivity, stability and lifetime.
The problem of the protection diode for the pCl-ISFET can be solved by a modification of the connection between gate and protection diode, whereas the adhesion problem can be solved with an additional metal layer [24]. The additional shift in threshold voltage for the pH-ISFET can be compensated by changing the fabrication parameters.

References

1. Matsuo,T., Esashi,M., *Sensors Actuators* **1,** 77 (1981).
2. Wen,C.C., Chen,T.C., Zemel,J.N., *IEEE Trans. Electron Devices* **ED-6,** 1945 (1979).
3. Huang,J.C.M., Wise,K.D., *Int.Elec.Dev.Meeting Tech.Digest* p.316, 1982.
4. Chapter 3 of this thesis.
5. Harame,D., Shott,J. Plummer,J., Meindl,J., *Int.Elec.Dev.Meeting Tech.Digest* p.467, 1981.
6. Ho,N.J., J.Kratochvil, Blackburn,G.F., Janata,J., *Sensors Actuators* **4,** 413 (1983).
7. Sanada,Y., Akiyama,T., Ujihara,Y., Niki,E., *Fres.Z.Anal.Chem.* **312,** 526 (1982).
8. Ko,W.H., Bao,M.H., Hong,Y.D., *IEEE Trans. Electron Devices* **ED-29,** 48 (1982).
9. Engelkrout,D.W., Day,A.C., Horne,W.E., *16th IEEE Photovoltaic Spec. Conf.,* 108, (1982).
10. Kratochvil,J., *Proc. of a Symposium on Electrochemical Sensors in Medicine and Medical Research,* Park City,Utah, 1982.
11. Pomerantz,D.I., *U.S.Patent 3.397.278,* 1968.
12. Ko,W.H., Suminto,J.T., Yeh,G.J., in *Micromachining and Micropackaging of Transducers* (C.D.Fung et. al. Ed, Elsevier, Amsterdam), p.41, 1985.
13. Herman,J.H., Pendelton,J.M., Rhodes,L.M., Sander,C.S., Terry,S.C., Walsh,G.V., Meindl,J., *EE 412 Report Stanford University,* 1977.
14. Shapiro,F., Terry,S.C., Meindl,J., *EE 412 Report Stanford University,* 1977.
15. Anthony,T.R., *J.Appl.Phys.* **54 (5),** 2419 (1983).
16. Barth,P.W., Burn,B.E., Lee,K.F., Meindl,J., *EE 412 Report Stanford University,* 1980.
17. Decroux,M., De Rooij,N.F., to be published.
18. Tomazzi,W., Jodzwerwicz,W., *Prz.Chem.* **11,** 129 (1955).
19. Ives,J.G., Janz,G.J., in *Reference electrodes,* Academic Press, 1981.
20. Koudelka,M., *Proc. Journeé d'Electrochimie,* p.3, 1985.
21. Sze,S.M., *Physics of semiconductor devices,* Wiley & Sons, New York, 1981
22. Antoniadis,D.A., Hansen,S.E., Dutton,R.W., *Technical report no 5019-2,* Stanford University, 1978.
23. Janata,J., Huber,R.J., *in* Ion selective electrodes in analytical chemistry Vol 2, (H.Freiser Ed., Plenum Press), 1980
24. Lambrechts,M., Suls,J., Sansen,W., *Proc.of the 2nd Int. Meeting on Chemical Sensors,* Bordeaux, p.572, 1986.

Chapter 7 Solvent polymeric membranes combined with chemical solid state sensors

accepted for publication:

The Analyst:

Solvent polymeric membranes combined with chemical solid state sensors

H.H. van den Vlekkert, C.G. Francis, A. Grisel, N.F. de Rooij

Abstract

The operation of ion-selective field effect transistors (ISFET) with solvent polymeric membranes is described and their chemical performance is discussed. It is shown that the stability of these devices can be increased by the introduction of an intermediate electrolyte solution with fixed ion-concentration, between the insulator and the membrane. Using the same method interference from carbon dioxide and organic acids can be diminished. The encapsulation method with glass is found to provide furthermore a suitable method for hydrogel and membrane fixation, and ensures a long lifetime of the sensor.

Introduction

Since the introduction by Bergveld [1] in 1970 of the ISFET (ion sensitive field effect transistor) much attention has been given to improving the sensitivity and selectivity of these devices. Considerable improvements in all aspects of device performance can be achieved when an additional inorganic layer is deposited on top of the native gate oxide. Thus, excellent pH-sensors have been made in this way with metal oxides (like Al_2O_3 or Ta_2O_5) or silicon nitride [2,3]. In order to change the sensitivity of such pH sensitive devices to for example potassium or sodium, ionophore materials supported in inert matrices [4] can be deposited on top of the gate insulator [5-9], similar to the well known coated wire electrodes (CWE). However two main problems are encountered when these so-called solvent polymeric membranes are applied to ISFETs:

1) the lifetime is limited due to the poor fixation of the membrane
2) the membrane/insulator interface is undefined

The lifetime of these sensors is limited because the poor adhesion of the membrane material to the surface of the sensor enables water to creep in between the sensor surface and the membrane. As soon as the sensitive gate area is reached the sensor can be considered to be short-circuited to the solution. In addition, the membrane on the planar surface is susceptible to any physical force applied to the chip. Possible solutions to this problem have been described by Blackburn and Janata [10], Ho *et al.* [11] and Covington and Whalley [12].

The more serious problem however is the second one. The ISFET can be considered to be a MAOSFET in which the metal is replaced by a reference electrode and a solution with unknown pH. To change the sensitivity of such a system, a solvent polymeric membrane, sensitive to ion i (ISM), can be placed on top of the gate insulator and immersed in a solution with an ion activity of a_i (pI-ISFET). The arrangement of the contacting phases, including the reference electrode, is shown below for all systems:

M'	Si	SiO_2/Al_2O_3	M"
	1 2		7

System 1: MAOSFET

M'	Si	SiO_2/Al_2O_3	sol.pH_2	sat.KCl	AgCl	Ag	M"
	1 2		3 4		5	6	7

System 2: pH-ISFET

M' |Si | SiO_2/Al_2O_3 | ISM | sol a_i || sat.KCl |AgCl | Ag | M"
1 2 8 9 4 5 6 7

System 3: pI-ISFET

From a thermodynamical point of view, these are multiphase systems for which the Gibbs equation must apply at equilibrium when M' is in contact with M":

$$\sum_i dn_i\mu_i = 0 \qquad (1)$$

where dn_i is the number of species i transported across individual intertaces and μ_i is the electrochemical potential of species i.
The flat-band voltage of system 1 can be described by [13]:

$$V_{FB} = \frac{1}{q}(\Phi^M - \Phi^{Si}) - \frac{Q_{ins}}{C_{ins}} \qquad (2)$$

with Φ^M the metal work function, Φ^{Si} the silicon work function, Q_{ins} the charge inside the insulator which is assumed to be located at the insulator/silicon intertace per unit area, q the unit charge and C_{ins} the insulator capacitance per unit area.
The measured parameter for a transistor is the drain current I_D, which is related to the flat-band voltage, in the so-called linear region, as follows:

$$I_D = \mu_n \frac{W}{L} C_{ins} \left(V_G - V_T - \frac{1}{2}V_D\right)V_D \qquad (3)$$

The threshold voltage V_T is given by:

$$V_T = V_{FB} - \frac{Q_B}{C_{ox}} + 2\phi^F \qquad (4)$$

with V_G the gate to source voltage, V_D the drain to source voltage, Q_{inv} the charge per unit area at the silicon surface at inversion, Φ^F the Fermi potential, μ_n the mobility of electrons (or holes) in the inversion layer, W the channel width and L the channel length.
Combination of Equations 2 and 3 yields:

$$(5) \qquad I_D = \mu_n \frac{W}{L} C_{ins} \left(V_G - \frac{\Phi^M}{q} + V_{ss} \right) V_D$$

with V_{ss} equal to:

$$(6) \qquad V_{ss} = \left(\frac{\Phi^{Si}}{q} + \frac{Q_{ins} + Q_{inv}}{C_{ins}} - 2\phi^F - \frac{1}{2} V_D \right)$$

When transforming the MAOSFET into the ISFET the interface M''/Al_2O_3, (system 1) has to be replaced with 3-4, 4-5,5-6 and 6-7 of system 2 to which the Gibbs equation has also to be applied. Based on the site-binding model, as proposed e.g. by Bousse [14] the following expression for I_D can be derived:

$$(7) \qquad I_D = \mu_n \frac{W}{L} C_{ins} \left(V_G - E_{Ag/AgCl} - E_J + \Psi_o - \chi + V_{ss} \right) V_D$$

with $E_{Ag/AgCl}$ the reference electrode potential (5-7), E_J the liquid junction potential (4), for which frequently the Henderson approximation is used [15] and 2-3, 3-4 is described by Ψ_o the potential difference between the insulator surface and the bulk of the solution and χ the surface dipole potential at the insulator/solution interface.
In the case of Al_2O_3 the potential difference Ψ_o is given by [14]:

$$(8) \qquad \Psi_o = 2.303 \frac{kT}{q} \frac{\beta}{\beta+1} (pH_{pzc} - pH)$$

where k denotes the Boltzmann constant, T the absolute temperature, ß the sensitivity parameter and pH_{pzc} the pH at the point of zero charge of the oxide material. In ß all the constants of the surface reactions and of the electrical double layer are lumped together.
In a similar way the expression for I_D for the membrane coated ISFET

(system 3) has been described by Bergveld and De Rooij [16], where 2-3 and 3-4 is replaced with 2-8, 8-9 and 9-4:

$$I_D = \mu_n \frac{W}{L} C_{ins} \left(V_G - E_{Ag/AgCl} - E_J + \frac{\mu_i^{sol\,2}}{z_i q} + \frac{kT}{z_i q} \ln a_{i2} + \frac{\alpha_i^{ISM}}{z_i q} + V_{ss} \right) V_D \qquad (9)$$

with $\mu_i^{sol\,2}$ the standard chemical potential of ion i in the solution, z_i the charge number and α_i^{ISM} the so called real potential (phase 8), consisting of the dipole potential at the ISM/insulator interface and the chemical potential of species i in the membrane. This formula is identical to the equation given by Buck [17] for a structure where SiO_2 is coated with AgBr.
The question of the stability of the term α_i^{ISM} is similar to the situation for coated wire electrodes, first described by Hirata and Date [18] where the membrane/metal potential is also undefined. It was found that CWEs showed a potential dependence on oxygen partial pressure, especially for electrodes with platinum conductors [19,20]. Therefore the CWE function can be considered to be due to the formation of an oxygen half-cell on the membrane/metal interface owing to water penetration, which can be fast for solvent polymeric membranes [21]. A similar mechanism was proposed by Srianujata *et al.* [22], who used a CWE made of chloridated silver wire, covered by a membrane (PVC and DOP) for metal ion determination. Prepared electrodes were soaked for 12 hours in 0.1 M potassium chloride. According to these authors, the membrane contact with Ag/AgCl was through a thin film of salt water (KCl) solution rather than directly. In both cases the electrode potential can be described using the standard expression for ion-selective electrodes with an internal filling solution. The stability of the devices depends now on the stability of the reference system and the concentration of the measured species i in the water layer between membrane and reference system.

For ISFETs covered with polymeric membranes, and in particular potassium sensitive membranes based on valinomycin, contradictory results regarding stability have been reported in the literature. A possible explanation of these contradictions could be the membrane/insulator interface, which may be stable under certain conditions as for CWEs. In a recent paper Fogt *et al.* [23] reported that pH sensitive ISFETs, coated with a potassium sensitive membrane, are subject to a number of unexpected interferences. Carbon dioxide, benzoic acid and acetic acid caused significant shifts in the output of these potassium-sensitive ISFETs. Since conventional potassium membranes are normally not susceptible to these species [24], the mechanism involved must be related to the membrane/insulator interface. Supposing that there is a thin water layer at this interface, a change in pH of this layer would be seen as a change in output potential of the ISFET. Dissociation of species, which diffuse through the membrane, such as CO_2 and benzoic acid can induce this change of this ill defined hydrated layer. Similar results were reported by Harrison [25] for MIS capacitors.
Assuming that there is a hydrated layer between the membrane and insulator, the following system can be described for an ISFET covered with a potassium sensitive membrane:

$M'|Si|SiO_2/Al_2O_3|$ sol. pH_1, $a_{K^+}{}_1$ |ISM | sol. $a_{K^+}{}_2$‖ KCL sat.|AgCl| Ag| M"

System 4:

which results in the following expression for I_D:

$$I_D = \mu_n \frac{W}{L} C_{ins} \left(V_G - E_{Ag/AgCl} - E_J + \Psi_o - \chi + \frac{kT}{q} \ln \frac{a_{K_2^+}}{a_{K_1^+}} + V_{ss} \right) V_D \qquad (10)$$

It can be seen from this equation that the stability of the system depends on the pH and a_{K+1} of the hydrated layer. When these are stable, the system will react to changes of the activity of potassium ions in the outside solution (a_{K+2}). This indicates for example that the influence of carbon dioxide can be eliminated when the pH of the inner hydrated layer is around 4 because at this pH the hydrogen carbonate does not dissociate. In order to achieve this a hydrogel with pH 4 has to be placed between the membrane and the insulator. Furthermore to ascertain that the membrane responds only to the outside potassium ion activity the hydrogel should also contain potassium ions. An ideal structure to deposit first a hydrogel and then the solvent polymeric membrane is described previously in chapter 6: the sensor consists of a pH sensitive ISFET, encapsulated with glass which has at the gate area a hole of about 500 µm diameter and depth around 200 µm.
In this chapter the validity of this configuration (system 4) will be investigated and compared to the simple membrane/insulator set-up (system 3). To simplify the question of the ion selective membrane we have used the well known potassium sensitive membrane, based on valinomycin first described by Stefanac and Simon [26].

Experimental

Electrodes:
The pH sensitive ISFETs, encapsulated with glass were first tested for pH response and drift rate, in order to verify their functionality. After these tests they were cleaned with water and iso-propanol and dried at room temperature. As a reference electrode a double junction Ag/AgCl electrode was used (Metrohm 6.1103.00). The inner solution was a saturated KCl solution, while the outer solution was a pH 4 buffer (Merck) to which 0.1 M KCl was added.
Chemicals:
Membrane composition:
The solution for dip coating consisted of 1400 mg DOS (Bis(2-ethylhexyl) sebacate, Fluka, purum p.a.), 600 mg PVC (Poly(vinyl chloride),Fluka, purum p.a.), 20 mg Valinomycin(Fluka, purum p.a.) and 8 mg KtpClpB (Potassium-tetrakis(4-chlorophenyl)borate, Fluka, purum p.a.) dissolved in 8 ml Tetrahydrofuran(p.a.).
Hydrogel:
Different hydrogels were tested for their applicability with the glass encapsulated ISFETs. It was established that, although it is not a real hydrogel, a solution of 20% Dextran was very suitable for filling up the glass hole. Different solutions were then prepared for the inner electrolyte:

20% Dextran in buffer pH 4 (Merck)
20% Dextran in Buffer pH 4 and 0.1 M KCl
20% Dextran in Buffer pH 8 (Merck) and 0.1 M KCl
For the stability test the sensors were tested in a pH 4 buffer with 0.1 M KCl or in a pH 8 buffer with 0.1 M KCl. To test the sensitivity several solutions were prepared with different KCl concentrations, to which NaCl was added in order to maintain a constant ionic strength.of 0.1 M.

Dip coating procedure
The glass holes were filled with the hydrogel and the surface was allowed to become tacky (5 to 10 min). Then the sensor was dip-coated in the solution and allowed to dry for 5 min, after which another dip-coating was carried out. After 15 min drying in air the sensors were stored in the buffer and were ready for testing. The estimated membrane thickness was about 50μm. It was noted that if the hydrogel surface was not tacky enough the membrane took up a lot of water and no homogeneous membranes could be formed.

Test procedure:
After dip coating, the ISFETs were connected to a specially developed amplifier system, which operated the devices at constant drain current and constant drain source voltage. The reference electrode to source voltage (V_G) was the determined quantity.
After a drift test and sensitivity test, the sensors were tested for carbon dioxide and organic acid sensitivity. All experiments were carried out at 25°C.

Results and discussion

In order to verify our theory that stable sensors can only be made if an inner solution with constant pH and KCl is present, the stability of the different systems has been measured. It was already shown that the stability of the ISFET is not dependent on pH [Ch 2] and the inner membrane potential is not dependent on the absolute KCl concentration [27]. Therefore only the systems without inner electrolyte, with inner electrolyte with constant pH and with inner electrolyte with constant pH and pK had to be investigated. The results are summarized in Table 1.

Table 1: *Stability of potassium sensitive ISFETs, as a function of inner electrolyte.*

inner electrolyte	drift rate pH -ISFET	drift rate membrane covered pH-ISFET			
time*	5-15	0-1	5-15	15-25	72-120
no	0.08	200	2.6	1.3	0.4 to -0.4
pH 4	0.10	40	0.8	0.4	0.12
pH 4, 0.1M KCl	0.25	15	0.4	0.2	0.07

**time interval over which the drift rate (in hours) is determined.*

As can be seen from Table 1 there is a remarkable difference in stability of the different sensors. The results from the sensor without inner electrolyte are comparable to those reported in the literature [5,6,7]: After a long stabilisation time the drift rate becomes small and more or less stable. Furthermore when the inner electrolyte has a constant pH and KCl the drift rate of the total sensor (column 3 Table 1) is nearly equal to the drift rate of the bare pH-ISFET (column 2 Table 1). It can also be seen that when no potassium is present in the inner electrolyte the sensor exhibits a much higher initial drift, probably due to the unstable boundary potential at the membrane/inner electrolyte interface. The total lifetime of the sensors was about 7 days, after which the sensitivity decreased and the drift increased, in agreement with other measurements on similar configurations [5,6,28].
In order to test the influence of carbon dioxide, the gas was bubbled through the solution with pH 4 and a background of 0.1 M KCl. The influence of CO_2 was investigated as a function of the pH of the inner electrolyte. The external pH was also measured with a conventional glass electrode. The results are summarized in Table 2, together with the sensitivity to potassium ion activity.

Table 2: *Sensitivity and carbon dioxide interference of membrane covered ISFETs*

inner electrolyte	sensitivity (mV/pK) after			response to CO_2 (ΔV_G)		
	1day	5days	7days	air	10 %	20 %
no	54.0	53.9	49.4	0	-143	-161
pH 4, 0.1M KCL	57.8	58.5	56.0	0	0	0
pH 8, 0.1 M KCl	57.0	56.9	30.0	0	-76	-93

As can be seen from Table 2 there is an enormous difference in carbon dioxide response when the inner electrolyte pH is changed.
At pH 8 CO_2 reacts with water and the formed hydrogen carbonate dissociates (pK = 6.37), causing thus a drop in pH. The shift observed for the sensor with pH 8 as inner electrolyte, is equal to the changes in pH for a pH 8 buffer saturated with 10 and 20% CO_2 as measured with a glass electrode. The shift in potential when no inner electrolyte solution is used, is more or less comparable to the concentration change going from air (0.033% CO_2) to 10 and 20% CO_2 supposing that $[CO_2]=[H^+]$. These results indicate that both sensors show a linear response to CO_2. The response time to an increase in carbon dioxide concentration is rather short. However when the CO_2 concentration is reduced the response is much slower, consistent with observations for normal gas sensors.
As predicted no change in potential was observed when the inner electrolyte has a pH of 4. At pH 4 hydrogen carbonate does not dissociate and therefore causes no change in pH. It should furthermore be noted that carbonate ions do not diffuse through the membrane because no potential shift was observed when the pH of the outer solution saturated with CO_2 was raised to 8.

The influence of organic acids was tested on the device with a pH 4, 0.1 M KCl inner solution. To different buffers (Merck) 10 or 20 mMol of an organic acid were added. All solutions had a background of 0.1M KCl. Before and after each test the sensor response was determined in the buffer solution with pH 3.85, 0.1 M KCl. It was found that all responses were reversible. The pH of the different solutions was also registrated. The results are summarized in Table 3. With respect to the pK values of the different organic acids it should be noted that at pH 4 around 25 % of the acid is not dissociated, and with increasing pH this amount diminishes so that at pH 8 the dominant species is the conjugated base form (>99%).

Table 3: *Influence of organic acids on the response of a potassium sensitive ISFET with an inner electrolyte solution with pH = 4 and 0.1 M KCl.*

acid	pH test solution			response($-\Delta V_G$ (mV))	
	0	10 mMol	20mMol	10mMol	20mMol
benzoic acid	3.86	3.75	3.68	7.6	15.7
pK= 4.19	7.81	6.60	4.08	2.7	14.7
$(C_6H_5)CO_2H$			6.57*		2.5
		8.28*		0.1	
ascorbic acid	3.85	3.75	3.68	0.1	-0.2
pK= 4.10					
$C_6H_8O_6$					
citric acid	1.00	0.99		0.0	
pK= 3.14	3.85	3.58		0.7	
$HOC(CH_2CO_2)$-	7.81	3.59		-1.7	
CO_2H		7.97*		0.0	
acetic acid	3.82	3.82	3.77	3.0	8.0
pK= 4.75			8.10*		1.1
CH_3CO_2H					

**pH changed in-situ by adding 0.5 M NaOH ($-\Delta V_G$ corrected for change in potassium concentration)*

From Table 3 it can be seen that the sensor reacts differently to different organic acids and that the response is a function of the outer pH of the solution. From the fact that, at pH 8, the response of the sensor to organic acids is negligible, it can be deduced that the conjugate base does not diffuse through the membrane, in contrast to the conclusion of Harrison [25], but in agreement with the findings of Kobos [24] and Fogt [23]. At pH 4, however, the acid is present and can diffuse into the membrane. In the hydrogel it will then dissociate, thereby changing the pH of the solution. The non-Nernstian behavior can be explained in terms of the buffer capacity and the difference in response with the different pK values. Furthermore it is evident that the rate of diffusion of the organic acids through the membrane is determined by their structure.

Conclusions

Although no statistical data are yet available, the following conclusion can be drawn based, on our experiments and data from the literature.
It has been shown that the sensitivity of a pH-ISFET can be modified with solvent polymeric membranes. The method of glass encapsulation did not only provide devices with a long lifetime (> 4 weeks) but the existence of a well-defined cavity also contributes to an excellent fixation for the membrane. The stability of such modified sensors can be compared to that for an unmodified device, when an appropiate solution is placed between the insulator and the membrane. The undefined interface potential of the membrane/insulator is now replaced with two interfaces: insulator/solution and membrane/solution which can be described with the site-binding theory resp. with the theory for solvent polymeric membranes. In the case of the pH sensitive ISFETs the choice of the inner electrolyte pH should be made according to its application. For biomedical measurements, the interference of carbon dioxide can be eliminated by using an inner electrolyte with a pH of 4, whereas at the same time interference of organic acids can be ruled out at physiological pHs since the conjugate bases do not diffuse through the membrane.

References

1. Bergveld,P., *IEEE Trans. Biomed.Eng.* **BME-17 no 1,** 70 (1970)
2. Abe,H., Esahi,M., Matsuo,T., *IEEE Trans. Electron Devices* **ED-26,** 1939 (1979).
3. Akiyama,T., Ujihara,Y., Okabe,Y., Sugano,T., Niki,E., *IEEE Trans. Electron Devices* **ED-29,** 1936 (1982).
4. Ammann,D., Morf,W.E., Anker,P., Meier,P.C., Pretsch,E., Simon,W., *Ion Selective Electrode Review* **5,** 3 (1983).
5. Moss,S.D.,Janata,J., Johnsson, C.C., *Anal.Chem.* **47,** 2238 (1975).
6. McBride,P.T., Janata,J., Comte,P.A., Moss,S.D., Johnson,J., *Anal.Chim.Acta* **101,** 239 (1978).
7. McKinley,B.A., Staffle,J., Jordon,J., Janata,J., Moss,S.D., Westenskow,D.R., *Med.Instrum.* **14,** 93 (1980).
8. Oesch,U., Caras,S., Janata,J., *Anal.Chem.* **53,** 1983 (1981).
9. Sibbald,A., Covington,A.K., Carter,R.F., *Med.Biol.Eng.&Comp.* **23,** 329 (1985).
10. Blackburn,G.F., Janata,J., *J.Electrochem.Soc.* **129,** 2580 (1982).
11. Ho,N.J., Kratochvil,J., Blackburn,G.F., Janata,J., *Sensors Actuators* 4, 413 (1983).
12. Covington,A.K., Whalley,P.D., *J.Chem.Soc., Faraday Trans. 1* **82,** 1209 (1986).
13. Sze,S.M., *in* "Physics of Semiconductor Devices", 2nd ed., Wiley and Sons, 1984.
14. Bousse,L., *Thesis,* University of Twente, The Netherlands, 1982.
15. Henderson,P., *Z.Phys.Chem.* **59,** 118 (1907); **63,** 325 (1908).
16. Bergveld,P., De Rooij,N.F., *in* Vaste Stof Sensoren, (Kluwer B.V. Deventer), p.119 1980.
17. Buck,R.P., Hacklemann,D.E., *Anal.Chem.* **49 no. 14,** 2315 (1977).
18. Hirata,H., Date,K., Talanta 17, 883 (1970).
19. May-Zurawska,M., Hulanicki,A., *Anal.Chim.Acta.* **136,** 395 (1982)
20. Schindler,J.G., Stork,G., Strüh,H.J., Schmid,W., Karaschinski,K.D., *Fres.Z.Anal.Chem.* **295,** 248 (1979).
21. Oesch,U., *Thesis,* ETH Zürich, Switzerland, 1979.
22. Srianujata,S., White,W.R., Higuchi,T., Sternson,L.A., *Anal.Chem.* **50,** 232 (1978).
23. Fogt,E.J., Untereker,D.F., Norenberg,M.S., Meyerhoff,M.E., Anal.Chem. **57,** 1998 (1985).
24. Kobos,R. K., Parks,S.J., Meyerhoff,M.E., *Anal.Chem.* **54,** 1976 (1982).
25. Harrison,D.J., Verpoorte,E.M.J.,Xizhong,L., *in* Proc. of Transducers '87, Tokyo, Japan, p.301, 1987.
26. Stefanac,Z., Simon,W., *J.Microchem.* **12,** 125 (1967).
27. Jalkanen,L., Virtatanen,R., *Anal.Letters* **14(A7),** 479 (1981).
28. Kawakami,S., Akiyama,T., Ujihara,Y., *Fres.Z.Anal.Chem.* **318,** 349 (1984).

Summary

Since the introduction by Bergveld in 1970 of the ion selective field effect transistor (ISFET) much attention has been paid to improve the performance of these devices. Considerable improvements in all aspects of device performance have been achieved when an additional inorganic layer is deposited on top of the native gate oxide.
In this thesis some remaining fundamental and practical problems, which have hampered the application of these types of sensors on a large scale, have been discussed
After a short introduction, chapter 1, the design, fabrication and characterization of a pH sensitive ISFET, with alumina as pH sensitive layer was discussed in chapter 2. A method has been outlined to achieve reliable pH measurements, despite their drift and temperature behavior. With the outlined method a residual standard deviation of 0.01 pH is observed between a pH-ISFET and a conventional glass electrode
In chapter 3 it was shown that ISFETs can fullfil the specific requirements for biomedical application when carefully designed. A pH sensitive ISFET, with back-side contacts, will be discussed for the determination of dental plaque pH. Furthermore, a combined pH-pressure sensor has been presented for oesophageal studies.
In chapter 4 attention was paid to the drift behavior of the ISFETs. A method was presented to reduce the drift rate of pH-ISFETs, without pretending that the origin of this decrease is fully understood. The drift rate could be reduced from typically 0.1 to 0.2 mV/h to 50 μV/h
In chapter 5 the temperature sensitivity of ISFETs was discussed. It can be described accurately using standard MOS theory in combination with the site-binding theory. The results showed that careful measurement of the temperature sensitivity of ISFETs, with metal oxides as sensitive layer, can provide information about the reactions occurring at the oxide/solution interface.
In Chapter 6 a method has been outlined to improve and simplify the encapsulation of ISFETs. The described encapsulation technique is based on the anodic bonding of glass to silicon. It was shown that, provided care is taken to protect the devices against the hazardous circumstances of the anodic bonding process, an efficient encapsulation of ISFETs can be achieved. Furthermore the development of a pCl-ISFET has been discussed.
Finally in Chapter 7 the transformation of the sensitivity of pH sensitive ISFETs with solvent polymeric membranes has been discussed. It was shown that, in order to obtain stable sensors, an intermediate layer is neccessary between the insulator and the solvent polymeric membrane.